

8. SITE 887¹

Shipboard Scientific Party²

HOLE 887A

Date occupied: 9 September 1992
Date departed: 11 September 1992
Time on hole: 2 days, 30 min
Position: 54°21.921'N, 148°26.765'W
Bottom felt (rig floor; m, drill-pipe measurement): 3642.8
Distance between rig floor and sea level (m): 11.57
Water depth (drill-pipe measurement from sea level, m): 3631.2
Total depth (rig floor; m): 3928.8
Penetration (m): 286.0
Number of cores (including cores with no recovery): 31
Total length of cored section (m): 286.0
Total core recovered (m): 239.89
Core recovery (%): 83.9
Oldest sediment cored:
Depth (mbsf): 279.4
Nature: clay and gravel slurry
Age: middle Miocene
Measured velocity (km/s): 1.56

HOLE 887B

Date occupied: 11 September 1992
Date departed: 12 September 1992
Time on hole: 13 hr, 15 min
Position: 54°21.921'N, 148°26.778'W
Bottom felt (rig floor; m, drill-pipe measurement): 3647.5
Distance between rig floor and sea level (m): 11.57
Water depth (drill-pipe measurement from sea level, m): 3635.9
Total depth (rig floor; m): 3687.5
Penetration (m): 40.0
Number of cores (including cores with no recovery): 5
Total length of cored section (m): 40.0
Total core recovered (m): 41.38
Core recovery (%): 103.4
Oldest sediment cored:
Depth (mbsf): 40.0
Nature: clayey siliceous ooze with calcite and diatom calcareous ooze with clay
Age: early Pliocene

HOLE 887C

Date occupied: 12 September 1992
Date departed: 13 September 1992
Time on hole: 1 day, 11 hr, 45 min
Position: 54°21.934'N 148°26.778'W
Bottom felt (rig floor; m, drill-pipe measurement): 3645.2
Distance between rig floor and sea level (m): 11.57
Water depth (drill-pipe measurement from sea level, m): 3633.6
Total depth (rig floor; m): 3919.0
Penetration (m): 273.8
Number of cores (including cores with no recovery): 30
Total length of cored section (m): 273.8
Total core recovered (m): 269.44
Core recovery (%): 98.4
Oldest sediment cored:
Depth (mbsf): 273.8
Nature: clayey siliceous ooze and calcareous ooze
Age: middle Miocene
Measured velocity(km/s): 1.56

HOLE 887D

Date occupied: 13 September 1992
Date departed: 16 September 1992
Position: 54°21.935'N, 148°26.788'W
Bottom felt (rig floor; m, drill-pipe measurement): 3645.2
Distance between rig floor and sea level (m): 11.57
Water depth (drill-pipe measurement from sea level, m): 3633.6
Total depth (rig floor; m): 4018.3
Penetration (m): 373.1
Number of cores (including cores with no recovery): 13
Total length of cored section (m): 115.7
Total core recovered (m): 19.92
Core recovery (%): 17.2
Oldest sediment cored:
Depth (mbsf): 289.37
Nature: clay with ash and iron oxides
Age: Oligocene (at 145-887D-6R-1, 10 cm)
Hard rock:
Depth (mbsf): 373.1
Nature: basalt
Measured velocity (km/s): 4.5 (at 292 mbsf)
Comments: Washed from 0 to 257.4 mbsf.

Principal results: The site survey at proposed Site PM-1A (Site 887; Figs. 1 and 2) on the Patton-Murray Seamount platform in the northern portion of

¹ Rea, D.K., Basov, I.A., Janecek, T.R., Palmer-Julson, A., et al., *Proc. ODP, Init. Repts.*, 145: College Station, TX (Ocean Drilling Program).

² Shipboard Scientific Party is as given in list of participants preceding the contents.

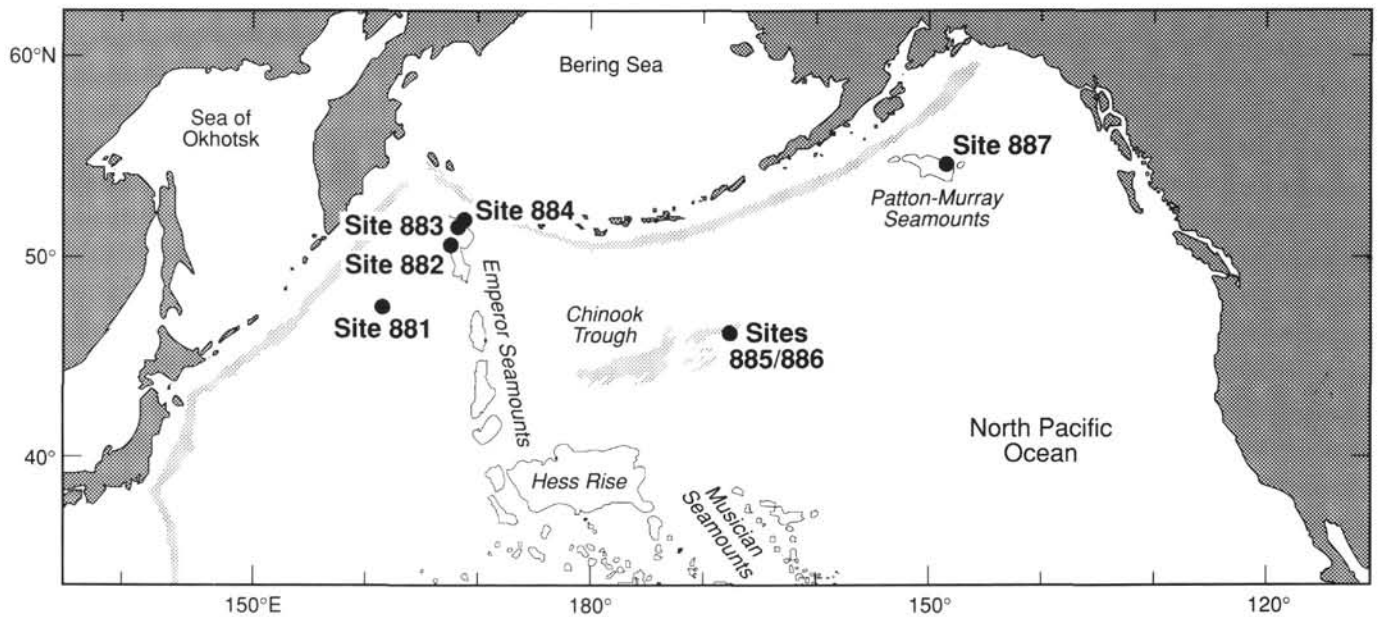


Figure 1. Index map of the North Pacific Ocean showing location of Leg 145 drill sites.

the Gulf of Alaska began about 0945 hr (local time) on 9 September 1992—the first daylight survey of the cruise. The survey was routine, and a beacon was dropped for Site 887 at about 1130 hr. Hole 887A was spudded with a good mud-line core at 2200 hr that same evening. Hole 887A penetrated 285 m with 84% recovery and bottomed, after penetrating about 15 m of basaltic pea gravel, at basement. The attempt to spud Hole 887B, beginning at about 0600 hr on 11 September, met with failure twice, apparently because the APC apparatus was inoperable, which necessitated a pipe trip for a new bit assembly. Hole 887B finally was spudded at 0200 hr on the morning of 12 September and consisted of five APC cores (41.4 m cored and 103.5% recovery) raised for high-resolution studies of sediment and pore-water chemistry. With the recovery of Core 145-887B-2H, Leg 145 passed the 4000-m total core recovery level and became part of the now five-member elite group of ODP/DSDP cruises that has exceeded 4 km in total recovery. Hole 887C was spudded at 0600 hr on 12 September and was continued using the APC-coring system down to 274 mbsf with 98.4% recovery, a testament to the efficacy of the new aggressive piston-coring techniques. At 1100 hr on 13 September, we began the round trip to change the bit and set a bottom-hole assembly (BHA) for rotary-coring in the basement of the seamount platform. Hole 887D penetrated to 373.1 mbsf, about 84 m into basalt, with a low recovery of 20% in the rock. The last core of Leg 145, 145-887D-13R, arrived on deck at 0210 hr on 15 September, when preparation for logging began. The first two logging runs with the Quad combo and the formation microscanner (FMS) tools went well, but at about 0000 hr on 16 September, the FMS tool became stuck in the drill pipe during retrieval. Normal procedures could not dislodge it, so the crimper and then the cable cutter were sent down the wire, the cable was cut, and we started out of the hole. The suspect section of pipe arrived on deck about 1230 hr, the FMS tool was extracted, and the *JOIDES Resolution* got under way for Victoria, Canada, at 1500 hr on the 16th of September, about half a day sooner than expected. We were carrying 4321.40 m of sediment and basalt recovered from the sites of the North Pacific Transect, about 1 km more recovery than anticipated—thanks to the hard work and efficiency of the SEDCO drilling crews and the ODP operations group.

The 289 m of sediment recovered at Site 887 can be divided into three lithologic units. Lithologic Unit I (0–90 mbsf) is an upper Pliocene to Quaternary siliceous silty clay (Subunit IA, 0–45 mbsf) and clay (Subunit IB, 45–90 mbsf). Dropstones are numerous, and ash layers are common in Unit I. Lithologic Unit II (90–270 mbsf) is a lower Miocene to upper

Pliocene siliceous ooze with scattered carbonate. Lithologic Unit II can be divided into three subunits. Lithologic Subunit IIA (90–174 mbsf) is an essentially pure diatom ooze of late Pliocene–late Miocene age. Subunit IIB (174–235 mbsf) is an upper Miocene to middle Miocene calcareous diatom ooze, and Subunit IIC (235–270 mbsf) is a middle to lower Miocene siliceous ooze. Lithologic Unit III (270–289 mbsf) is a sparsely fossiliferous clay of presumably early Miocene age that overlies the basalt. At Hole 887A, several meters of basaltic pea gravel in a clay slurry were recovered from this interval. Unit IV (289–373 mbsf) is basalt that, from drilling, appears to occur in flows or sills that trap at least two horizons of intervening sediment. One small piece of chalk that contained an undifferentiated Oligocene nannofossil assemblage was recovered at 298 mbsf from Core 145-887D-6R.

Calcareous fossils are present in the Miocene and lower Pliocene parts of the section, but Pleistocene sediments are present only in discrete, apparently cyclic, horizons; most of the Pleistocene is barren. Diatoms are abundant, and radiolarians common throughout the section. Reworked middle Miocene forms of these fossils occur in the upper Miocene and lower Pliocene sediments.

In addition to the biostratigraphy provided by the siliceous microfossils, a magnetic reversal stratigraphy complete to 18 Ma has been constructed for essentially the entire section of APC-cored Hole 887C (0–270 mbsf). This stratigraphy provides a framework for calibration of microfossil zonation and allows one to determine well-constrained sedimentation rates. Subunit IA (the siliceous clays) has a linear sedimentation rate of about 61 m/m.y. that pertains from 0 to 0.74 Ma. Sedimentation rates decline more or less continuously down the core and are about 25 m/m.y. in the Pliocene and lower Pleistocene portions of the section, which is 0.74 to 5.8 m.y. in age, and 10 m/m.y. in the middle and upper Miocene parts. The lower Miocene clays may have a linear sedimentation rate of perhaps 2 m/m.y. Casting the sedimentation rates as MARs allows for differentiation of the influx of major sedimentary components. Terrigenous materials, recorded aboard the ship as clay plus quartz, increase in flux by nearly an order of magnitude at the time of the onset of Northern Hemisphere glaciation from 0.10 to 0.15 $\text{g}(\text{cm}^2 \cdot \text{k.y.})^{-1}$ in the Miocene and lower and middle Pliocene sediments to about 1.0 $\text{g}(\text{cm}^2 \cdot \text{k.y.})^{-1}$ in sediments younger than 2.6 Ma. Diatoms, the other major sedimentary component, reached their flux maxima in the lower and middle Pliocene portions of the section, where they accumulated at more than 1.0 $\text{g}(\text{cm}^2 \cdot \text{k.y.})^{-1}$ in the time interval between 2.6 and 5.7 Ma. The lower Pliocene period of greatly enhanced

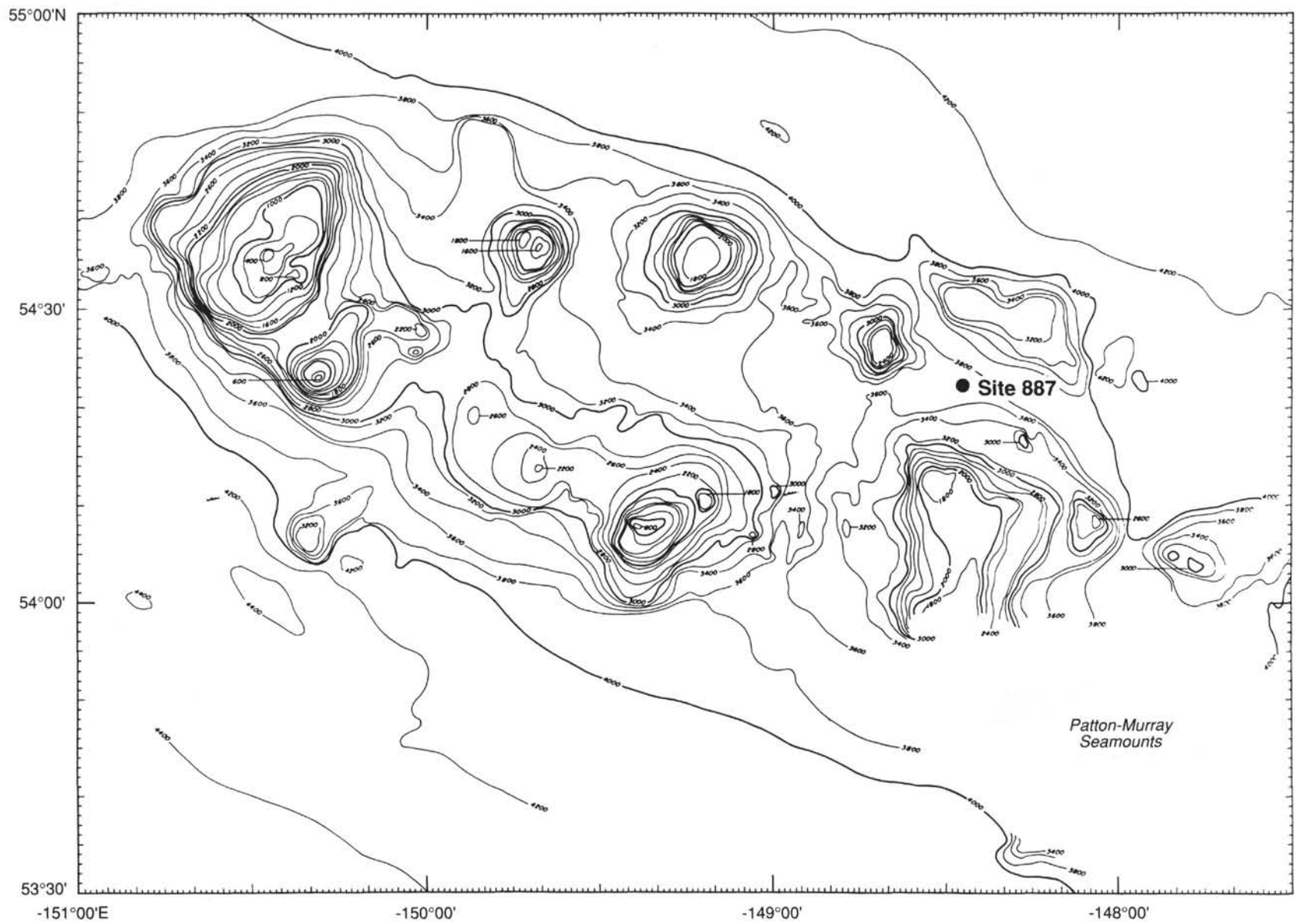


Figure 2. Bathymetric map of the Patton-Murray Seamounts; contours in meters with a 200-m interval. Site 887 is on the platform level in the eastern end of the seamount group. Map by C. Brenner of the Lamont-Doherty Earth Observatory.

diatom deposition, observed during Leg 145 throughout the North Pacific Ocean, also is present in the Gulf of Alaska.

Using logging runs into basement with the Quad combo tool and the FMS, we were able to define a compound basement structure that consists of at least three and possibly four flows or sills with intervening sediment layers. Hole 887D bottomed in pillow lavas at 373 mbsf and 84 m into the seamount platform and provides a first glimpse into the geology of these kinds of volcanic constructions.

BACKGROUND AND SCIENTIFIC OBJECTIVES

Site 887 (proposed Site PM-1) was chosen on a flat, elevated surface in the eastern part of the Patton-Murray Seamount group in the Gulf of Alaska at a water depth of 3630 m. This site is the eastern termination of the Leg 145 latitudinal transect across the subarctic Pacific Ocean. The *Parizeau-87* seismic profile from the site survey shows (1) an approximately 300-m-thick sedimentary sequence having pronounced reflectors parallel to acoustic basement in the upper 100 m and (2) a more homogeneous transparent unit having separate strong reflectors in the deeper portion. The sedimentary section rests on basaltic basement and has an age of 26.3 Ma for Patton Seamount and 25.7 Ma for Murray Seamount and, presumably, consists of hemipelagic clays with some admixture of biogenic siliceous and calcareous material. Sedimentation rates are thought to average 10 to 15 m/m.y., with a several-fold increase during the Quaternary. Examination of 10 piston and gravity cores from this locality revealed moderate carbonate content, up to 55% in separate layers and repetitive succession of distinct lithologies, testifying to significant changes in biological productivity and terrigenous influx that occurred in this area during the latest Cenozoic.

Neogene high-resolution biostratigraphy, paleoceanography, and paleoclimatology were the main goals for drilling at Site 887. A presumably continuous sequence of uppermost Oligocene through Quaternary pelagic sediments will provide for the first time in the eastern subarctic Pacific Ocean detailed diatom and radiolarian zonations, which will then be compared to western subarctic and subtropical Pacific Ocean zonations. The diatom distribution record will also add information about the middle Miocene "silica shift" (Barron and Baldauf, 1990). At the same time, drilling at Site 887 also provided us with the opportunity for obtaining a reliable Neogene-Quaternary paleomagnetic reversal stratigraphy in this region to obtain good age control of biostratigraphic and paleoceanographic events.

Location of the site on the Patton-Murray Seamounts platform, well-elevated above the abyssal plain, precludes turbidite sedimentation and ensures recovery of pelagic sediments with both calcareous benthic and planktonic foraminifers suitable for stable isotope analysis. This can provide a record of successive changes in oceanographic parameters, both surface and deep-water circulation and biological productivity during the entire Neogene that may have been controlled by global changes in deep-water circulation during the Miocene (Woodruff and Savin, 1989). Data from Site 887 in the center of the Alaskan gyre might make it possible to distinguish large-scale oceanographic changes in the subarctic Pacific Ocean from those caused by local or regional events. Watermass evolution in the North Pacific throughout the latest Quaternary (based on the benthic and planktonic stable isotope record) was also a first priority for this site (Keigwin, 1987; Zahn et al., 1991).

Ice-rafted material of Alaskan origin (expected in the upper portion of the sequence) may provide evidence for the onset and evolution of continental glaciation in western North America; this, along with data obtained in other Leg 145 sites and during DSDP Leg 86 (Heath, Burckle, et al., 1985), should help us to understand the history of Northern Hemisphere glaciation during the latest Cenozoic.

Previous studies showed that the Aleutian Arc and Alaska Peninsula were volcanically active throughout the Cenozoic and that composition of extruded material has been changing through time (Scheidegger and Kulm, 1975; Scholl et al., 1976). Volcanic ashes, which are likely

in Site 887 sediments, will help us to trace the changes in intensity and composition of Aleutian Arc volcanism and will permit comparison with Northwest Pacific Ocean ashes to define the scenario of late Cenozoic volcanism for the entire North Pacific Ocean.

Basalts recovered from Site 887 should provide information about the chemistry, age, nature, and paleolatitude for the formation of the basement of the Patton-Murray Seamounts platform.

On the whole, information obtained from Site 887 should add an important (key) piece for the puzzle called North Pacific paleoceanography.

To achieve these objectives, we planned to double-core the sedimentary section with APC/XCB tools, then to change to the rotary bit for basement drilling. The standard suite of logs was to be collected.

OPERATIONS

Transit to Proposed Site PM-1A

At 0930 hr (local time), 9 September, near the end of the 955-nmi transit to proposed Site PM-1A, our seismic gear was deployed and a 34-nmi site survey was conducted at an average speed of 5.7 kt. A beacon was deployed at the proposed location at 1130 hr, and the survey continued past the site. At 1500 hr, the survey ended, the gear was retrieved, and the vessel came about to return to the location. Shortly after the beacon signal was acquired at 1530 hr, the hydrophones and thrusters were lowered and the ship was on location.

Hole 887A

The first piston core was spudded at 2145 hr, 9 September, and 6.65 m of sediment was recovered to establish the mud line at 3642.8 mbrf (see Table 1 for a summary of coring operations). Piston-coring advanced to 130.2 mbsf (Core 145-887A-14H), where an overpull of 130,000 lb required a switch to XCB-coring. Coring continued with the XCB system from 130.2 to 193.4 mbsf (Core 145-887A-26X), where the formation began to soften again. Piston-coring was resumed and continued until 269.7 mbsf (Core 145-887A-29H), where the final switch to the XCB was done in anticipation of basement contact. The last two cores advanced 16.3 m in unstable hole conditions (gravel). With total depth designated as 286 mbsf, the pipe was pulled out of the hole to the surface, and the vessel was offset 20 m east. At this hole, piston-coring penetrated 196.7 m and 190.51 m was retrieved (96.9% recovery). XCB-coring penetrated 89.30 m and 49.38 m was recovered (55.3% recovery).

Hole 887B

Our objective at this hole was to provide five cores for analyzing high-resolution sediments and pore-water chemistry. The APC did not completely stroke out during the first two attempts at retrieving mud-line cores, and only a handful of gravel was recovered. We also noted that the core-catcher flapper was missing on each of the two barrels. To determine whether the core barrel was being prevented from a complete stroke by an internal obstruction or by the formation, the pipe was picked up and an intentional water core was attempted. The absence of proper bleed-off suggested that the barrel did not stroke out completely in the water column; however, when the core barrel was retrieved with the shear pins severed, it was clear that whatever obstruction was being encountered was in the BHA.

We reluctantly pulled the bit out of the hole, and it was on deck at 1600 hr, 11 September. The bit and lockable float valve were replaced, and the APC system was tested twice just below the sea's surface. After these two successful tests, the pipe was run to the seafloor, where Hole 887B was spudded at 0100 hr on 12 September. The first core contained 2.05 m of sediment to establish the mud-line depth at 3647.5 mbsf. After obtaining five cores, which penetrated 40 m (103.5% recovery), we pulled the pipe out of the hole and cleared the mud line at 0515 hr. The vessel was offset 20 m north, and the last piston-cored hole of Leg 145 was initiated.

Table 1. Coring summary for Site 887.

Core no.	Date (Sept. 1992)	Time (UTC)	Depth (mbsf)	Length cored (m)	Length recovered (m)	Recovery (%)
Hole 887A						
1H	10	0700	0.0-6.7	6.7	6.65	99.2
2H	10	0800	6.7-16.2	9.5	9.72	102.0
3H	10	0835	16.2-25.7	9.5	10.02	105.5
4H	10	0925	25.7-35.2	9.5	9.78	103.0
5H	10	1015	35.2-44.7	9.5	10.01	105.3
6H	10	1100	44.7-54.2	9.5	10.07	106.0
7H	10	1145	54.2-63.7	9.5	9.96	105.0
8H	10	1235	63.7-73.2	9.5	9.92	104.0
9H	10	1315	73.2-82.7	9.5	8.15	85.8
10H	10	1405	82.7-92.2	9.5	9.90	105.0
11H	10	1505	92.2-101.7	9.5	10.08	106.1
12H	10	1610	101.7-111.2	9.5	9.99	105.0
13H	10	1715	111.2-120.7	9.5	10.06	105.9
14H	10	1825	120.7-130.2	9.5	9.77	103.0
15X	10	1915	130.2-139.7	9.5	8.27	87.0
16X	10	1955	139.7-145.1	5.4	4.67	86.5
17X	10	2030	145.1-154.8	9.7	7.42	76.5
18X	10	2115	154.8-164.4	9.6	8.89	92.6
19X	10	2200	164.4-174.1	9.7	0.00	0.0
20X	10	2245	174.1-183.7	9.6	9.25	96.3
21X	10	2330	183.7-193.4	9.7	3.43	35.3
22H	11	0030	193.4-202.9	9.5	8.68	91.3
23H	11	0115	202.9-212.4	9.5	9.95	105.0
24H	11	0150	212.4-221.9	9.5	8.83	92.9
25H	11	0240	221.9-231.4	9.5	10.00	105.2
26X	11	0610	231.4-241.2	9.8	0.00	0.0
27H	11	0700	241.2-250.7	9.5	5.20	54.7
28H	11	0830	250.7-260.2	9.5	9.16	96.4
29H	11	0945	260.2-269.7	9.5	4.56	48.0
30X	11	1205	269.7-279.4	9.7	7.45	76.8
31X	11	1350	279.4-286.0	6.6	0.00	0.0
Coring totals				286.0	239.84	83.9
Hole 887B						
1H	12	1100	0.0-2.0	2.0	2.05	102.0
2H	12	1145	2.0-11.5	9.5	9.88	104.0
3H	12	1230	11.5-21.0	9.5	9.92	104.0
4H	12	1310	21.0-30.5	9.5	9.58	101.0
5H	12	1350	30.5-40.0	9.5	9.95	105.0
Coring totals				40.0	41.38	103.4
Hole 887C						
1H	12	1500	0.0-4.3	4.3	4.32	100.0
2H	12	1555	4.3-13.8	9.5	9.86	104.0
3H	12	1640	13.8-23.3	9.5	0.05	0.5
4H	12	1725	23.3-32.8	9.5	9.31	98.0
5H	12	1805	32.8-42.3	9.5	10.02	105.5
6H	12	1845	42.3-51.8	9.5	9.99	105.0
7H	12	1930	51.8-61.3	9.5	10.06	105.9
8H	12	2015	61.3-64.8	3.5	3.58	102.0
9H	12	2100	64.8-74.3	9.5	9.47	99.7
10H	12	2155	74.3-83.8	9.5	10.00	105.2
11H	12	2245	83.8-93.3	9.5	10.01	105.3
12H	12	2340	93.3-102.8	9.5	9.86	104.0
13H	13	0030	102.8-112.3	9.5	10.01	105.3
14H	13	0115	112.3-121.8	9.5	9.93	104.0
15H	13	0200	121.8-131.3	9.5	9.84	103.0
16H	13	0320	131.3-140.8	9.5	9.32	98.1
17H	13	0425	140.8-150.3	9.5	10.09	106.2
18H	13	0550	150.3-159.8	9.5	7.86	82.7
19H	13	0655	159.8-169.3	9.5	9.32	98.1
20H	13	0830	169.3-178.8	9.5	9.63	101.0
21H	13	1005	178.8-188.3	9.5	9.78	103.0
22H	13	1110	188.3-197.8	9.5	9.57	101.0
23H	13	1200	197.8-207.3	9.5	10.00	105.2
24H	13	1310	207.3-216.8	9.5	9.34	98.3
25H	13	1415	216.8-226.3	9.5	9.95	105.0
26H	13	1515	226.3-235.8	9.5	9.53	100.0
27H	13	1600	235.8-245.3	9.5	9.92	104.0
28H	13	1700	245.3-254.8	9.5	9.63	101.0
29H	13	1830	254.8-264.3	9.5	9.39	98.8
30H	13	1945	264.3-273.8	9.5	9.80	103.0
Coring totals				273.8	269.44	98.4
Hole 887D						
			Washed/drilled from 0-257.4 mbsf			
1R	14	1220	257.4-267.4	10.0	0.00	0.0
2R	14	1300	267.4-277.1	9.7	0.00	0.0
3R	14	1340	277.1-286.7	9.6	0.91	9.5
4R	14	1530	286.7-291.9	5.2	4.30	82.7
5R	14	1730	291.9-296.4	4.5	1.35	30.0
6R	14	1910	296.4-305.8	9.4	1.10	11.7
7R	14	2220	305.8-315.3	9.5	5.21	54.8
8R	15	0200	315.3-324.7	9.4	3.32	35.3
9R	15	0330	324.7-334.5	9.8	0.22	2.2
10R	15	0510	334.5-344.2	9.7	2.45	25.2
11R	15	0650	344.2-353.8	9.6	0.20	2.1
12R	15	0850	353.8-363.4	9.6	0.52	5.4
13R	15	1105	363.4-373.1	9.7	0.34	3.5
Coring totals				115.7	19.92	17.2

Hole 887C

The first core was taken at 0600 hr, and 4.32 m of sediment was recovered to establish the mud-line depth at 3645.2 mbrf. In an attempt to improve recovery over the results of the APC/XCB-coring of Hole 887A (83.9%), this hole was piston-cored to total depth, while being washed over whenever the overpull exceeded 130,000 lb. The total cored interval was 273.8 m, with 269.44 m recovered (98.4% recovery). Cores 145-887C-4H through -16H were oriented. To achieve this enhanced recovery, 10 core barrels had to be extracted by washing over. When drilling stopped at this hole, the pipe was pulled out of the hole, and the bit and BHA changed to an RCB-coring configuration.

Hole 887D

The final hole of Leg 145 was an RCB excursion into basement. This hole was spudded at 2200 hr on 13 September and washed down to 257.4 mbsf, where rotary-coring was initiated just above basement. Drilling of the first three cores advanced effortlessly through the soft sediment overlying basement, with a total recovery of only 0.91 m. Contact with the basement occurred at approximately 295 mbsf (Core 145-887D-4R), where the rate of penetration slowed to 5.2 m/hr. Rotary-coring advanced into alternating layers of sediment(?) and unstable basalt for the next 78 m. The rate of penetration increased markedly with the last five cores to an average of 15.4 m/hr. Finally, at 373.1 mbsf (Core 145-887D-13R), drilling was terminated because of deteriorating hole conditions.

Logging (Hole 887D)

After an extensive wiper trip and flushing of the hole, the pipe was pulled to a logging depth of 78.8 mbsf. The logging program began at 1100 hr, 15 September, when the Schlumberger equipment was rigged up (see Table 2 for a summary of logging operations). The logging program for this hole was to include the standard three suites (Quad combo, FMS, geochemical) plus the French susceptibility tool (SUMT). Unfortunately, only the Quad combo and FMS tools were run, as the FMS tool became stuck in the pipe, necessitating a pipe trip out of the hole. The logging runs were as follows:

Log No. 1:(NGT/HLDT/SDT/DITE). On the first pass, the tool string was lowered to 347.8 mbsf (within 25.3 m of total depth) and the bottom 150 m of the hole was logged. On the repeat pass, the hole was logged from 347.8 mbsf to the mud-line. The tool was out of the hole at 1830 hr, 15 September.

Log No. 2:(FMS/GPIT/NGT). The first five passes concentrated on logging the bottom 100 m of the hole from 242.8 to 342.8 mbsf; the sixth pass logged from the bottom of the hole up to the base of the pipe.

At the end of the FMS logging run, the logging cable had to be worked rigorously to fix the FMS tool into the pipe. After we had succeeded in moving FMS 170 m up the pipe, it became permanently stuck. To retrieve the tool, we had to pull the pipe out of the hole; logging was then terminated. Once the tool was on deck, the drilling assembly was secured for transit, and the vessel turned on a south-easterly heading toward Victoria.

LITHOSTRATIGRAPHY**Introduction**

Three sediment holes were drilled at Site 887 (Figs. 1 and 2): Hole 887A (0-286 mbsf, APC and XCB drilling), Hole 887B (0-40 mbsf, APC), and Hole 887C (0-273 mbsf, APC). Hole 887D was washed through sediment to 257.9 mbsf and then was rotary drilled into basement; 5 m of sediment were recovered.

Table 2. Summary of logging operations, Site 887.

Time (local)	Depth (mbsf)	Comments
15 September 1992		
0200		End coring operations, begin wiper trip.
1400	Surface	Make up Quad and Lamont temperature tools and run in hole.
1510	3770	Quad at base of pipe, down-going log at 3000 ft/hr.
1530	3969	CSU fails, continue down-going log.
1540	3993	At total depth, begin up-going Log 1 at 1500 ft/hr.
1550	3930	CSU fails again, end up-going Log 1, begin up-going Log 2.
1630	3772	WHC turned off.
1650	3640	At mud line, end up-going Log 2, pull out of hole.
1800	Surface	Test NGT and CNT-G calibrations.
1930	Surface	Make up FMS and run in hole.
2100	3988	At total depth, begin up-going Log 1 at 1000 ft/hr to 3983 mbrf.
2150	3988	Begin up-going Log 2 to 3939 mbrf.
2210	3988	Begin up-going Log 3 to 3945 mbrf.
2220	3988	Begin up-going Log 4 to 3900 mbrf.
2240	3988	Begin up-going Log 5 to 3905 mbrf.
2300	3988	Begin up-going Log 6 to base of pipe.
16 September 1992		
0100	3747	WHC turned off.
	3727	End up-going Log 6, difficulty entering pipe.
0200	3600	FMS tool string stuck in pipe.
0230	3600	Kinley crimper/cutter tool used to cut and crimp wireline. End of logging operations. Begin tripping drill pipe.

The sediments at Site 887 consist of terrigenous clay, ash, dropstones, and biogenic siliceous and calcareous oozes. Terrigenous materials range from homogeneous fine-grained clay to clay with silt-sized quartz, feldspars, opaque and accessory minerals, vitric ash, and dropstones. Vitric ash layers and dropstones are abundant in the top of the section (0–90 mbsf). Dropstones display a wide range of compositions, but are primarily fine-grained, black sedimentary rocks. The oldest occurrence of dropstones is at 130 mbsf (Hole 887A, 125 mbsf, Hole 887B, 135 mbsf); ashes are present throughout the entire length of the column. Biogenic sediments are dominated by diatom ooze. Calcareous oozes are important, but never major, components of some intervals. Minor amounts of radiolarian and spicule oozes are present.

The sediments have been divided into three units based on the lithology (Fig. 3). Unit I is composed of upper Pliocene–Pleistocene terrigenous and biogenic sediments, Unit II is composed of lower Miocene–upper Pliocene biogenic sediments, and Unit III is clay and iron oxides overlying basalt.

Description of Units

Unit I

Intervals: Cores 145-887A-1H to -10H
Cores 145-887B-1H to -5H
Cores 145-887C-1H to -11H
Depth: 0–90 mbsf
Age: Pleistocene-late Pliocene

Unit I is composed of siliceous silty clay mixed sediments with quartz and calcite, diatom ooze, and clay, together with minor amounts of calcareous ooze and spicule ooze. Bioturbation is ubiquitous, as indicated by burrows and mottles throughout Unit I. Subunit IA (0–45 mbsf) consists of mixed sediment interbedded with diatom ooze; Subunit IB (45–90 mbsf) is composed of relatively homogeneous clay interbedded with diatom ooze in the interval from 45 to 74 mbsf, and is primarily clay from 74 to 90 mbsf. The boundary between Subunits IA and IB is gradational over 10 m and extends from Cores 887A-6H to -7H in Hole 887A and from Cores 145-887C-6H to -7H in Hole 887C. This boundary represents a change in the texture of the terrigenous component, which changes from a mixed silty clay matrix to a homogeneous clay matrix; this texture change can be observed in the smear slide data and has been recorded in the core barrel sheets.

The sediments in Unit I reflect terrigenous sedimentation interbedded with discrete diatom-rich horizons. The clays are usually gray to dark gray (7.5GY 4/1), except in the top 5 m of the hole, when the silty clays have been oxidized to red (5R 4/1). Diatom oozes are yellow green (5Y 4/1) and calcareous-rich intervals are usually light gray (8.0Y 7/1). Vitric ash layers are abundant in Unit I (Fig. 4); the ashes range in color from black to light brown and in thickness from 1 to 50 cm. The lower contact of each ash layer is usually sharp, but some are bioturbated; the upper contacts are usually gradational. Dropstones, with the exception of a single occurrence in Subunit IIA, occur exclusively in lithologic Unit I (Fig. 4). These dropstones range in size from 5 mm to 7 cm in diameter. Dropstone lithology is commonly fine-grained, black, lithofeldspathic sandstones and siltstones, but a wide variety of lithologies can be observed, including arkose, quartzose graywacke, schist, metabasalt, pyroxene andesite, pyroxenite, potash granite, and acid porphyry clasts.

Subunit IA

Intervals: Cores 145-887A-1H to -6H
Cores 145-887B-1H to -5H (end of hole)
Cores 145-887C-1H to -6H
Depth: 0–45 mbsf
Age: Pleistocene

Subunit IA consists of 45 m of siliceous silty clay mixed sediment with quartz and calcite, (i.e., a mixture of clay with diatoms, silt-sized quartz, feldspar, calcite, opaque minerals, and accessory minerals) that grades into calcareous-rich intervals. Both the siliceous silty clay mixed sediment and the calcareous-rich intervals are interbedded with discrete units of diatom ooze. These diatom ooze layers have sharp lower boundaries and gradational upper boundaries, range from 1 to 125 cm thick, and occur at roughly a 1-m spacing. The diatom ooze layers sometimes exhibit millimeter-scale color variations, but smear slide analysis reveals no compositional differences across these color changes. Vitric ash layers and dropstones are abundant within Subunit IA (Fig. 4). The only primary structural feature seen in Unit I occurs in Subunit IA (Fig. 5); this feature is a vertical crack in Section 145-887C-4H-6. This crack is filled with foraminifer-bearing sand and may record fluid migration along a fracture in the indurated sediment.

Subunit IB

Interval: Cores 145-887A-6H to -10H
Cores 145-887C-6H to -11H
Depth: 45–90 mbsf
Age: Pleistocene to late Pliocene

Subunit IB consists of clay interbedded with discrete diatom ooze layers from 45 to 74 mbsf; uniform fine-grained clay present from 74 to 90 mbsf (Fig. 3). Calcareous ooze intervals occur intermittently within this subunit, and dropstones and vitric ash are common (Fig. 4). The layers of diatom ooze present from 45 to 74 mbsf have sharp lower and gradational upper contacts.

One layer of subangular clasts occurs in both Holes 887A (Core 145-887A-10H-3; Fig. 6) and 887C (Core 145-887C-11H-2) at 86 mbsf. It is not clear whether mass flow or iceberg dumping is responsible for this feature. Three layers of quartz sand, each 5 cm thick and possibly representing turbidites, are present in Core 145-887C-10H (74–84 mbsf).

Unit II

Intervals: Cores 145-887A-11H to -30X
Cores 145-887C-12H to -30H
Depth: 90–270 mbsf
Age: late Pliocene–early Miocene

Lithologic Unit II is primarily composed of diatom ooze with minor amounts of carbonate and radiolarian ooze. The boundary between

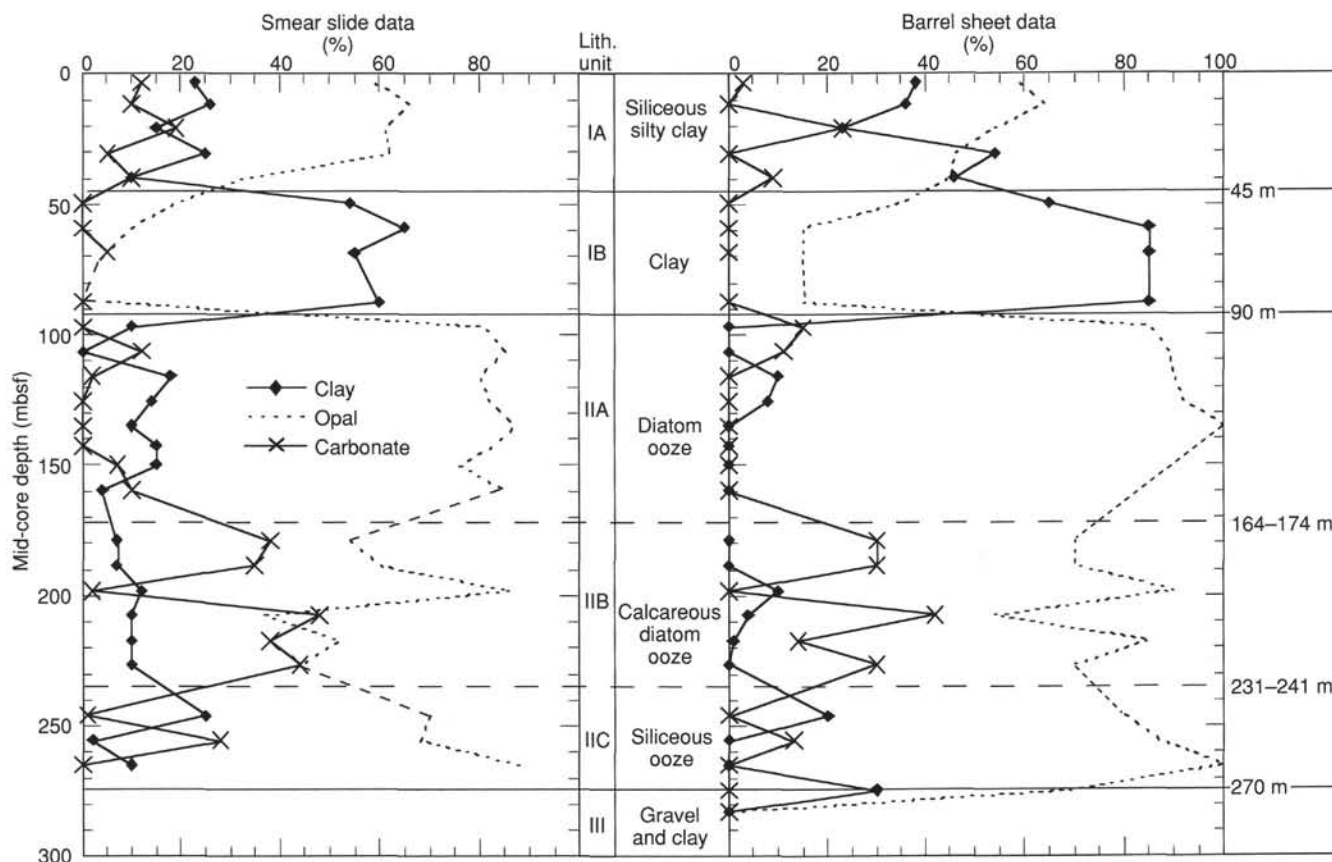


Figure 3. Summary of lithology, Hole 887A.

lithologic Units I and II at 90 mbsf is clearly defined by the smear-slide estimates of sediment composition (Fig. 3) as well as the abrupt loss of dropstones down the sediment column (Fig. 4). This lithologic boundary is also clearly defined by magnetic susceptibility and intensity records (see "Paleomagnetism" section, this chapter) and GRAPE and grain density records (see "Physical Properties" section, this chapter). The subunits of Unit II are defined by the occurrence of the minor calcareous and siliceous biogenic components. Subunit IIA consists of diatom ooze; Subunit IIB, diatom ooze with carbonate; and Subunit IIC, siliceous ooze, which is a mixture of poorly preserved diatoms and radiolarians. The contacts between these subunits are gradational and were defined on the basis of smear slide data. Isolated dropstone occurrences can be seen at 125 mbsf in Hole 887A and 135 mbsf in Hole 887C (Fig. 4).

The sediments in Unit II represent lower Miocene to upper Pliocene biogenic sedimentation. Few primary sedimentary structures are present in this unit. Thin, green clay layers within an otherwise homogeneous diatom ooze in Cores 145-887A-12H, -13H, -14H (110–125 mbsf), and Core 145-887C-13H (105–110 mbsf) may represent periods of nondeposition or erosional. The only examples of color lamination (green) also occur in Cores 145-887A-12H and -887C-13H (Fig. 7). No compositional difference is evident in this color lamination. Bioturbation can be observed throughout the sediment. Vitric ash layers are present in Subunits IIA and IIC, but are rare in Subunit IIB.

Subunit IIA

Intervals: Cores 145-887A-11H to -18X
Cores 145-887C-12H to -20H
Depth: 90–174 mbsf
Age: late Pliocene–late Miocene

Subunit IIA consists of homogeneous gray (5Y 4/1) to brown (2.5Y 4/2) diatom ooze with small amounts of clay and carbonate (<20% combined). The interval is slightly bioturbated throughout, as indicated by faint mottling and bioturbation at the bases of some ash layers (Fig. 8). Vitric ash layers are common in this subunit, but their importance generally decreases downhole (Fig. 4). One dropstone horizon occurs in Subunit IIA at 125 mbsf in Hole 887A and at 135 mbsf in Hole 887C.

Subunit IIB

Intervals: Cores 145-887A-20X to -25H
Cores 145-887C-20H through -26H
Depth: 174–235 mbsf
Age: late Miocene–middle Miocene

Subunit IIB consists of calcareous diatom ooze. The contact between Subunits IIA and IIB at 174 m is sharp and occurs in Core 145-887C-20H in Hole 887C. This contact was not recovered in Hole 887A. The location of the contact is also apparent in magnetic and physical properties records (see "Paleomagnetism" and "Physical Properties" sections, this chapter). The carbonate-rich intervals are light gray (6.7Y 6.4/1.0) in a dark gray (7.1Y 4.2/1.2) diatom ooze. The carbonate intervals display gradational upper contacts and bioturbated or sharp lower contacts with the diatom ooze. A few ash layers can be seen in this interval, especially near the bottom of the subunit (Fig. 4).

Subunit IIC

Intervals: Cores 145-887A-27H to -29H
Cores 145-887C-27H to -30H (end of hole)
Depth: 235–270 mbsf
Age: middle Miocene–early Miocene

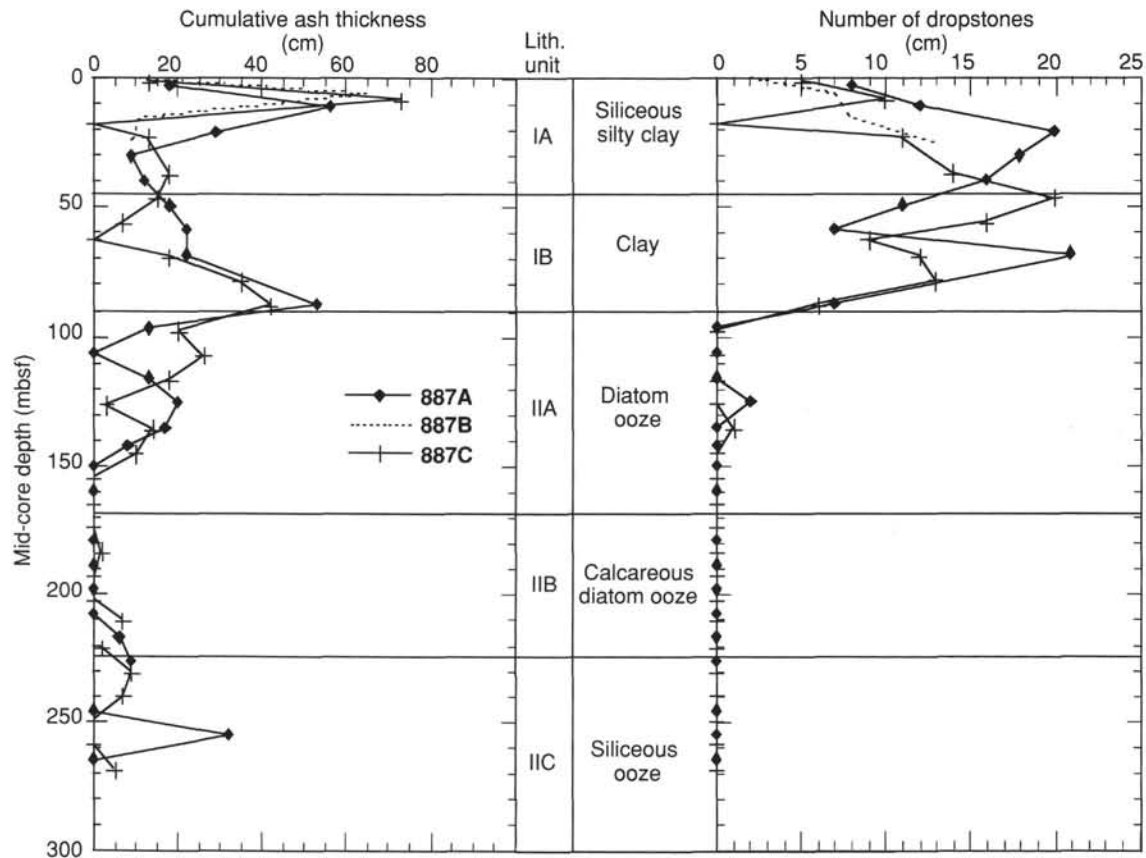


Figure 4. Cumulative ash thickness and number of dropstones, Site 887.

Subunit IIC consists of clayey siliceous ooze, primarily composed of poorly preserved diatoms and radiolarian skeletons approximately 80% of the sedimentary column together with smaller amounts of clay and carbonate approximately 20% of the sedimentary column. The contact between the overlying Subunit IIB calcareous diatom ooze and the Subunit IIC siliceous ooze is gradational over Core 27H in both Holes 887A and 887C. The lithologic change at the boundary between Subunit IIC and Unit III is manifested as a clear break at 270 mbsf in magnetic susceptibility and physical properties measurements (see "Paleomagnetism" and "Physical Properties" sections, this chapter). Within Subunit IIC, the siliceous oozes display gradational upper and lower contacts with the interbedded carbonates. The siliceous ooze is dark brown (8.1YR 3.6/2.1) and the carbonate layers are light gray (1.2Y 6.7/2.1). The sediments in Subunit IIC are heavily bioturbated, as indicated by burrows and mottles. *Zoophycos* tracks are common throughout the interval. Ash layers occur throughout the unit (Fig. 4).

Unit III

Intervals: Core 145-887A-30X
Cores 145-887D-3R to -4R
Depth: 270–289 mbsf
Age: early Miocene

Unit III contains dark brown (9.5YR 3.5/1.7) clay with ash and iron oxides, recovered just above basalt in Hole 887D, and gravel and clay in Hole 887A.

Unit IV

Intervals: Cores 145-887D-4R to -13R
Depth: 289–373 mbsf
Age: Oligocene

The basalts range from highly clinopyroxene-plagioclase phyric basalt in the upper portion to moderately plagioclase phyric basalt to sparsely plagioclase phyric basalt near the bottom of the hole (see "Igneous Petrology" section, this chapter).

Discussion

Site 887 sediments record the transition in the northeasternmost Pacific Ocean from Miocene pelagic sedimentation to Quaternary hemipelagic sedimentation. The major step in this transition occurs at the boundary between lithologic Units I and II, and correlates to the onset of Northern Hemisphere glaciation at 2.6 Ma.

The lower Miocene–upper Pliocene portion of the record (lithologic Unit II) documents the importance of biosiliceous deposition, dominated by diatoms, observed in the other North Pacific Ocean sites of Leg 145 (see "Lithostratigraphy" sections, this volume). Poor preservation of siliceous sediments in lithologic Subunit IIC may indicate reworking of the sediment. Subunit IIB, largely composed of diatom ooze, also contains a significant amount of calcareous sediments, which may indicate a deepening of the carbonate compensation depth (CCD) from middle to late Miocene time. Upper Miocene to upper Pliocene sediments in lithologic Subunit IIA are composed almost exclusively of diatom oozes, and sedimentation rates at Site 887 are highest during this period.

Evidence of volcanic activity increases above a middle Miocene low in Subunit IIB at 150 mbsf (~5 Ma), as indicated by the abundance of ash layers in lithologic Subunit IIA. The first evidence of ice rafting at Site 887 is the dropstone in the upper portion of Subunit IIA (~4.5 Ma). The presence of green clay layers at 110–120 mbsf (~3.5 Ma), in the top of the diatom ooze, may record the effects of bottom-water circulation.

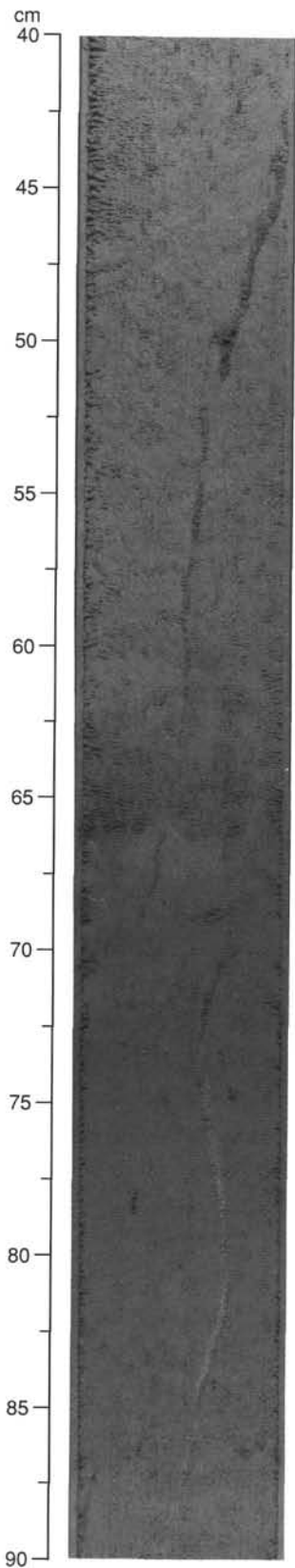


Figure 5. Vertical crack filled with sand (interval 145-887C-4H-6, 40–90 cm).

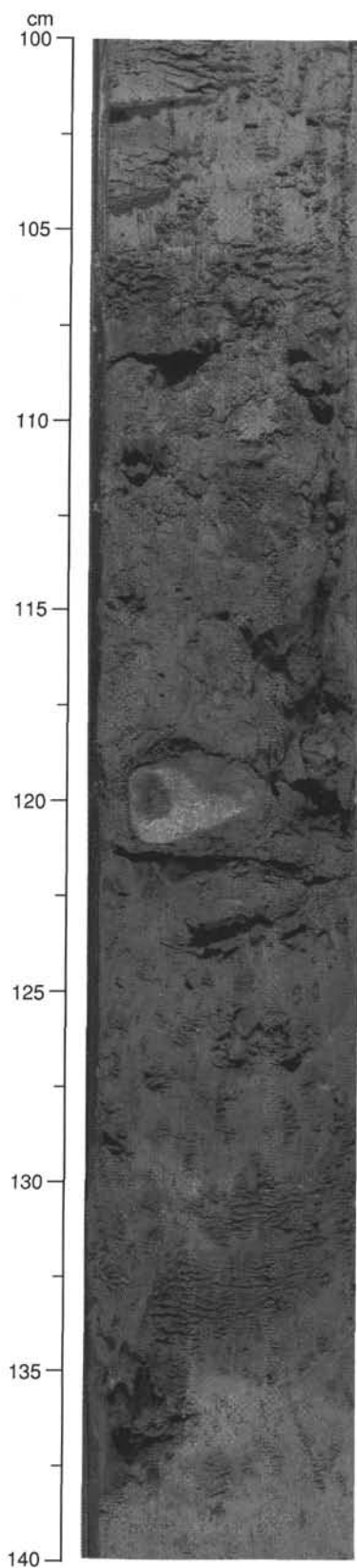


Figure 6. Subangular clast layer (interval 145-887A-10H-3, 100–140 cm).

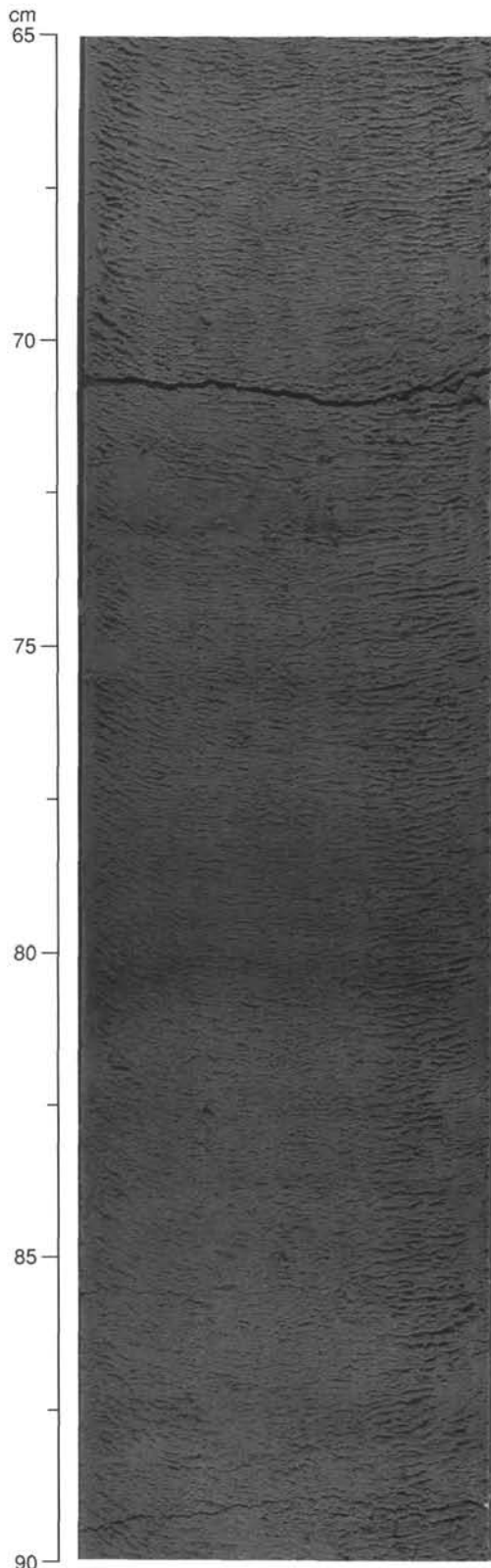


Figure 7. Color laminations (interval 145-887A-12H-6, 65–90 cm).

Hemipelagic sedimentation begins abruptly at 90 mbsf (2.6 Ma), the boundary between lithologic Units I and II. At that level, diatom ooze is replaced by relatively uniform clay, ash frequency and thickness increase dramatically, and dropstones appear continuously and in large numbers for the first time. These trends also were observed at all the other sites of Leg 145 (see “Lithostratigraphy” sections, this volume). The uniform clay gradually grades into a siliceous silty clay mixed sediment at 45 mbsf and coarsens upward to the top of Unit I. Preliminary X-ray diffraction data suggest that the relative abundances of illite and chlorite increase up the core, which is consistent with enhanced mechanical weathering as a result of glaciation. Discrete diatom layers occur from 0 to 74 mbsf and probably represent oceanic responses to short-term climate fluctuations from 1.7 Ma to the present.

IGNEOUS PETROLOGY

Hole 887D penetrated 83.7 m into basement (289.4–373.1 mbsf), and 16.35 m of basalt was recovered (20% recovery). In areas of good recovery, the basalts are massive flows or sills, while areas of poor recovery consist of angular basalt cobbles, often with black to reddish-brown glass margins. Whether these cobbles were originally pillows, flows, or sills is not known. Chalky sediments occur in chunks and also coat some of the basalt cobbles, suggesting that these basalts were interbedded with sediments, an observation confirmed by logging (see “Downhole Measurements” section, this chapter). Many of the cobbles have weathered and oxidized outer surfaces and may not have been parts of a coherent flow or pillow at the time of drilling.

The basalts were divided into five lithologic units, based upon the presence of chilled or glassy margins. The units range from highly clinopyroxene-plagioclase phyric basalt in the top unit to moderately plagioclase phyric basalt to sparsely plagioclase phyric basalt in the lowest unit. Plagioclase phenocrysts up to 11 mm in diameter were observed in Units 3 through 5. Clinopyroxene phenocryst size increases with depth to a maximum of 3 mm. Rare olivines were noted in a few places, but are completely altered to iddingsite. The groundmass in all of the units is moderately to highly altered to light brown to greenish-brown clays. Many of the glass margins are palagonitized on the outer surface, but otherwise appear to be fairly fresh.

Intact fractures are rare and have been filled in with calcite. The outer surfaces of some of the angular cobbles are covered with calcite (and occasionally pyrite) and are probably fracture surfaces. Vesicles usually make up less than 10% of the rock and are lined with calcite, pyrite, and iron oxides.

BIOSTRATIGRAPHY

At Site 887, about 285 m of lower Miocene to Quaternary sediments overlie a basalt encountered in Core 145-887D-4R. Below this interval, a thin layer of sediment is found between basalt flows in Sample 145-887D-6R-1, 10–15 cm, which contains calcareous nanofossils indicative of an undifferentiated Oligocene age. Calcareous microfossils (foraminifers and calcareous nanofossils) range from barren to abundant and are moderately well preserved to poorly preserved. The low diversity of the calcareous microfossil assemblages prevents the assignment of biostratigraphic zones to the samples. By contrast, siliceous microfossils (diatoms, radiolarians, and silicoflagellates) are more common in the sediments from Site 887 and typically are well to moderately well preserved; however, persistent reworking of middle Miocene diatoms and radiolarians is present in the uppermost Miocene and Pliocene section. Most of the Miocene to Quaternary section can be zoned using diatoms, but only the upper part of the Site 887 section can be assigned to radiolarian zones (Table 3). Numerous early Miocene to Quaternary diatom and radiolarian datum levels can be identified in the Site 887 sequence (Table 3), and the inferred ages agree well with those suggested by magnetostratigraphy (see “Paleomagnetism” section, this chapter).

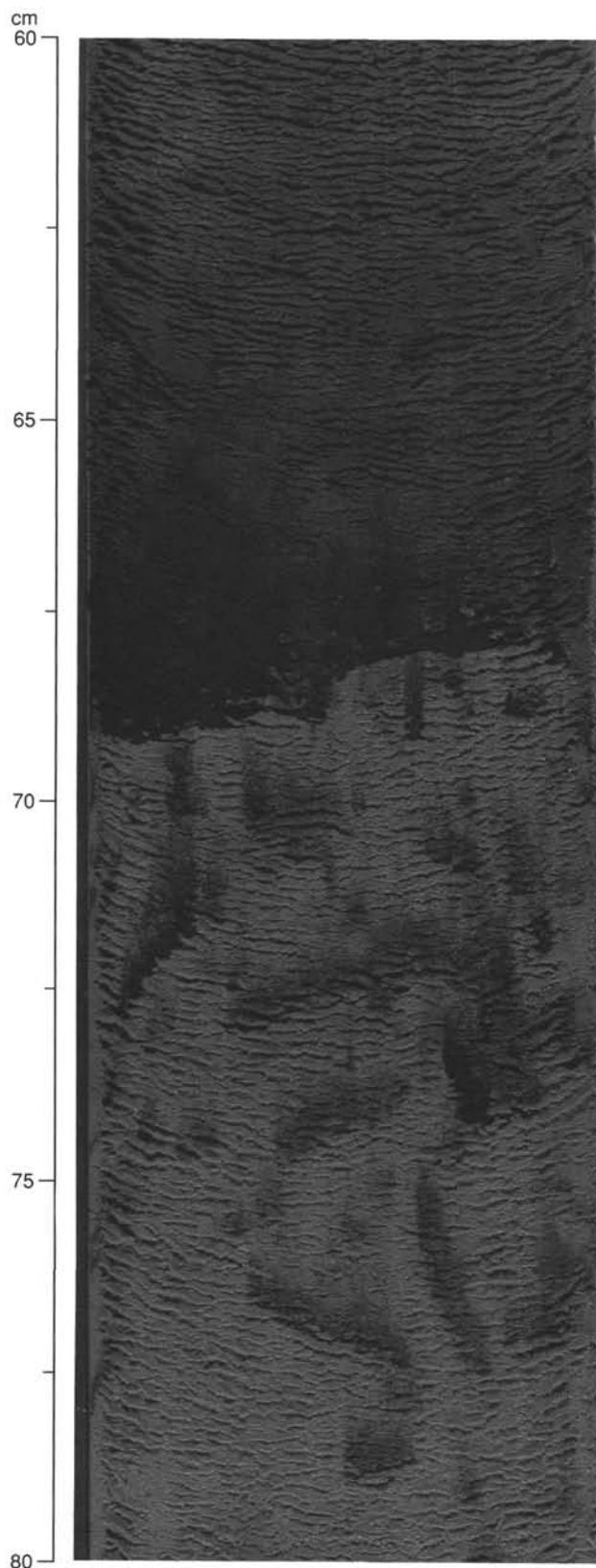


Figure 8. Bioturbated ash layer (interval 145-887A-14H-3, 60–80 cm).

The absence of the *Crucidentacula nicobarica* Zone of diatoms (12.8–13.3 Ma) between Samples 145-887A-27H-3, 20 cm (244.4 mbsf) and -27H-3, 124 cm (245.44 mbsf) is inferred as resulting from a hiatus.

Foraminifers

All core-catcher samples from Holes 887A and 887C were processed and examined for foraminifers. Foraminiferal abundances range from barren to common and generally are most abundant in the Miocene and upper Pliocene sections. Planktonic foraminifers are rare and moderately to poorly preserved, with evidence of dissolution becoming more prevalent in the Pleistocene section. Pleistocene assemblages are dominated by *Globigerina bulloides* and *Neoglobobulimina pachyderma* (sinistral). Pliocene assemblages consist of *G. bulloides* and *Orbulina universa*, as well as rare occurrences of *G. venezuelana* and *G. scitula*. Most of the Miocene section is barren of planktonic foraminifers, with the exception of one late Miocene sample (Sample 145-887C-20H-CC) and one early Miocene sample (Sample 145-887C-30H-CC).

Benthic Foraminifers

Samples from Sections 145-887A-1H-CC to -10H-CC and 145-887C-1H-CC to -10H-CC are barren, or nearly barren, of benthic foraminifers. Samples of late Pliocene age (Samples 145-887A-10H-CC and -11H-CC, 145-887C-11H-CC to -13H-CC) contain a moderately well-preserved assemblage of *Cibicides bradyi*, *Cibicides mundulus*, *Cibicides robertsonianus*, *Epistominella exigua*, *Laticarinina pauperata*, *Nuttallides umbonifera*, *Oridorsalis* sp., *Planulina rugosa*, *Pullenia* spp., *Uvigerina senticosa*, and *Uvigerina proboscidea*. Samples 145-887A-13H-CC to -18X-CC, and 145-887C-14H-CC to -19H-CC are barren of all calcareous foraminiferal taxa. These samples contain rare occurrences of the agglutinated taxa *Cyclammina cancellata*, *Eggerella bradyi*, and *Martinottiella* sp.

Benthic foraminifers are present in all Miocene age samples (Samples 145-887A-20X-CC to -30X-CC, Samples 145-887C-20H-CC to -30H-CC), with the exception of Samples 145-887A-18H-CC, -887C-18H-CC, -19H-CC, -22H-CC, -24H-CC, and -26H-CC. Common taxa include *Anomalinoidea globulosus*, *Anomalinoidea semicribriatus*, *Cibicides havanensis*, *Cibicides mundulus*, *Epistominella exigua*, *Globocassidulina subglobosa*, *Laticarinina pauperata*, *Melonis barleeianum*, *Nuttallides umbonifera*, *Oridorsalis* spp., and *Pullenia bulloides*. Additional taxa include *Cibicides bradyi*, *Eggerella bradyi*, *Fissurina* sp., *Martinottiella* sp., *Pleurostomella* spp., and *Sphaeroidina bulloides*.

Two samples were processed from Hole 887D (145-887D-3R-CC and 145-887D-6R-1, 10–15 cm). These contain common, moderately well-preserved benthic foraminifers, including *Cibicides havanensis*, *Cibicides mundulus*, *Cibicides robertsonianus*, *Globocassidulina subglobosa*, *Nuttallides umbonifera*, *Oridorsalis* sp., and *Stilostomella* spp. In addition, Sample 145-887D-6R-1, 10–15 cm, contains single specimens of *Cibicides laurissae* and *Cibicides* sp. 13, which suggest a late Oligocene age.

Paleoenvironment

The benthic foraminiferal faunas of Site 887 indicate lower-bathyal to abyssal paleodepths (>1000 mbsf) throughout the section recovered (based on van Morkhoven et al., 1986).

Calcareous Nannofossils

Calcareous nannofossil assemblages were examined from all the core-catcher samples obtained from Site 887. Significant fluctuations in abundances of calcareous nannofossils are observed in the sediments. The samples in the upper part of the section (Samples 145-887A-1H-CC to 145-887A-18X-CC and 145-887C-1H-CC to 145-

Table 3. Age and stratigraphic position of radiolarian (R) and diatom (D) datum levels in Holes 887A and 887C.

Sample no.	Datum	Age (Ma) CK92	Hole 887A		Hole 887C	
			Interval	Depth (mbsf)	Interval	Depth (mbsf)
R1	LO <i>Lychnocanoma grande</i>	0.05	/1H-CC	/6.7	/1H-CC	/4.3
D2	LO <i>Simonseniella curvirostris</i>	0.3	2H-CC/3H-CC	16.2/25.7	2H-CC/3H-CC	13.8/23.3
R2	LO <i>Druppatractus acquilontius</i>	0.35	2H-CC/3H-CC	16.2/25.7	2H-CC/3H-CC	13.8/23.3
R3	LO <i>Stylatractus universus</i>	0.45	3H-CC/4H-CC	25.7/35.2	3H-CC/4H-CC	23.3/32.8
D5	LCO <i>Actinocyclus oculatus</i>	1.00	6H-CC/7H-CC	54.2/63.7	6H-CC/7H-CC	51.8/61.3
R5	LO <i>Eucyrtidium matuyamai</i>	1.05	8H-CC/9H-CC	73.2/82.7	8H-CC/9H-CC	64.8/74.3
D6	FO <i>Simonseniella curvirostris</i>	1.58	7H-CC/8H-CC	63.7/73.2	9H-CC/10H-CC	74.3/83.8
R7	FO <i>Eucyrtidium matuyamai</i>	1.9	9H-CC/10H-CC	82.7/92.2	9H-CC/10H-CC	74.3/83.8
D9	LO <i>Neodenticula koizumii</i>	2.0	8H-CC/9H-CC	73.2/82.7	9H-CC/10H-CC	74.3/83.8
D12	LCO <i>Neodenticula kamschatica</i>	2.63-2.7	9H-CC/10H-CC	82.7/92.2	10H-CC/11H-CC	83.8/93.3
D13	FO <i>Neodenticula seminae</i>	2.7	9H-CC/10H-CC	82.7/92.2	10H-CC/11H-CC	83.8/93.3
R8	FO <i>Cycladophora davisiana</i>	2.8	9H-CC/10H-CC	82.7/92.2	10H-CC/11H-CC	83.8/93.3
R9	LO <i>Stichocorys peregrina</i>	2.9	13H-CC/14H-CC	112.3/121.8		
D14	LO <i>Thalassiosira marujamica</i>	3.2	11H-CC/12H-CC	101.7/111.2	11H-CC/12H-CC	93.3/103.8
N15	LO <i>Reticulofenestra pseudoumbilica</i>	3.71	11H-CC/12H-CC	93.3/103.8		
D17	FO <i>Neodenticula koizumii</i>	3.75	12H-CC/13H-CC	111.2/120.7	13H-CC/14H-CC	112.3/121.8
R11	LO <i>Theocorys redondoensis</i>		16H-CC/17X-CC	145.1/154.8	14H-CC/15H-CC	121.8/131.3
R12	FO <i>Lamprocyrtis heteroporos</i>	4.6	14H-CC/15X-CC	130.2/139.7	15H-CC/16H-CC	131.3/140.8
D19	FO <i>Thalassiosira latimarginata</i>	5.05	16X-CC/17X-CC	145.1/154.8	17H-CC/18H-CC	150.3/159.8
D21	FO <i>Thalassiosira oestrupii</i>	5.4	17X-CC/18X-CC	154.8/164.4	17H-CC/18H-CC	150.3/159.8
D23	LO <i>Thalassiosira miocenica</i>	5.7	18X-CC/20X-CC	164.4/183.7	19H-CC/20H-CC	169.3/178.8
D24B	FO <i>Thalassiosira miocenica</i>	6.3	20X-CC/21X-CC	183.7/193.4	20H-CC/21H-CC	178.8/188.3
R	FO <i>Druppatractus acquilontius</i>	6.75	20X-CC/21X-CC	183.7/193.4	21H-CC/22H-CC	188.3/197.8
R	FO <i>Stichocorys peregrina</i>	6.75	20X-CC/21X-CC	183.7/193.4	22H-CC/23H-CC	197.8/207.3
D25	FO <i>Neodenticula kamschatica</i>	7.25	21X-CC/22H-CC	193.4/202.9	22H-CC/23H-CC	197.8/207.3
D26	LCO <i>Thalassionema schraderi</i>	7.45	21X-CC/22H-CC	193.4/202.9	22H-CC/23H-CC	197.8/207.3
D30	LCO <i>Denticulopsis hustedtii</i>	8.4	22H-CC/23H-CC	202.9/212.4	23H-CC/24H-CC	207.3/216.8
R	LO <i>Lychnocanoma nipponica magnacornuta</i>	8.5	23H-CC/24H-CC	212.4/221.9	23H-CC/24H-CC	207.3/216.8
D32	LO <i>Denticulopsis dimorpha</i>	9.0	23H-CC/24H-CC	212.4/221.9	23H-CC/24H-CC	207.3/216.8
D33	FO <i>Denticulopsis katayamae</i>	9.3	24H-CC/25H-1,133	221.9/223.23		
D32A	FO <i>Thalassionema schraderi</i>		24H-CC/25H-CC	216.8/223.3		
D34	FO <i>Denticulopsis dimorpha</i>	9.8	25-3,133/25H-4,133	226.23/227.73	24H-CC/25H-CC	216.8/223.3
D36	LCO <i>Denticulopsis praedimorpha</i>	10.8	25H-CC/27H-1,60	231.4/241.26	25H-CC/26H-CC	223.3/235.8
D38	FO <i>Simonseniella barboi</i>	11.5	25H-CC/27H-CC	231.4/250.7	25H-CC/26H-CC	223.3/235.8
R	LO <i>Cyrtocapsella tetrapera</i>	12.1	25H-CC/27H-CC	231.4/250.7	26H-CC/27H-CC	235.8/245.3
R	FO <i>Lychnocanoma nipponica magnacornuta</i>	12.15	25H-CC/27H-CC	231.4/250.7	26H-CC/27H-CC	235.8/245.3
R	LO <i>Eucyrtidium inflatum</i>	12.2	25H-CC/27H-CC	231.4/250.7	26H-CC/27H-CC	235.8/245.3
D41	LO <i>Crucidentacula nicobarica</i>	12.4	27-1,60/27H-2,20	251.3/252.4		
D42	FO <i>Denticulopsis praedimorpha</i>	12.8	27-3,20/27H-3,124	244.4/245.44	26H-CC/27H-CC	235.8/245.3
D44	FCO <i>Denticulopsis hustedtii</i>	13.3	27-3,20/27H-3,124	244.4/245.44	26H-CC/27H-CC	235.8/245.3
D46	FO <i>Denticulopsis hustedtii</i>	14.2	27H-CC/28H-CC	250.7/260.2	27H-CC/28H-CC	245.3/254.8
R	FO <i>Eucyrtidium inflatum</i>	14.8	28H-CC/29H-CC	260.2/269.7	28H-CC/29H-CC	254.8/264.3
D49	FO <i>Denticulopsis hyalina</i>	14.9	28H-CC/29H-CC	260.2/269.7	27H-CC/28H-CC	245.3/254.8
D50	FO <i>Actinocyclus ingens nodus</i>	15.1	28H-CC/29H-CC	260.2/269.7	28H-CC/29H-CC	254.8/264.3
D52	FO <i>Denticulopsis lauta</i>	15.9	30X-5,90/30X-CC	270/279		
D53	FO <i>Denticulopsis praelauta</i>	16.2	Not seen		Not seen	
D54	FO <i>Crucidentacula sawamurae</i> ^a	18.4	>30X-CC		30H-6,21/30H-7,21	272.0/273.7
D55	FO <i>Actinocyclus ingens</i> ^a	18.4	>30X-CC	>279.4	30H-6,21/30H-7,21	272.0/273.7
D57	FO <i>Thalassiosira fraga</i>	20.1			<30H-CC	<273.8

^aNew paleomagnetic calibration this site.

Notes: Samples constraining each datum level are separated by a slash (/), as are the sub-bottom depths (mbsf) of these samples. LO = last occurrence; LCO = last common occurrence; FO = first occurrence; FCO = first common occurrence. CK92 refers to the Cande and Kent (1992) geomagnetic polarity time scale.

887C-19H-CC) are generally barren or contain low abundances of calcareous nannofossil assemblages. In the lower part of the section (from Samples 145-887A-20X-CC, -887C-20H-CC, and -887D-3R-CC), abundances are higher. When present, the calcareous nannofossils are poorly to moderately well preserved.

Diversity of nannofossils is extremely reduced. The assemblages consist of *Coccolithus pelagicus* and *Reticulofenestra minutula*, *R. pseudoumbilica*, *R. perplexa*, *Cyclicargolithus floridanus*, *Calcidiscus leptoporus* (Sample 145-887C-20H-CC), and *Discoaster deflandrei* (Samples 145-887A-30X-CC, 145-887C-29H-CC, 145-887C-30H-CC, and 145-887D-3R-CC). This reduced diversity prevents the use of calcareous nannofossils for biostratigraphy. Although, the LO of *Reticulofenestra pseudoumbilica* in Sample 145-887C-12H-CC indicates that the lower/upper Pliocene contact lies within this core.

In Hole 887D, the basalts were reached in Section 145-887D-4R-2, 120 cm. Three samples were examined in this core above this level: 145-887D-4R-1, 137-138 cm, -4R-2, 95-96 cm, and -4R-2, 115 cm. The former sample contains only rare and badly preserved *R. pseudo-*

umbilica, the last two are barren. The presence of *D. deflandrei* in Sample 145-887D-3R-CC and that of *R. pseudoumbilica* suggest that the sediments overlying the basalts are early Miocene in age. In Core 145-887D-6R, a thin layer of sediment was recovered from within the basalts. From this interval, Sample 145-887D-6R-1, 10-15 cm, contains an abundant and well-preserved calcareous nannofossil assemblage, dominated by *R. bisecta*, which suggests an Oligocene age for this level. Because of the absence of Oligocene sediments above this level, this layer cannot be attributed to downhole transport.

Radiolarians

Radiolarians examined in sediments from core-catcher samples at Site 887 range in age from Oligocene(?)/Miocene through Quaternary. The highest concentrations (common to abundant) of radiolarians are recorded in upper Pleistocene and lower through middle Miocene sequences. Most middle-upper Miocene through lower Pliocene (~8.5-3.5 Ma) samples contain various amounts of reworked middle

Miocene(?) radiolarians, with the percentage of reworked specimens in some samples exceeding 30%. Preservation of radiolarians varies between moderately well and well preserved, except for an upper Miocene through lower Pliocene interval within which nearly half of the samples contain a poorly preserved siliceous faunal assemblage.

The moderately well- to well-preserved radiolarians in sediments from samples taken from the first three cores in all three holes at Site 887 (Samples 145-887A-1H-CC through -3H-CC, 145-887B-1H-CC through -3H-CC, -887C-1H-CC through -3H-CC) are characteristic of the late Quaternary *Botryostrobus aquilonaris* Zone (Hays, 1970). Radiolarians range from rare to abundant in these samples. *Lychnocanium grande* is present in the uppermost core-catcher samples from Holes 887A and 887C (Samples 145-887A-1H-CC and -887C-1H-CC), but not in Sample 145-887B-1H-CC from Hole 887B, indicating that the sediments from the uppermost 2.0 m of this core are younger than 0.05 Ma. The faunal assemblage in the bottom of Core 3 from all three holes (Samples 145-887A-3H-CC, 145-887B-3H-CC and 145-887C-3H-CC) contains *Drupptractus aquilonius*, but lacks *Stylatractus universus*, which places a narrow age range on these samples of between 0.35 and 0.45 Ma (Morley et al., 1982; Hays and Shackleton, 1976; Morley and Shackleton, 1978).

The boundary between the *B. aquilonaris* and *S. universus* (Hays, 1970) zones occurs between core-catcher samples from Cores 3 (Samples 145-887A-3H-CC, 145-887B-3H-CC, 145-887C-3H-CC) and 4 (Samples 145-887A-4H-CC, 145-887B-4H-CC, 145-887C-4H-CC) in all the holes at Site 887. The abundance of moderately well- to well-preserved radiolarians varies from common at the uppermost part of the zone to rare at its base. The remainder of the sediments in samples from Hole 887B contains faunas typical of the *S. universus* Zone.

Eucyrtidium matuyamai is present in only a single core-catcher sample (Sample 145-887A-9H-CC, 145-887C-9H-CC) in both Holes 887A and 887C. Therefore, it appears that the *E. matuyamai* Zone (Hays, 1970; Foreman, 1975) at this site is confined to a short sediment sequence. The radiolarians range in abundance from rare to common in this narrow zone and are moderately well to well preserved.

The succeeding interval at Hole 887C, from Samples 145-887C-10H-CC through -13H-CC, has been tentatively assigned to the late Pliocene *Lamprocyrtis heteroporos* Zone (Hays, 1970; Foreman, 1975), based on the absence of both *E. matuyamai* and *Stichocorys peregrina* (with the FO of *E. matuyamai* and the LO of *S. peregrina* marking the top and bottom of this zone, respectively) even though only one of the four core-catcher samples from this sequence contains *L. heteroporos*. Although the siliceous fauna varies in preservation between poor and good in the lower Pliocene section at Site 887, radiolarian concentrations are low. This zone is much more difficult to recognize at Hole 887A because of our inability to locate accurately the LO of *S. peregrina* at as young a level as that found in sediments in Hole 887C (164 vs. 121 mbsf). The LO of *Cycladophora davisiana* var. *davisiana*, which falls within the *L. heteroporos* Zone, is located between Samples 145-887A-9H-CC and -10H-CC and between Samples 145-887C-10H-CC and -11H-CC.

Beginning in Core 12 (Samples 145-887A-12H-CC and 145-887C-12H-CC) at Holes 887A and 887C and continuing through the section to the middle part of the upper Miocene, reworked specimens of probable middle to early late Miocene age are present in the sediments. This factor, coupled with rare abundances of generally moderately well to poorly preserved radiolarians throughout this interval, makes it difficult to place the radiolarian fauna within specific zones.

Although *L. heteroporos* has been positively identified in only a single core-catcher sample from Hole 887A, the species is present in several samples from Hole 887C. The FO of *L. heteroporos* in Hole 887C, between Samples 145-887C-15H-CC and -16H-CC, most likely marks the boundary between the *Sphaeropyle langii* (Foreman, 1975) and the *Stichocorys peregrina* (Riedel and Sanfilippo, 1970, 1978) zones. Only one sample from the interval directly above this

faunal boundary in both Holes 887A and 887C contains concentrations of radiolarians higher than rare. Radiolarians are rare in much of the interval that has been tentatively assigned to the *S. peregrina* Zone at Site 887, with preservation ranging between moderately well and poor. The base of this zone occurs between Samples 145-887A-20X-CC and -21X-CC in Hole 887A and between Samples 145-887C-22H-CC and -23H-CC in Hole 887C, based on the first common occurrence of *S. peregrina*. This event nearly coincides with the FO of *D. aquilonius* (see Table 3). The next several cores from both holes at Site 887 do not contain diagnostic species of late Miocene radiolarian zonations, which precede the North Pacific *S. peregrina* Zone. However, samples from this sediment sequence (145-887A-21X-CC through -23H-CC; 145-887C-23H-CC) do contain what appears to be a late Miocene fauna characterized by the presence of *Theocorys redondoensis*, *Sphaeropyle robusta*, and *Phormostichoartus fistula*, in addition to reworked middle Miocene forms. Poor to moderately well-preserved radiolarians exist throughout this interval and abundances vary between rare and common.

Samples 145-887A-24H-CC and -25H-CC from Hole 887A and 145-887C-24H-CC through -26H-CC from Hole 887C are most likely middle to late Miocene age, based upon the dominance of *Lychnocanoma nipponica nipponica* and *Lychnocanoma nipponica magnacornuta* and the absence of *Eucyrtidium inflatum*. *L. nipponica magnacornuta* ranges from the late middle Miocene through early late Miocene (Sakai, 1980). Radiolarian concentrations range from rare to abundant in this sediment section and have moderate-to-poor preservation.

The succeeding two core-catcher samples (Samples 145-887A-27H-CC and -28H-CC, and 145-887C-27H-CC and -28H-CC) from both Holes 887A and 887C contain rare-to-abundant radiolarians of varying degrees of preservation. The presence of *Eucyrtidium inflatum* along with *T. redondoensis*, *S. robusta*, *Eucyrtidium asanoi*, and *Cryptocapsella tetrapera* indicates that this interval is most likely middle Miocene in age.

The abundant, well-preserved radiolarians in Sample 145-887A-29H-CC from Hole 887A are of probable late early Miocene to early middle Miocene age, based on the presence of *Acanthodesmid* sp. (Ling, 1973), along with *C. tetrapera* and *Cryptocapsella cornuta* and *Lithocarpium polyacantha*.

The lowermost sample from both Holes 887A and 887C (Samples 145-887A-30X-CC and -887C-30H-CC) contains common-to-abundant radiolarians. The presence of *C. tetrapera*, *C. cornuta*, *Cryptocapsella japonica*, *Collosphaera* sp. cf. *C. coronata* (?), combined with the absence of *E. inflatum* and *E. asanoi*, indicates that these sediments are of early Miocene age (possibly middle early Miocene). The radiolarian assemblage in Sample 145-887D-3R-CC consists of *C. tetrapera*, *C. cornuta*, and *Collosphaera* sp. cf. *C. coronata* (?), indicating a probable early Miocene age for these sediments. The few rare radiolarians present in sediments from Sample 145-887D-6R-CC do not yield a narrow age for this sample, but suggest a wide age range from Oligocene through early Miocene.

Diatoms

Diatoms are generally common to abundant, and their preservation ranges from good to poor in the lower Miocene to Pleistocene section cored above about 280 mbsf at Site 887 (Core 145-887D-3R). Except for parts of the lower middle Miocene and lower Miocene, all of the assemblages can be zoned readily by the Leg 145 North Pacific diatom zonation (Fig. 9), and standard North Pacific diatom datum levels are recognizable from the late Pleistocene *Neodenticula seminiae* Zone through the late early Miocene *Actinocyclus ingens* Zone (Table 3).

In contrast to the sites from the Northwest Pacific Ocean (Sites 881 through 884), Pleistocene assemblages (Cores 145-887A-1H through -8H; 145-887B-1H through -5H; and 145-887C-1H through -9H) typically are well preserved and easily zoned. Reworking seems

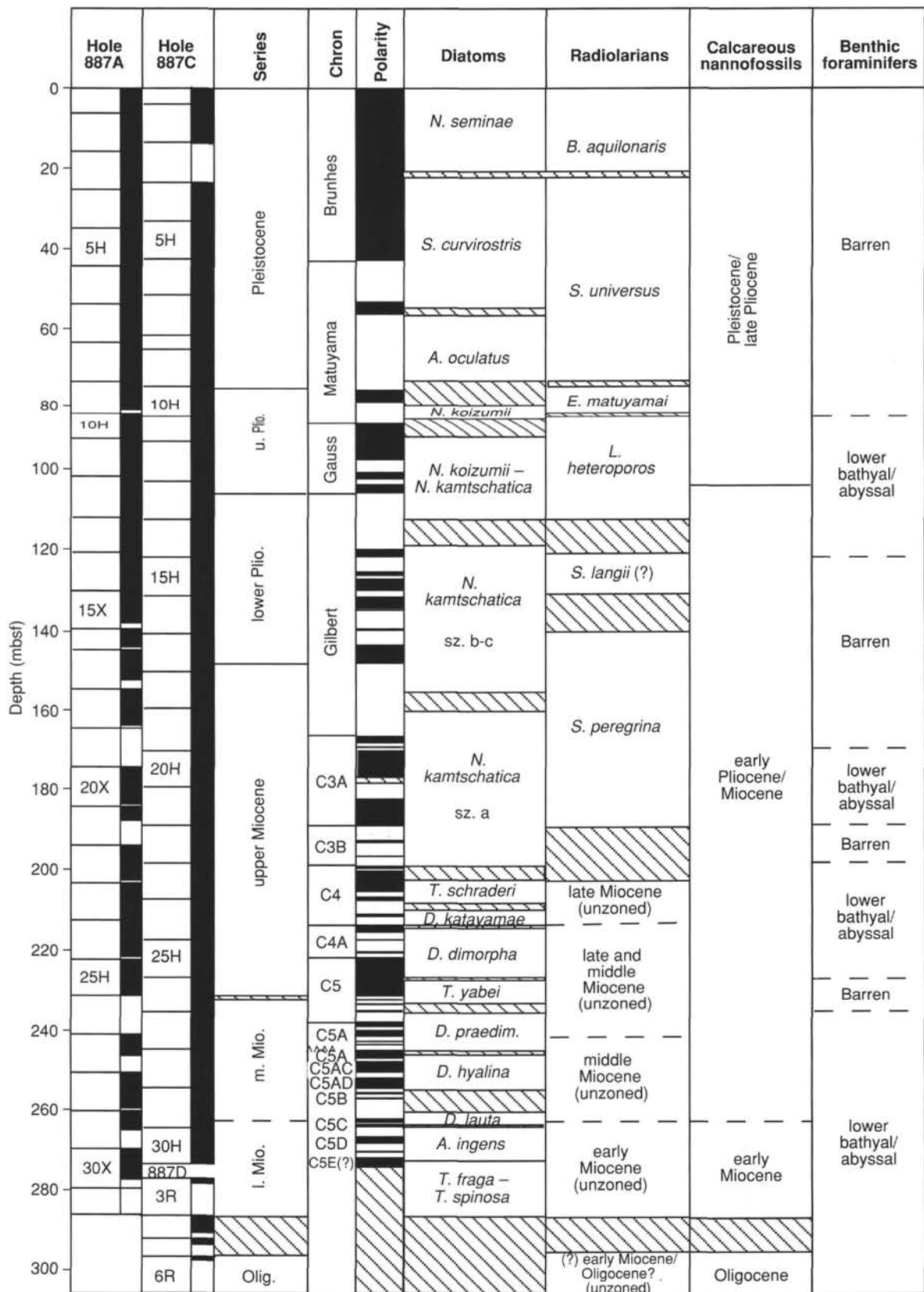


Figure 9. Stratigraphic position of cores; recovery (black); ages; placement of magnetostratigraphic chrons and subchrons; polarity log; and placement of diatom, radiolarian, calcareous nannofossil zones; and the bathymetric range of benthic foraminifers in Holes 887A and 887C. Intervals filled by slanted lines indicate uncertainty in the placement of biostratigraphic boundaries. The magnetostratigraphy shown is that of Hole 887C (see "Paleomagnetism" section, this chapter) and the interpreted paleomagnetic chron boundaries are based on the Leg 145 biostratigraphy and may differ from those interpreted by the paleomagnetists.

to be at a minimum, with the exception of Sample 145-887B-4H-CC, where common *Actinocyclus oculatus*, which is typical of the lower part of the Pleistocene, appears to have been reworked into the late Pleistocene *Simonseniella curvirostris* Zone. Diatom datum levels from Hole 887B (from which only five cores were recovered) are reported in Table 3; however, the LO of *Simonseniella curvirostris* (0.30 Ma) falls between Samples 145-887B-2H-CC and -3H-CC, where it separates the *Neodenticula seminae* Zone from the underlying *S. curvirostris* Zone.

Persistent reworking of middle Miocene forms of *Actinocyclus ingens* and *A. ingens nodus* is documented in the Pliocene and upper Miocene section of Hole 887C (Cores 145-887C-11H through -23H [84–207 mbsf]). Hole 887A also contains reworked middle Miocene taxa in the Pliocene and upper Miocene section, but these have not been documented as thoroughly as those of Hole 887C. Reworked specimens are typically rare (<2% of the assemblage); however, in Sample 145-887C-23H-CC, these are relatively common (perhaps 5%–10% of the assemblage).

The middle Miocene *Crucidenticula nicobarica* Zone appears to have been removed at an unconformity at about 245 mbsf in Hole 887A. Sample 145-887A-27H-3, 20 cm (244.4 mbsf), contains *Denticulopsis praedimorpha* and common *D. simonsenii* and can be assigned to the *D. praedimorpha* Zone (10.8–12.8 Ma), whereas the dominance of *D. hyalina* over *D. simonsenii* without *D. praedimorpha* in Sample 145-887A-27H-1, 124 cm (245.44 mbsf) argues for correlation of that sample with the *Denticulopsis hyalina* Zone (13.3–14.9 Ma).

Dissolution in the lower middle Miocene appears to have removed selectively the marker species *Denticulopsis lauta* in Samples 145-887C-28H-CC (254.8 mbsf) and -29H-CC (264.3 mbsf). The presence of *Actinocyclus ingens nodus* in the former sample, however, indicates an age no older than the upper part of the *D. lauta* Zone. In Hole 887A, Samples 145-887A-28H-CC (260.2 mbsf) and -29H-CC (269.7 mbsf) contain *Denticulopsis hyalina* and *D. lauta*, respectively, and can be correlated with the *D. hyalina* (-28H-CC) and *D. lauta* (-29H-CC) zones.

The FO of *Actinocyclus ingens* and *Crucidenticula sawamurae* in Sample 145-887C-30H-6, 21 cm (272.0 mbsf), are correlative with the uppermost part of a normal polarity event that appears to be Chron C5En (see "Paleomagnetism" section, this chapter). The FO of *C. sawamurae* at Site 887 thus is slightly older than the Chron C5Dn correlation reported by Barron (1985) (as *C. nicobarica*) at equatorial Pacific Ocean DSDP Site 575, but this age is in accord with the correlations of Baldauf et al. (1987) at DSDP Site 610 in the North Atlantic.

Samples 145-887C-30H-CC (273.8 mbsf) and 145-887D-3R-CC (286.7 mbsf) contain a low diversity early Miocene assemblage of *Stellarima* spp., *Cavitatus jouseana*, and *Coscinodiscus marginatus* and cannot be zoned readily. However, the presence of the silicoflagellate *Naviculopsis lata obliqua* in these samples indicates an assignment to the *N. quadrata* Zone of silicoflagellates (Perch-Nielsen, 1985), which is correlative to the middle part of the lower Miocene and, therefore, likely to be equivalent to the *Thalassiosira fraga* Zone. The absence of *Thalassiosira fraga* in these samples, one assumes, results from ecological exclusion.

PALEOMAGNETISM

Procedures

At Site 887, pass-through measurements of magnetic susceptibility and remanence were performed on all APC and XCB cores from Holes 887A, 887B, and 887C. Readings were taken at 10-cm spacings. Measurements of NRM after 15 mT demagnetization were performed for all sections of all cores and, usually, the undermagnetized NRM of at least one section per core was also measured (Table 4). Two to three cubic samples were taken from all sections of Hole 887A and from Hole 887C, Cores 145-887C-19H, -26H, and -27H. Measurements were performed using both the Molspin and the Japa-

nese spinner magnetometers. Samples were demagnetized in five steps up to 30 or 35 mT. In addition to the NRM demagnetization, the Japanese instrument also provided anhysteretic remanent magnetization (ARM) data. The multishot orientation device was deployed in the upper parts of Holes 887A and orientations obtained for Cores 145-887A-4H to -8H and -10H to -12H. Susceptibilities (K) were measured at 5-cm intervals for all cores from Holes 887A, 887B, and 887C, in conjunction with other measurements performed using the multisensor track (MST).

Results

Pass-through measurements of natural remanent magnetization, after 15 mT demagnetization, and whole-core susceptibility are shown in Figure 10 for Hole 887C. As at the other sites of Leg 145, Site 887 is characterized by a high remanence and susceptibility within the top 100 mbsf, which decreases abruptly below this depth as the abundance of diatoms increases. In contrast to previous sites, no significant recovery in intensity toward the bottom of the section is evident. However, values for both the remanence and susceptibility remain well within measurable levels. At Site 887, the remanence intensity curve follows the susceptibility curve, which shows particularly well the sharp transition between lithologic Units I and II. There is almost an order-of-magnitude decrease in susceptibility below this boundary. Mean remanence intensities after demagnetization at 15 mT are about 40 mA/m from 0 to 89.5 mbsf (varying between 2 and 200 mA/m), and between about 5 and 15 mA/m from 89.5 to 269.7 mbsf. An abrupt low value in K is seen between 165.5 and 168.95 mbsf, marking the boundary between lithologic Subunits IIA and IIB. An increase in K coincides with the boundary between lithologic Subunits IIA and IIB.

ARM measurements, demagnetized at 30 mT using the Japanese spinner magnetometer, are shown in comparison to susceptibility in Figure 11. The ratio of ARM to susceptibility (seen qualitatively in the separation between the two curves) is an indicator of magnetic grain size. This is because ARM is mostly held in the finer-grained fraction, while K is controlled by the coarse fraction. Above and below the lithologic boundary between Units I and II (89.5 mbsf), the two curves parallel each other, indicating a constant ARM/ K ratio (Fig. 11). In these regions, the various troughs and peaks of the two curves reflect only dilution changes of a magnetic fraction whose basic properties are constant. However, between these two regions, a significant change is evident in the ratio. Above 89.5 mbsf, the ARM/ K ratio is approximately one-half that of the ratio below this depth. This difference indicates either a significant upward-coarsening of the magnetic grain size, or a change in magnetic mineralogy. It cannot be explained by dilution effects. An upward-coarsening is consistent with the sedimentological observations (see "Lithostratigraphy" section, this chapter).

As at earlier sites, a reversed drilling overprint was observed in cores from Hole 877A. Hole 887C, however, shows a normal overprint (Fig. 12); this must be related to a change in the dominant magnetization of the core barrel and drill string. Discrete sample demagnetizations show that this overprint is removed by 5- to 10-mT demagnetization fields. Discrete samples held a measurable and, apparently, stable remanence throughout most of Hole 887B. A few examples of weakly magnetized samples did not show stable demagnetizations using the spinner magnetometers. Examples of sample demagnetizations are shown in Figures 13 and 12, together with a comparison of the whole-core measured inclinations, after 15 mT demagnetization, and with the discrete sample results. The individual sample directions were obtained by linear regression fits to the demagnetization data between 10 and 40 mT. With the exception of disturbed parts of the cores, the sediments appear to record stable normal and reversed-field directions between 0 and 269.7 mbsf at the base of Hole 887C (the axial dipole field inclination is about $\pm 70.3^\circ$ at a latitude of $54^\circ 22'N$).

Table 4. Depths of polarity chron boundaries in Holes 887A and 887C.

Chron	Age (Ma)	Hole 887A		Hole 887C	
		Depth (mbsf)	Notes	Depth (mbsf)	Notes
C1n	(?)				
	0.780	45.55		42.70	
C1r.1n	0.984	55.60		52.60	
	1.049	58.95		56.25	
C1r.2r-1n	1.201				
	1.212				
C2n	1.757		f	75.35	
	1.983		f	78.95	
C2r.1n	2.197				
	2.229				
C2An.1n	2.600	88.90		87.30	
	3.054	101.10		98.30	
C2An.2n	3.127	101.85		100.55	
	3.221	104.20		102.70	
C2An.3n	3.325	106.55		103.40	
	3.553	110.35		105.90	
C3n.1n	4.033	121.10		120.35	
	4.134	125.20			cb
C3n.2n	4.265				
	4.432	134.70		134.80	
C3n.3n	4.611			139.65	
	4.694	142.20			
C3n.4n	4.812	145.80		143.55	
	5.046	149.95		148.65	
C3An.1n	5.705			169–169.3	cb
	5.946			177.10	
C3An.2n	6.078			181.75	
	6.376				
C3Bn	6.744				
	6.901				
C3Br.1n	6.946				
	6.981				
C3Br.2n	7.153				
	7.187				
C4n.1n	7.245				
	7.376			199.20	
C4n.2n	7.464			199.80	
	7.892			205.45	
C4r.1n	8.047			206.80	
	8.079				
C4An	8.529			211.80	
	8.861			215.95	
C4Ar.1n	9.069				

Conclusions

Results from Holes 887A and 887C provide at least 270 m of coherent and continuous magnetostratigraphy (Table 4). Directional results from XCB-coring in Hole 887A contain more noise than results from APC-coring in Hole 887C. In the intermediate to deep parts of Hole 887A, recovery from XCB-coring was low, while, at the same depths in Hole 887C, recovery was good. In fact, the quality of the magnetic results from Hole 887C is extremely high. As a result, below 180 mbsf, the magnetostratigraphy has been interpreted almost exclusively using results from Hole 887C. In the upper parts of the section (above 180 mbsf), a continuous magnetostratigraphy has been constructed using the results from both Holes 887A and 887C. Figure 14 illustrates the magnetostratigraphy between 0 and 180 mbsf, how it was constructed from the two holes, and its correlation to the polarity time scale of Cande and Kent (1992). Figure 15 illustrates the magnetostratigraphy between 180 and 270 mbsf.

The magnetostratigraphic results from Site 887 are extraordinary. A clear interpretation of this magnetostratigraphy is possible from 0 Ma as far back as the top of Chron 5En (18.317 Ma) at about 272 mbsf. The record from 0 to 18.317 Ma appears to be continuous, with no suggestion of substantial missing time intervals. A detailed and coherent picture of sedimentation rate variation is produced and an age-vs.-depth curve, based on the magnetostratigraphy, is shown in Figure 16. The sedimentation rates near the base of the section are close to 0.5 cm/k.y., an order of magnitude lower than rates near the top. As at other sites of Leg 145, a low value in sedimentation rate is centered near the level (60–90 mbsf) of the Olduvai event. Thus, the

Table 4 (continued).

Chron	Age (Ma)	Hole 887A		Hole 887C	
		Depth (mbsf)	Notes	Depth (mbsf)	Notes
	9.149				
C4Ar.2n	9.428			219.75	
	9.491			220.65	
C5n.1n	9.592			221.30	
	9.735			222.85	
C5n.2n	9.777			223.05	
	10.065				
	10.330				
	10.595				
	10.834			231.45	
C5r.1n	10.940				
	10.989				
C5r.2n	11.378			235.15	
	11.434				cb
C5An.1n	11.852			238.25	
	12.000			239.50	
C5An.2n	12.108			240.05	
	12.333			241.65	
C5Ar.1n	12.618				
	12.649				
C5Ar.2n	12.718				
	12.764				
C5AAn	12.941				
	13.094				
C5ABn	13.263				
	13.476				
C5ACn	13.674			248.45	
	14.059			250.85	
C5ADn	14.164			251.75	
	14.608				cb
C5Bn.1n	14.800			255.60	
	14.890			256.25	
C5Bn.2n	15.038			257.05	
	15.162			257.55	
C5Cn	16.035			262.10	
	16.755				cb
C5Dn	17.310			266.75	
	17.650			268.40	
C5En	18.317			271.95	

Note: The annotation "cb" indicates that a reversal occurred in a core break; "f" indicates depth of poorly recovered Olduvai internal (see text).

Olduvai appears shorter than expected in the reversal stratigraphy. Low sedimentation rates near the Olduvai appear to occur across the entire North Pacific Ocean.

SEDIMENTATION RATES AND FLUXES

Sedimentation Rates

To calculate sedimentation rates and sediment fluxes (mass accumulation rates), we considered the sedimentary section at Site 887 to consist of five time-stratigraphic intervals. The limits of these intervals were chosen on the basis of changes in sedimentation rate and dry-bulk density, as well as changes in sediment composition. Thus, they should represent intervals of relatively constant flux, and with one exception, they coincide with lithostratigraphic units defined for this site. Whereas lithostratigraphy divides Unit I into two subunits at 45 m, two time-stratigraphic intervals are divided at ~56 m on the basis of a change in linear sedimentation (Fig. 17). Linear rates of sedimentation were calculated for this site using magnetostratigraphy at Hole 887C. In general, rates decrease down the core from ~54 m/m.y. during the late Pleistocene to ~5 m/m.y. during the middle Miocene. It is important to stress that our estimated rates of sedimentation reflect averages for intervals of time millions of years long. Significant variability exists within these intervals, that might drive large changes in mass accumulation rate on shorter time scales. Note, for example, that sedimentation rates in upper Subunit IIB are higher than the unit average and lower than the unit average near the unit bottom (Fig. 17).

Sediment Fluxes

Sediment fluxes were determined in the conventional way, taking the product of the sedimentation rate, the dry-bulk density, and the concentration of the sediment component. Average fluxes were calculated for the five time-stratigraphic intervals, the results of which are shown as histograms in Figure 17, keyed to the depth intervals with dashed lines. Raw data for each of these intervals in Hole 887C were averaged and are presented in Table 5. Dry-bulk density values were taken from pycnometer measurements, and sedimentary component data come from smear slide estimates, with the exception of percentages of carbonate and total organic carbon (TOC), which were measured analytically. Flux results (in $\text{g/cm}^2 \cdot \text{k.y.}^{-1}$) for diatoms, clay, glass, quartz, and carbonate are listed in Table 5 and are shown in the histograms (values for TOC fluxes are too near zero to be visible in the histograms). These results are only semi-quantitative, because of the nature of smear slide abundance estimates as well as because of possible errors when calculating deposition rates. For example, Thiede and Rea (1981) noted previously that smear slide results tend to overestimate coarse-grained sedimentary components that were subsequently measured analytically in shore-based studies. Additional errors may stem from the assumption that the abundance estimates are directly proportional to the weight percentage of each sedimentary component.

Average sediment fluxes for the five time-stratigraphic intervals reveal distinctive changes with time (Fig. 17). As at Sites 881 through 886, at Site 887, the 2.6-Ma level has been marked by an abrupt increase in a clay flux that is associated with the onset of Northern Hemisphere glaciation. At this site, where we have subdivided the post-2.6 Ma interval, values for clay flux remain constant, but a jump in diatom flux values is evident within the past million years. Although we do not know the oceanographic significance of this change, the decreased values for diatom flux between ~1 and 2.6 Ma may account for the 50% decrease in linear sedimentation rate for that interval.

Within Subunit IIA, roughly equivalent to pre-glacial Pliocene time, sediment accumulation has been dominated by diatom flux. This finding is comparable to that observed far to the west at the Detroit Seamount sites, although values for diatom flux were three times higher at Site 883. This suggests that whatever the cause for this spike in diatom flux values during the early Pliocene and latest Miocene, its influence may have been felt across vast regions of the North Pacific Ocean.

For late Miocene time and older, values for fluxes at Site 887 are low. At the Detroit Seamount sites we found a similar pattern, although at relatively shallow depths, carbonate flux values increased with increasing age and at depths greater than those at which the Site 887 clay flux persisted. At those sites, changing flux patterns were attributed to the origin of the Meiji Drift (which may account for clay flux) and the backtracking of site locations to shallow, oligotrophic waters. Site 887 has probably lain beneath the Subpolar Gyre for most of its existence, yet during late and middle Miocene time, here the diatom flux was at least as low as that at the Detroit Seamount sites. By way of contrast, at about the same time to the south, offshore California, strong coastal upwelling produced one of the world's classic diatomites: the middle Miocene Monterey Formation.

INORGANIC GEOCHEMISTRY

Fourteen interstitial-water samples were collected from Hole 887A at depths ranging from 1.45 to 224.15 mbsf. The pore-water samples span all of lithologic Subunits IA (0–45 mbsf; alternating clay, ice-rafted debris, and diatom ooze), IB (45–90 mbsf; clay), IIA (91–169 mbsf; diatom ooze), and IIB (~174–235 mbsf; calcareous diatom ooze). No samples were collected from lithologic Subunit IIC (siliceous ooze) or from the basal chalks and dark brown clays of Unit III, which overlie the basement basalt (Unit IV; see "Lithostratigraphy" section, this chapter). All analytical results are listed in Table 6.

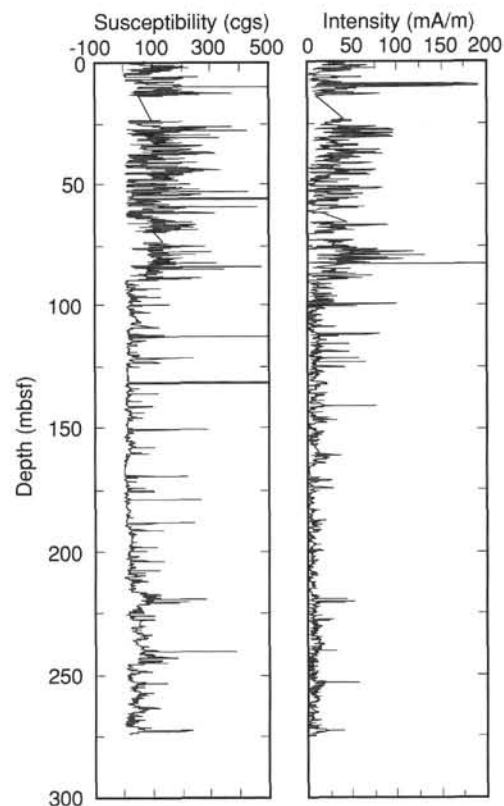


Figure 10. NRM intensities, after demagnetization at 15 mT (from Hole 887C), compared to whole-core susceptibilities.

Chloride concentrations in interstitial waters at Site 887 range from the North Pacific Deep Water value (554 mM) in the shallowest sample (1.45 mbsf; Fig. 18A) to a maximum of ~563 mM at 38.15 mbsf. As at Sites 881 through 886, the Cl^- maximum probably reflects the ongoing diffusive adjustment of the pore-water Cl^- distribution to the increased mean salinity of seawater during glacially dominated Pleistocene time and the fresher seawater of the Holocene (McDuff, 1985). The depth of the Cl^- maximum in Hole 887A is similar to that normally encountered in pelagic sections (McDuff, 1985). Below the maximum, the chloride concentration decreases progressively, reaching a near-constant value of ~557 mM at ~127 mbsf; this concentration persists to the base of the sampled section (Fig. 18A).

Nitrite is undetectable in the upper ~40 m (Table 6), even though sulfate reduction clearly is occurring at relatively shallow depths (see below). This suggests that the rate of nitrate reduction in shallow sediments at this site may be too slow to produce measurable concentrations of the biologically labile NO_2^- intermediate species. Alternatively, and more probably, the nitrite peak may have been missed because of the coarse sampling interval used at this site (one sample per core in the upper part of the section). At Site 883, where high-resolution sampling was employed (three samples in the upper 6 m), NO_2^- was undetectable at 1.5 mbsf, but was clearly observed in the 4.5- and 6-m-deep samples before decreasing to undetectable levels in deeper pore waters. Similar sampling may have defined a nitrite maximum in the shallow pore waters at Site 887.

The concentration of dissolved manganese in the shallowest sample at Site 887 (53 μM at 1.45 mbsf; Table 6) is sharply higher than that in the overlying bottom water (<100 nM in seawater; Landing and Bruland, 1980). Concentrations continue to increase to a shallow subsurface maximum of ~100 μM at ~29 mbsf (Fig. 18B) and generally decline with depth below this horizon, reaching ~75 μM in the deepest sample at 244 mbsf. The profile suggests that the manganese oxide reduction zone at this location is confined to the upper 20

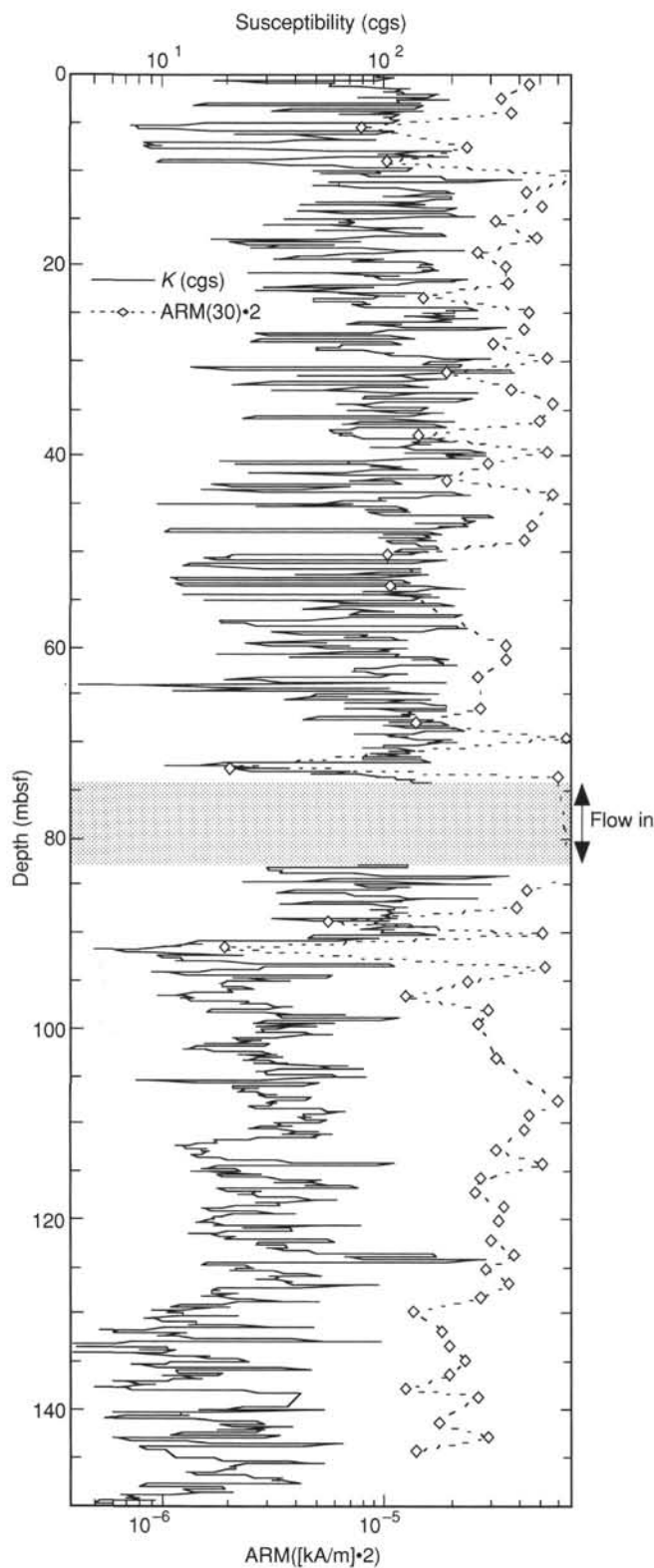


Figure 11. Comparison of results from whole-core measurements of susceptibility (solid line) with ARM, demagnetized to 30 mT, from discrete samples (open diamonds) for Hole 887A. Both are plotted on log scales spanning an equal number of orders of magnitude to preserve the relative magnitudes of the ARM and K values. Variation in the separation of the two curves indicates a change in the ARM/ K ratio.

mbsf. The gradual and slight general decline with depth may reflect precipitation of authigenic manganese carbonate or ongoing diffusive adjustment related to nonsteady-state deposition. The latter explanation is supported by the sulfate distribution, as discussed below.

Three noteworthy features characterize the pore-water sulfate profile at Site 887. The uppermost sample at 1.45 mbsf has the same concentration as the overlying seawater (28.6 mM, Table 6), indicating that no sulfate reduction is occurring in the upper 1.5 m at this location. Below this depth, the first-order decline in concentration (Fig. 18C) and the concentration minimum at ~50 mbsf indicate that the principal zone of sulfate reduction is confined to the upper 40 to 50 mbsf. Below this interval, the gradual, roughly linear increase in SO_4^{2-} is similar to those seen at Sites 883 and 884. This increase probably reflects upward diffusion from near the base of the section. Reduction of SO_4^{2-} is unlikely to be occurring at depths greater than 50 mbsf, which is consistent with the decline to low concentrations of organic carbon observed below 60 mbsf and with commensurately low organic carbon accumulation rates observed in the lower half of the drilled section (see "Organic Geochemistry" and "Sedimentation Rates and Fluxes" sections, this chapter). These data imply that a relatively low oxidant demand prevailed during the deposition of the lower Miocene to upper Pliocene siliceous and calcareous facies at this site.

Titration alkalinity in the pore waters increases gently with depth in the upper section at Site 887: from 3.6 mM at 1.45 mbsf toward a broad maximum of ~6 mM between 19 and 50 mbsf (Fig. 18C). Values progressively decrease below this interval, reaching ~3.2 mM at 244 mbsf. Downward diffusion from the base of the broad maximum toward a subtle mid-depth minimum is indicated by the concentration gradient. Minor consumption of alkalinity (precipitation of authigenic carbonate?) at mid-depths is implied by the slight downward concavity evident in this portion of the profile, while the overall distribution is consistent with the hypothesis that a low oxidant demand prevailed during deposition of the siliceous-calcareous facies intersected at depth.

Concentrations of dissolved ammonium in pore waters at Site 887 increase with depth from ~50 μM at ~1.5 mbsf to >300 μM between ~30 and ~80 mbsf and generally decline at progressively greater depths (Fig. 18D). The upward convexity in the interval between the uppermost sample and ~40 mbsf indicates that this is the principal zone of NH_3 release. This is consistent with the sulfate distribution, which indicates that the highest rate of anaerobic decomposition occurs over roughly the same depth range. The decline of the ammonium content below ~70 mbsf probably reflects downward diffusion from the zone of production in the more organic-rich upper portion of the section toward the organic-lean sediments overlying the basement. This suggestion is consistent with indications from other data that the oxidant demand was low during the deposition of the deeper sediments at this site.

Concentrations of magnesium in pore waters at this site are slightly lower than those in North Pacific Deep Water (~50–52 mM, compared with 53.5 mM) and vary little throughout the sampled section (Fig. 19A). The offset between the concentrations in the uppermost samples and bottom water may represent a temperature-of-squeezing artifact (see "Inorganic Geochemistry" section, "Site 883" chapter, this volume). A slight, but analytically reproducible, relative minimum between ~50 and 140 mbsf may reflect minor uptake of Mg^{2+} during alteration of volcanic ash; alternatively, the minimum may have been produced by the precipitation of trace amounts of dolomite in the interval near 100 mbsf, where minor consumption of dissolved carbonate species is indicated by concavity in the alkalinity profile (Fig. 19C).

Like magnesium, the concentrations of dissolved calcium exhibit little variation with depth. The concentration in the uppermost sample is the same as that in North Pacific Deep Water (10.5 mM), and values increase slightly with depth, rising by about 1.5 mM over the course of the sampled section (Fig. 19C).

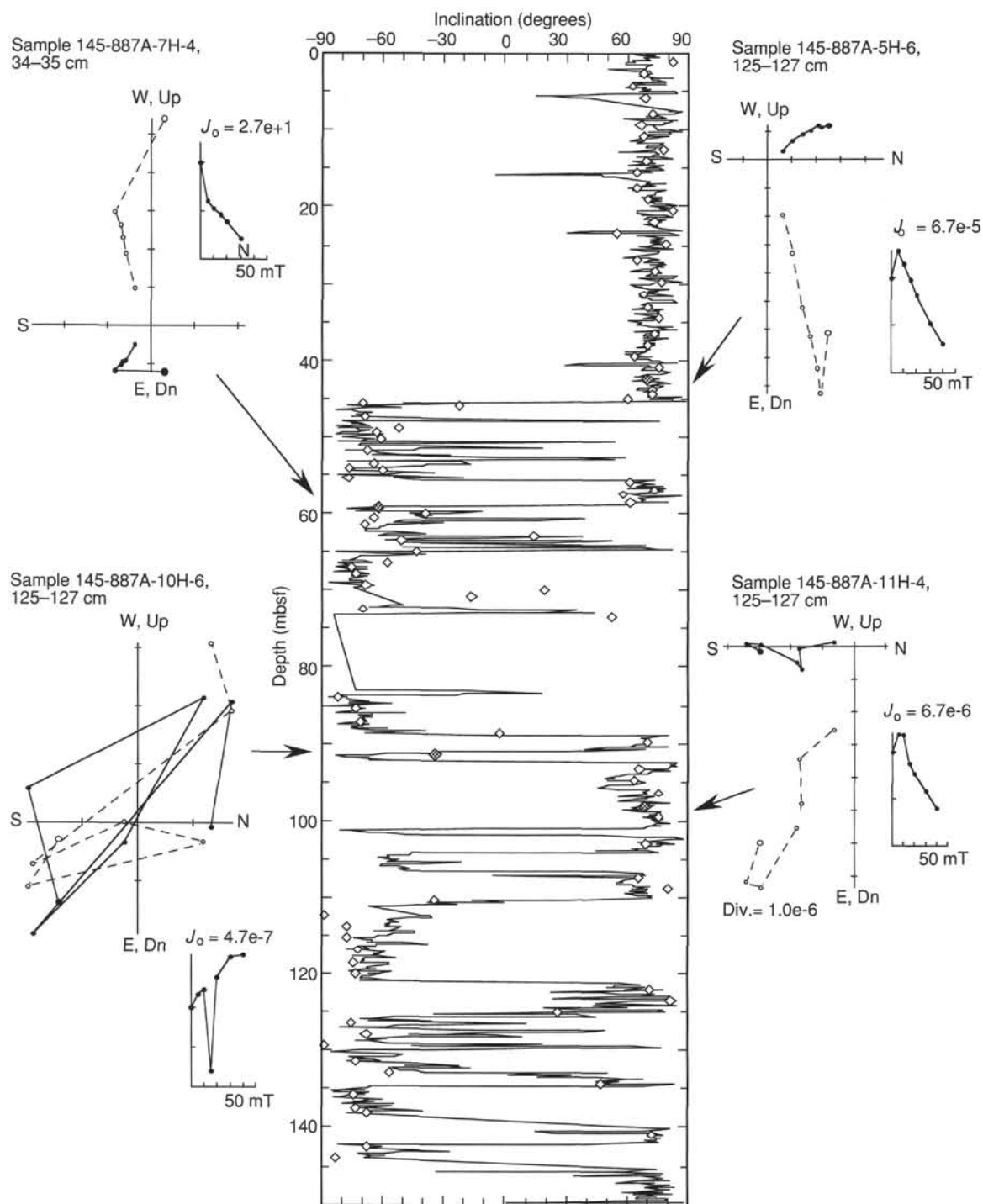


Figure 12. Comparison of discrete sample demagnetizations from Hole 887A with the whole-core results. For the Zijderfeld plots, the open circles joined by dotted lines indicate the vertical component plotted vs. the x (north-south) component.

The concentrations of dissolved silicate in the uppermost pore water sample at Site 887 ($\sim 863 \mu\text{M}$) are sharply higher than those in the overlying North Pacific Bottom Water ($\sim 160 \mu\text{M}$), reflecting pronounced dissolution of opaline diatom frustules within the uppermost sediment column (Fig. 19B), as observed previously at Sites 881 through 886. High concentrations prevail throughout the rest of the section, implying that pore waters at this location are everywhere saturated (or nearly so) with respect to opal.

The concentrations of strontium in the uppermost pore water sample ($87 \mu\text{M}$) are about the same as those in modern North Pacific Deep Water ($86.3 \mu\text{M}$; Fig. 19C). Little variation is seen throughout the rest of the sampled section, indicating that Sr is essentially conservative in the interstitial waters at Site 887. In contrast, the slight minimum in the concentration of lithium at 66 mbsf (Fig. 19C) suggests that clay minerals in the deposits above 100 mbsf are actively adsorbing Li^+ . Uptake by clays has been invoked to explain slight

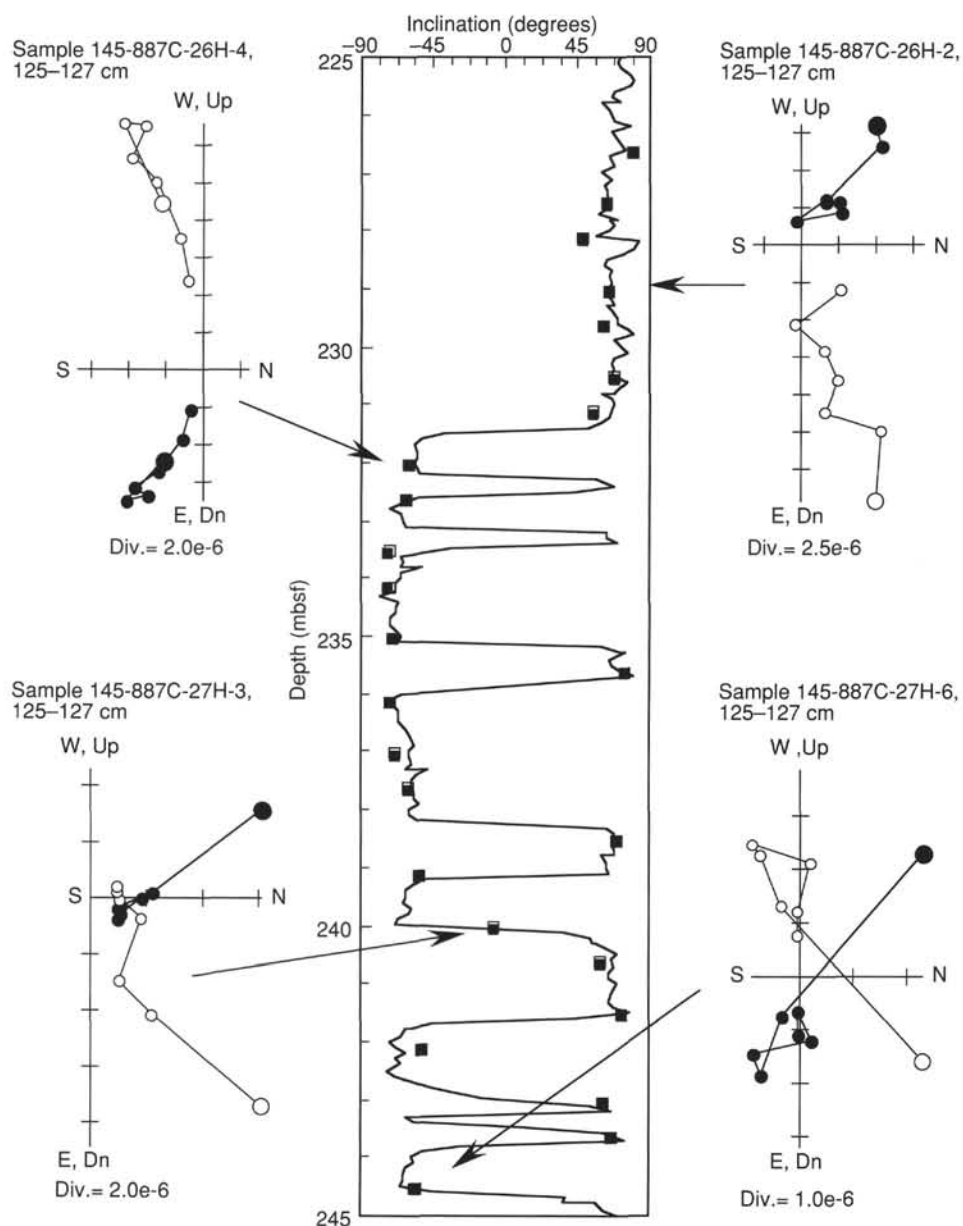


Figure 13. Comparison of discrete sample demagnetizations from Hole 887C with the whole-core results. For the Zijderfeld plots, the open circles joined by dotted lines indicate the vertical component plotted vs. the x (north-south) component.

relative lithium deficiencies in the pore waters at other North Pacific sites, including Sites 882 and 884.

Concentrations of sodium (calculated by charge balance at this site) show little variation in the pore waters down the core, with concentrations in the uppermost sample being equal to that of seawater (480 mM). A slight enrichment in sodium, similar to the chloride maximum, occurs between 30 and 48 mbsf (Table 6), reflecting the Quaternary salinity effect discussed earlier.

The concentration of potassium in the surface sample (11.8 mM) is higher than that in North Pacific Deep Water (10.35 mM) and remains within about 15% of this value throughout the section (Fig. 19D). The potassium data show some slight scatter, which may be the result of the temperature-of-squeezing effect (see "Inorganic Geochemistry" section, "Site 883" chapter, this volume). The general

absence of variation evident in the distribution suggests that K^+ is essentially conservative in the interstitial waters at Site 887.

ORGANIC GEOCHEMISTRY

Volatile Hydrocarbons

As part of the shipboard safety and pollution program, hydrocarbon gases were measured in the sediments at Site 887. Using the headspace technique and a Carle gas chromatograph (see "Organic Geochemistry" section, "Explanatory Notes" chapter, this volume) the concentrations of methane (C_1), ethane (C_2), and propane (C_3) were determined. The results of 51 headspace analyses are presented in Table 7. The volatile hydrocarbon concentrations are very low in Site 887 sediments, as recorded previously at all the Leg 145 sites.

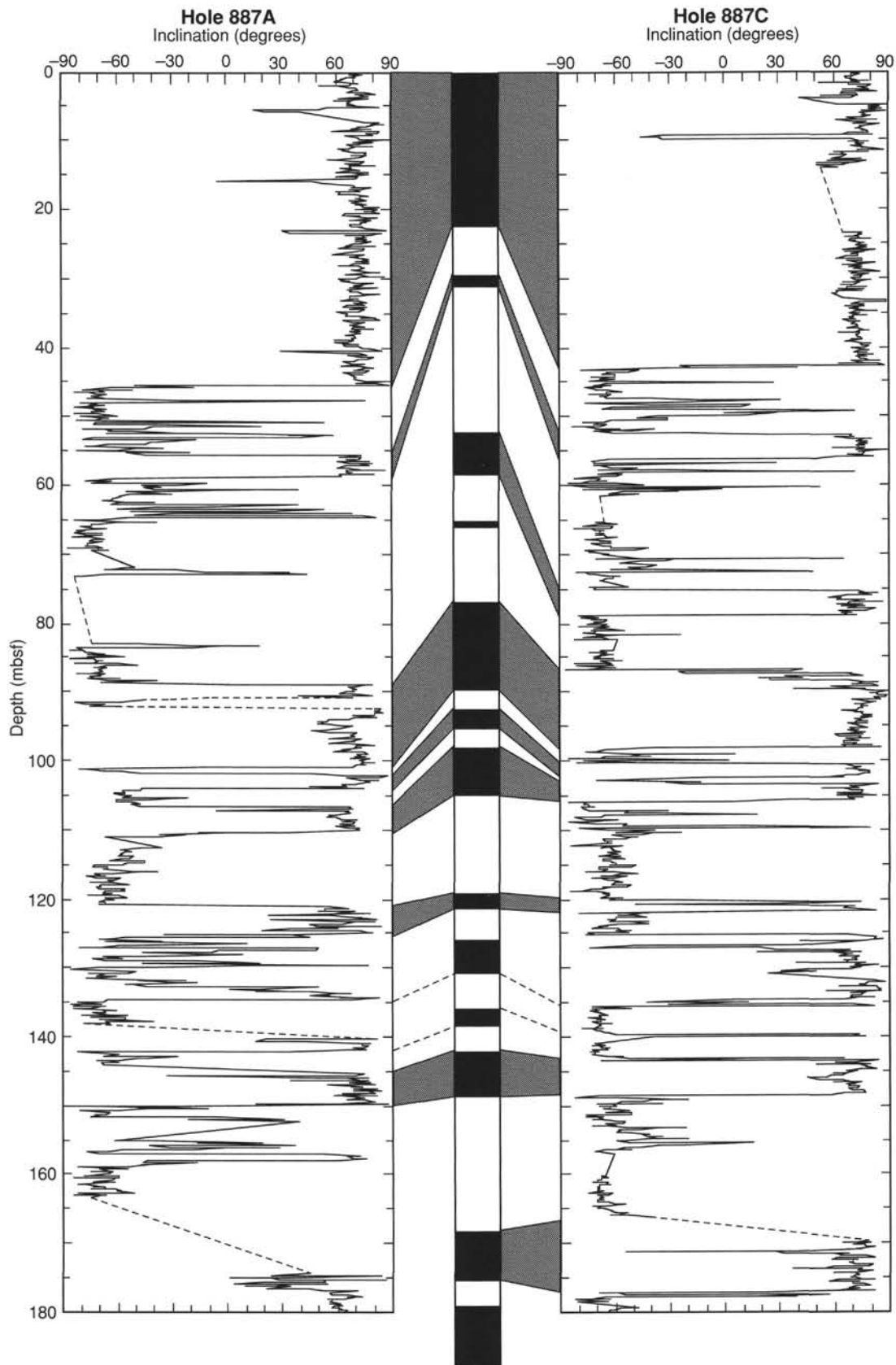


Figure 14. Whole-core measurements of inclination, after 15 mT demagnetization, from Holes 887A and 887C (0–180 mbsf). Correlation with the polarity time scale of Cande and Kent (1992) also is shown.

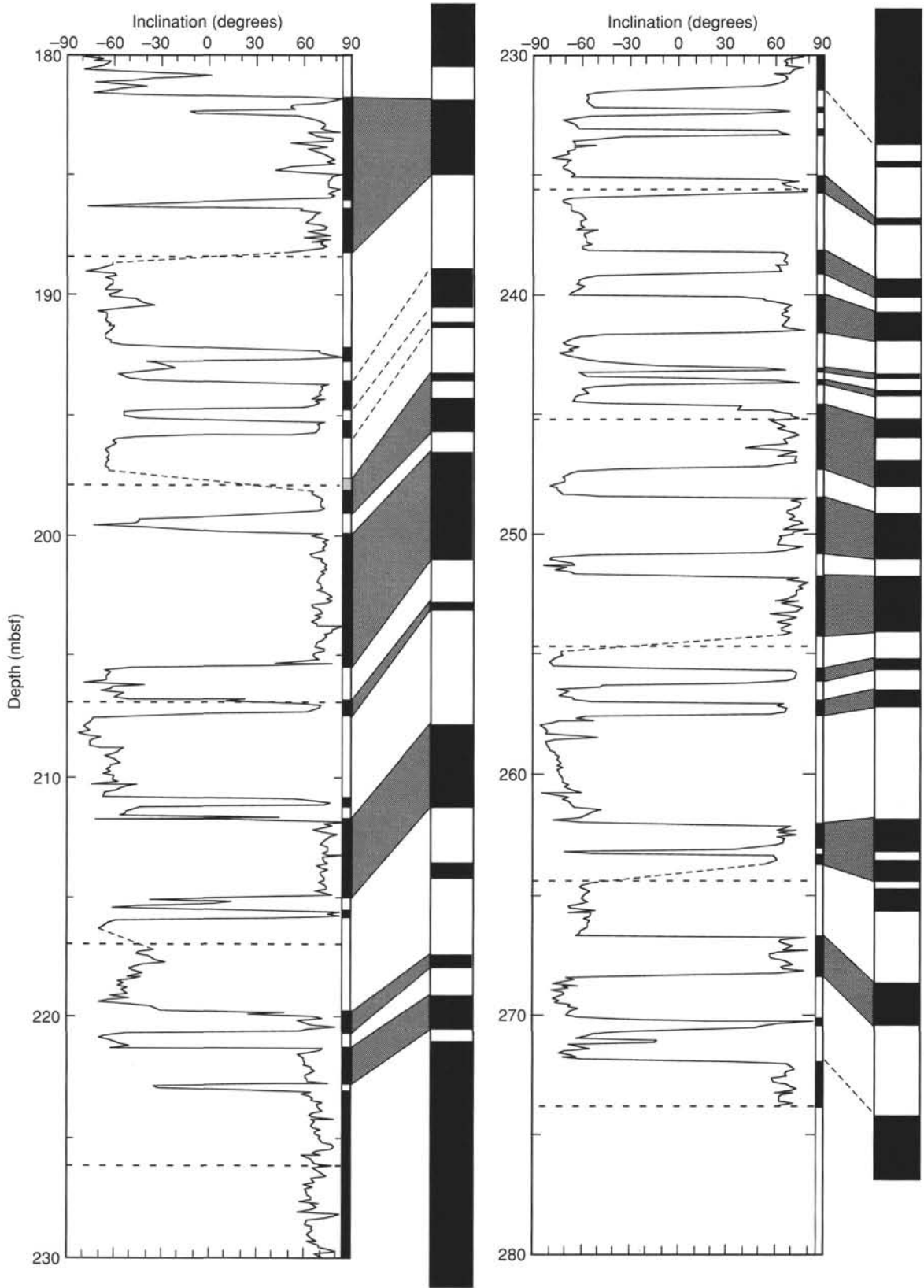


Figure 15. Whole-core measurements of inclination, after 15 mT demagnetization, from Hole 887C (180–270 mbsf). Correlation with the polarity time scale of Cande and Kent (1992) also is shown.

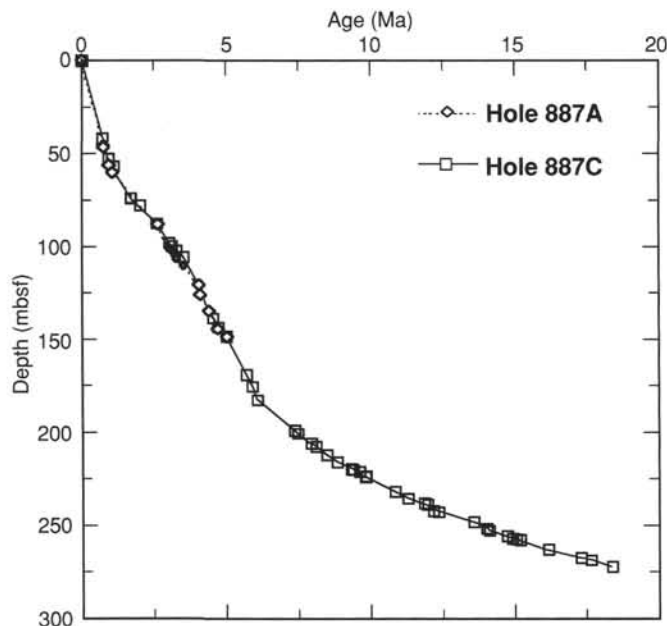


Figure 16. Plot of age vs. depth for Site 887 sedimentary section, based on magnetic reversal stratigraphy.

Methane values range from 2 to 7 ppm and indicate that no significant methanogenesis is occurring at this location. This result is consistent with the very low organic carbon contents throughout the sediment column. Ethane and propane concentrations were below the detection threshold of the gas chromatograph.

Carbonate Carbon

Carbonate concentrations at Site 887 were determined on 101 samples collected from Holes 887A and 887C. The inorganic carbon (IC) measurements were performed by means of a Coulometrics carbon dioxide coulometer and the results were multiplied by 8.334 to calculate percent CaCO_3 . No corrections for other carbonate phases were made. The results from Holes 887A and 887C are listed in Table 8 and are plotted vs. depth below seafloor in Figure 20.

The calcium carbonate concentration profile through lithologic Units I and II (see "Lithostratigraphy" section, this chapter) shows a very high amplitude variation with values ranging between 0 and almost 75 wt% CaCO_3 . Four intervals with distinctly increased values characterize the drilled section. The interval between the sediment surface and 15 mbsf displays carbonate contents up to 10 wt% and between 35 and 60 mbsf values reach about 20 wt%. These two intervals are within lithologic Unit I, which consists mainly of diatomaceous clay with carbonate. The transition between lithologic Units I and II is marked by the third interval (95–110 mbsf), where carbonate values increase up to 75 wt%; no carbonate depleted samples were encountered in this zone. Lithologic Subunits IIB and IIC are represented by the fourth interval of higher carbonate content. The transition between these two subunits is based on different amounts of opaline constituents (see "Lithostratigraphy" section, this chapter) and thus is not recorded by the carbonate record.

As seen at the other Leg 145 sites, the occurrence of calcium carbonate in the Site 887 sediments correlates fairly well with the abundance of calcareous nanofossils (see "Biostratigraphy" section, this chapter), indicating that this fossil group supplies the main portion of CaCO_3 measured in the samples.

Organic Carbon

Total organic carbon (TOC) values were calculated by difference between total carbon (TC), measured with a Carlo Erba NCS Ana-

lyzer, and IC from the coulometer. The data are presented in Table 8 and are plotted vs. depth below seafloor in Figure 21. Most of the total nitrogen values from the NCS analyzer were near or below the detection limit and thus were not used for further interpretations.

Two main features characterize the organic carbon pattern of the Site 887 sediment record. The upper 70 mbsf displays organic carbon contents of between 0.2 and 0.6 wt%. The sediments of this interval consist of gray clay-rich oozes alternating with greenish-brown, spicule-bearing diatom oozes (see "Lithostratigraphy" section, this chapter). A high-resolution profile was sampled over the transition of the diatom-spicule ooze to the gray clay-rich sediment (Fig. 22). The greenish-brown diatom ooze layer shows a slight enrichment in TOC and high CaCO_3 concentrations, whereas carbonate is absent in the gray sediments. This may indicate higher surface-water productivity and/or rapid burial and thus better preservation of the organic material in the diatom-rich layers.

The interval between 70 and 260 mbsf is characterized by low organic carbon contents, which do not exceed 0.25 wt%. As displayed by the pore-water sulfate profile of Site 887, no significant sulfate reduction occurred in the sediments of this section (see "Inorganic Geochemistry" section, this chapter), indicating low organic carbon accumulation rates during the deposition of this interval.

PHYSICAL PROPERTIES

Introduction

GRAPE bulk densities, magnetic susceptibilities, and P-wave velocities were measured continuously from Holes 887A, 887B, and 887C. Thermal conductivity was measured at 3-m intervals in cores from Holes 887A, 887B, and 887C. Index property (wet-bulk density, dry-bulk density, grain density, wet porosity, dry porosity, wet water content, dry water content, and void ratios) measurements were performed at approximately 1.5-m intervals in cores from Holes 887A, 887B, and 887C (Cores 145-887C-11H through -30H). In Cores 145-887C-1H through -10H from Hole 887C, measurements were performed at 75-cm intervals. Shear strength and digital sound velocimeter (DSV) measurements were performed at 1.5-m intervals in Hole 887A and 3-m intervals in Hole 887C. Compressional wave velocity and GRAPE bulk-density were measured on several discrete basalt samples from Hole 887D. Tables containing compressional wave velocity, thermal conductivity, index property, and shear strength data from Holes 887A, 887B, and 887C are included (Tables 9 through 16).

Index Properties and Vane Shear Strength

The downhole trends for bulk densities, grain density, porosities, and water contents are related to changes in the lithostratigraphy. The upper 90 mbsf of the sediment column (lithologic Unit I, see "Lithostratigraphy" section, this chapter), is characterized by high variability in the index property profiles (Figs. 23 through 27), the result of interbedded clay- and biogenic silica-rich intervals (see "Lithostratigraphy" section, this chapter). The clay-rich intervals are characterized by higher bulk densities and grain densities and lower porosities and water contents than those found in the biogenic silica-rich intervals (Fig. 28). In the clay-rich intervals, average wet-bulk density, dry-bulk density, grain density, dry water content, and dry porosity values are 1.5–1.65 g/cm^3 , 0.9–1.0 g/cm^3 , 2.6–2.8 g/cm^3 , 150%–200%, and 70%–80%, respectively. The biogenic silica-rich intervals are characterized by average wet-bulk density, dry-bulk density, grain density, dry water content, and dry porosity values of 1.2–1.4 g/cm^3 , 0.4–0.6 g/cm^3 , 2.2–2.4 g/cm^3 , 60%–80%, and 60%–65%, respectively. In the clay-rich Subunit IB (approximately 45–90 mbsf, see "Lithostratigraphy" section, this chapter) average grain-density and bulk-density values are slightly higher, with correspondingly lower porosities and water contents, than those in the diatom- and carbonate-rich Subunit IA (0–45 mbsf).

The top of lithologic Unit II, at approximately 90 mbsf, is marked by decreases in wet-bulk density, dry-bulk density, and grain density

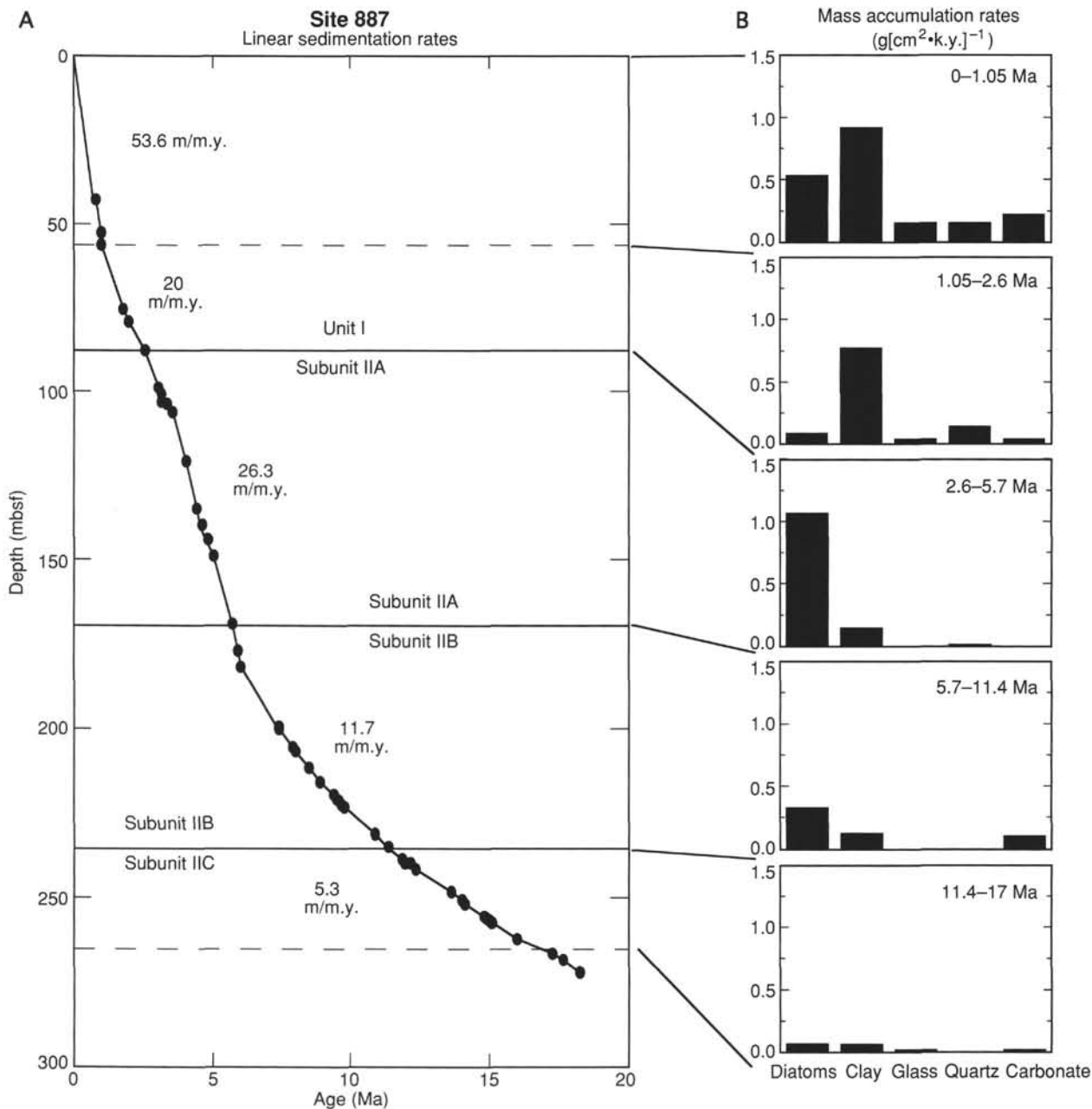


Figure 17. **A.** Plot of age vs. depth for Site 887 using magnetostratigraphy from Hole 887C. For flux (mass accumulation rate) calculations, the section was divided into five intervals where rates of sedimentation, dry-bulk density, and sediment composition are relatively constant. These intervals are identified by dashed lines tying the stratigraphic column to the flux results. **B.** Solid horizontal lines mark lithostratigraphic unit boundaries. Flux results quantify the late Neogene and Quaternary influence of terrigenous sedimentation associated with glaciation and the latest Miocene–early Pliocene pulse of diatom sedimentation.

(Figs. 23, 24, and 27) and increases in porosity and water content. The reduced clay content and increased biogenic silica in the sediments at approximately 90 mbsf might account for the changes noted. Below 110 mbsf, less variability is seen in the index property profiles than in the upper part (Figs. 23, 24, and 27), probably the result of the more homogeneous nature of the sediment. Below 110 mbsf, bulk densities and grain density decrease slightly downhole, corresponding to increases in water content and porosity. Below 165 mbsf, bulk densities and grain density increase slightly, again corresponding to decreases in porosities and water contents, probably the result of the increased carbonate content in the top of lithologic Subunit IIB.

At approximately 265 mbsf, a sharp increase is seen in grain-density and bulk-density values and a corresponding decrease in porosity and water content (Figs. 24 and 27), probably the result of the increased clay and gravel contents in lithologic Unit III. Basalt (lithologic Unit IV) was cored in the base of Hole 887D. The index properties from basalts are shown at the end of Table 11. The trend reflected in the index property profiles shows a sharp contact between lithologic Units I and II and also between Units II and III.

Shear strengths in cores from Holes 887A and 887C generally increase downhole (Fig. 29). At a depth of 130 mbsf in Hole 887A, shear strength values decrease from approximately 100 to 20 kPa.

Table 5. Listing of average sediment data and flux $\text{g}(\text{cm}^{-2}\cdot\text{k.y.})^{-1}$ results for five time-stratigraphic intervals at Site 887.

Depth (mbsf)	Age (Ma)	Dry-bulk density (g/cm^3)	Linear sed. rate ($\text{cm}/\text{k.y.}$)	Diatoms		Clay		Glass		Quartz		Carbonate		TOC	
				(%)	$\text{g}(\text{cm}^{-2}\cdot\text{k.y.})^{-1}$	(%)	$\text{g}(\text{cm}^{-2}\cdot\text{k.y.})^{-1}$	(%)	$\text{g}(\text{cm}^{-2}\cdot\text{k.y.})^{-1}$	(%)	$\text{g}(\text{cm}^{-2}\cdot\text{k.y.})^{-1}$	(%)	$\text{g}(\text{cm}^{-2}\cdot\text{k.y.})^{-1}$	(%)	$\text{g}(\text{cm}^{-2}\cdot\text{k.y.})^{-1}$
0–56.25	0–1.05	0.71	5.36	14	0.53	24	0.91	4.00	0.150	4.00	0.15	5.82	0.220	0.35	0.0100
56.25–87.30	1.05–2.60	0.86	2.00	5	0.09	44	0.76	2.50	0.040	7.50	0.13	2.16	0.040	0.29	0.0050
87.30–169.00	2.60–5.71	0.51	2.63	80	1.07	11	0.15	0.33	0.004	0.89	0.01	0.11	0.001	0.11	0.0010
169–235.15	5.71–11.38	0.54	1.17	54	0.34	18	0.11	0.71	0.004	0	0.00	15.99	0.100	0.07	0.0004
235.15–265.00	11.38–17.00	0.51	0.53	23	0.06	23	0.06	3.33	0.009	0	0.00	8.04	0.020	0.06	0.0002

Cores 145-887A-15X through -21X (130–193 mbsf) were cored using the XCB and were badly disturbed, which might account for the lower shear strength values. Below 193 mbsf in Hole 887A, values increase again downhole. In an attempt to reduce coring disturbance, Cores 145-887A-22H through -29H were taken with the APC. Below 250 mbsf, shear strengths increase sharply in Holes 887A and 887C, probably the result of a change in sediment type from siliceous ooze to clay and gravel, in the top of lithologic Unit III.

GRAPE Data

GRAPE bulk-density data have been plotted in Figures 24, 26, and 28. Data from the GRAPE have been smoothed using a 29-point moving average (except in Fig. 28). The GRAPE bulk-density trends from all holes drilled at Site 887 paralleled those measured with the helium pycnometer, although the GRAPE bulk-density values were consistently higher (by approximately $0.1 \text{ g}/\text{cm}^3$) than those obtained using the helium pycnometer (see "Physical Properties" section, "Sites 885/886," chapter, this volume). In lithologic Unit I, the GRAPE bulk-density values are highly variable. In the clay-rich Subunit IB (45–90 mbsf), the GRAPE values are more variable than those in Subunit IA (0–4 mbsf). GRAPE bulk-density values were higher in the clay-rich intervals (Fig. 28) than those in the biogenic silica-rich intervals. The distinct decrease in the GRAPE bulk density to an average $1.45 \text{ g}/\text{cm}^3$ at approximately 90 mbsf corresponds to a change in sediment type from clay above 90 mbsf to a diatom ooze below that. The increase in biogenic silica and decrease in clay content might easily account for the changes observed. Below 90 mbsf, GRAPE bulk densities decrease slightly downhole. The next change in the GRAPE bulk-density values occurs at approximately 155 mbsf in Hole 887A and 170 mbsf in Hole 887C. Below these points, GRAPE bulk densities increase downhole, probably the result of increased carbonate content in the top of lithologic Subunit IIB. Between 130 and 193 mbsf, GRAPE bulk-density values were lower in Hole 887A than those in Hole 887C, probably the result of the previously mentioned core disturbance. At approximately 265 mbsf, a distinct increase can be seen in GRAPE bulk density values. Below this point, GRAPE bulk-density values increase sharply to an average

$1.8 \text{ g}/\text{cm}^3$, probably the result of increased clay and gravel contents in the top of lithologic Unit III.

Compressional Wave Velocities

Figures 30 and 31 show profiles of compressional wave velocities from the P-wave logger and the digital sound velocimeter (DSV). The spiky nature of P-wave logger and DSV data, especially in the upper 90 mbsf (lithologic Unit I), corresponds to variations in sediment lithology between clay- and biogenic silica-rich intervals, and may also be attributed to the presence of ice-rafted debris (IRD) and ash layers. In the upper 90 mbsf, average P-wave velocity values range between 1520 and 1550 m/s. At approximately 90 mbsf, an increase in P-wave velocities occurs, the result of change in sediment type from clay to diatom ooze. Below this point, P-wave velocities range between 1540 and 1600 m/s and generally increase slightly downhole. The compressional wave velocities of the basalt cored in the base of Hole 887D were measured using the Hamilton Frame. The P-wave velocity values of the basalt range between 3840 and 5000 m/s (Table 16).

Thermal Conductivity

Thermal conductivity profiles are shown in Figures 29 and 31. In the upper 90 mbsf, thermal conductivity varies between 0.7 and $1.8 \text{ W}/(\text{m} \cdot ^\circ\text{C})$. The top of lithologic Subunit IIA is marked by a sharp decrease in thermal conductivity. Below 150 mbsf, thermal conductivity increases generally downhole. Thermal conductivity appears to be related to changes in the lithostratigraphy, not porosity.

DOWNHOLE MEASUREMENTS

Logging Operations and Quality of Logs

The Schlumberger Quad combination and formation microscanner (FMS) tools were the only tools run at Hole 887D. The FMS tool string stuck in the pipe as it was being pulled out of the hole, and tool recovery activities precluded any further logging. The wireline heave compensator (WHC) was used to counter any ship's heave resulting from mild sea-state conditions (1–2 m wave amplitude). Base of pipe

Table 6. Interstitial-water data for Hole 887A.

Core, section, interval (cm)	Depth (mbsf)	pH	Alk. (mM)	S (g/kg)	Cl (mM)	Mg (mM)	Ca (mM)	SO ₄ (mM)	NH ₄ (μM)	NO ₂ (μM)	H ₄ SiO ₄ (μM)	K (mM)	Li (μM)	Na (mM)	Sr (μM)	Mn (μM)	Mg/Ca (mol ratio)
145-877A-																	
H-1, 145-150	1.45	7.67	3.59	35.0	554	51.3	10.5	28.6	53	0	863	11.8	27.2	479	87	53	4.89
2H-2, 145-150	9.65	7.60	5.24	35.2	556	51.5	10.5	26.8	212	0	1059	11.5	24.5	479	90	86	4.90
3H-2, 145-150	19.15	7.60	6.00	36.0	558	52.3	10.8	26.6	269	0	864	10.7	24.1	480	92	99	4.86
4H-2, 145-150	28.65	7.64	5.84	36.0	561	51.1	10.5	25.9	328	0	974	11.6	23.8	483	91	98	4.86
5H-2, 115-120	38.15	7.72	5.62	36.0	563	50.6	10.6	25.7	332	n.m.	958	11.7	22.7	485	92	82	4.80
6H-2, 145-150	47.65	7.75	5.80	36.0	560	52.1	11.1	25.1	302	n.m.	830	10.2	23.0	479	94	95	4.69
8H-2, 145-150	66.65	7.67	5.12	35.5	562	50.5	10.9	25.7	428	n.m.	921	12.1	20.6	483	90	83	4.61
10H-2, 145-150	85.65	7.63	4.26	35.5	559	50.2	11.0	25.8	275	n.m.	824	11.0	22.5	481	90	90	4.57
12H-4, 145-150	107.65	7.72	3.57	35.5	558	50.8	10.9	26.5	242	n.m.	840	11.2	23.9	479	90	62	4.65
14H-4, 145-150	126.65	7.63	3.99	35.5	557	50.8	11.5	26.4	208	n.m.	990	11.2	23.8	478	92	82	4.43
16X-2, 145-150	142.65	7.47	3.74	35.5	556	51.8	11.5	26.6	178	n.m.	883	10.0	24.1	476	94	78	4.51
20X-4, 145-150	180.05	7.53	3.55	35.5	556	51.1	12.0	26.9	149	n.m.	1227	10.0	26.3	477	96	63	4.27
23H-4, 145-150	208.85	7.56	3.53	35.5	557	50.7	11.8	27.2	212	n.m.	835	10.5	26.1	479	96	79	4.29
27H-2, 145-150	244.15	7.55	3.19	35.0	557	50.6	11.8	27.3	163	n.m.	1062	11.2	27.2	478	94	73	4.31

Note: n.m. = not measured.

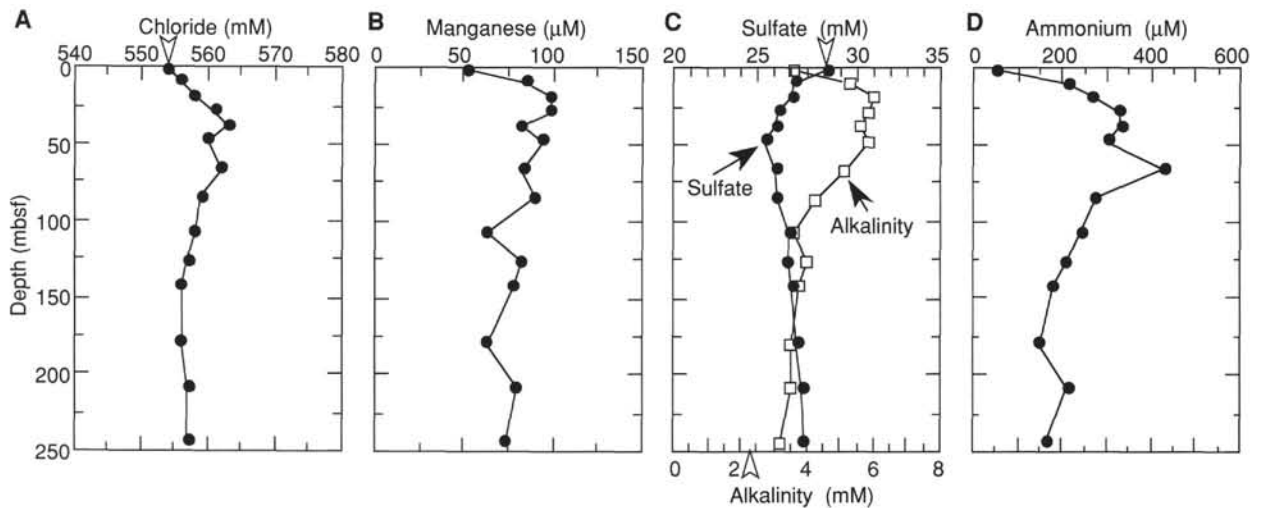


Figure 18. Interstitial-water profiles for Site 887. **A.** Chloride. **B.** Manganese. **C.** Sulfate and alkalinity. **D.** Ammonium. Open arrowheads indicate concentrations of chloride, sulfate, and alkalinity in modern North Pacific Deep Water.

was set at 79 mbsf. The entire depth of Hole 887D (373 mbsf) was logged with the Quad combination and FMS tool strings, although the accumulation of fill in the hole set the base of the logged interval to ~360 mbsf. The logging tool strings used during Leg 145, the basis of their measurement principles, and logging operations are discussed in the “Explanatory Notes” chapter (this volume). Log data presented in this section have not been corrected for environmental factors, nor have these data been depth-shifted to exactly match drilling depths.

The Quad combination tool string with the Lamont temperature tool was run first, and a down-going log was recorded from the end of pipe to total depth (360 mbsf). An up-going log was recorded at 1500 ft/hr from total depth to the mud line. All components of the tool string were functioning properly, with the notable exception of the neutron porosity tool (CNT-G). An uphole data acquisition software problem adversely affected CNT-G data quality, and these data are not considered reliable. For some unknown reason, the spectral resolution of the gamma-ray tool (NGT) was diminished during Quad logging, and while the total gamma-ray log (SGR) is reliable, the individual spectral components (K, Th, and U) must be interpreted with caution. The gamma-ray data shown in Figure 32 were measured by the NGT tool of the FMS string. The caliper on the high-temperature lithodensity tool (HLDT) tool and the two orthogonal FMS calipers indicated that the borehole diameter exceeded 18 in. over most of the sedimentary sections of the hole (above ~285 mbsf). High log density correction values and noisy bulk density above 115 mbsf data from the HLDT suggest that this HLDT tool was unable to maintain close contact with the borehole wall, because of extremely large diameters (much greater than 18 in.). The alternating hard and soft lithologies within lithologic Unit IV (interlayers of sediment and basalt) caused some cycle skipping within the sonic velocity log below 280 mbsf. The FMS caliper data are shown adjacent to the Quad bulk density, resistivity, and sonic velocity data in Figure 33.

The FMS tool string was run into the hole, and a total of six logs were recorded: five within lithologic Unit IV (basalt) and one main up going log from total depth (360 mbsf) to the base of the pipe at 80 mbsf. All logs were recorded at 1000 ft/hr. The FMS tool string became stuck in the pipe as the tool was being pulled out of the hole. After several unsuccessful attempts to pull the tool past the pipe crossover, which was roughly 120 m above the base of the BHA, we were forced to abandon further logging at Hole 887D and begin the operations to rescue the tools. A device was sent down the wire line to crimp, then cut, the wire line just above the tool so that it would not slip out while the drill pipe was being tripped out. The tool string was recovered intact at the depth where it had stuck; one imaging pad

had been damaged and almost completely severed away from its caliper arm. This damage was most probably incurred when the tool was abutting the hard basalt ledges within lithologic Unit IV (see FMS caliper data, Fig. 33).

Results

Borehole Temperatures

Borehole temperatures measured using the Lamont temperature tool (TLT) reflect the temperature of the seawater in the borehole, rather than the true temperature of the formation. The formation cools during drilling because of circulation of cold seawater during the wiper trip, and it is only after drilling has ceased that the temperatures can begin to rebound. The deployment of the TLT on the Quad tool string about 10 hr after the end of the wiper trip yielded a bottom-hole temperature of 1.8°C (Fig. 34). A similar temperature log was not recorded during the FMS run, so it is not possible to estimate heat flow from this single temperature log.

Lithology

Variations in the logging data reflect changes in the physical and chemical properties of the formation. Figures 32 and 33 show the Hole 887D logging data adjacent to the major lithology variations, as determined primarily from visual and smear slide analyses (see “Lithostratigraphy” section, this chapter). In contrast to logging data at the Detroit Seamount sites (Sites 883 and 884), there appears to be less expression of the major lithological boundaries in the logs at this site. This results, in part, to a scaling effect because the basalt layers within Unit IV have high density and resistivity values, and variations within the overlying sediments column are muted.

The natural gamma-ray logs from the FMS NGT (Fig. 32) show a sharp decrease in K and Th values, corresponding to the transition from lithologic Subunits IB to IIA at 90 mbsf. This transition from a clay-rich (Subunit IB) to a diatom-rich, clay-poor (Subunit IIA; 90–174 mbsf) lithology is indicated by reduced gamma-ray, resistivity, sonic velocity, and bulk density logging values. The diatom ooze lithology of Subunit IIA results in a higher porosity, lower density, and less rigid sediment section. Lithologic Subunit IIB (174–235 mbsf) is a calcareous diatom ooze, and the logs show several small increases in resistivity, sonic velocity, and bulk density that reflect the increased sediment rigidity caused by higher carbonate abundances. A short, but well-defined, increase in these physical properties identifies a thin carbonate-rich interval near 212 mbsf (Figs. 32 and 33).

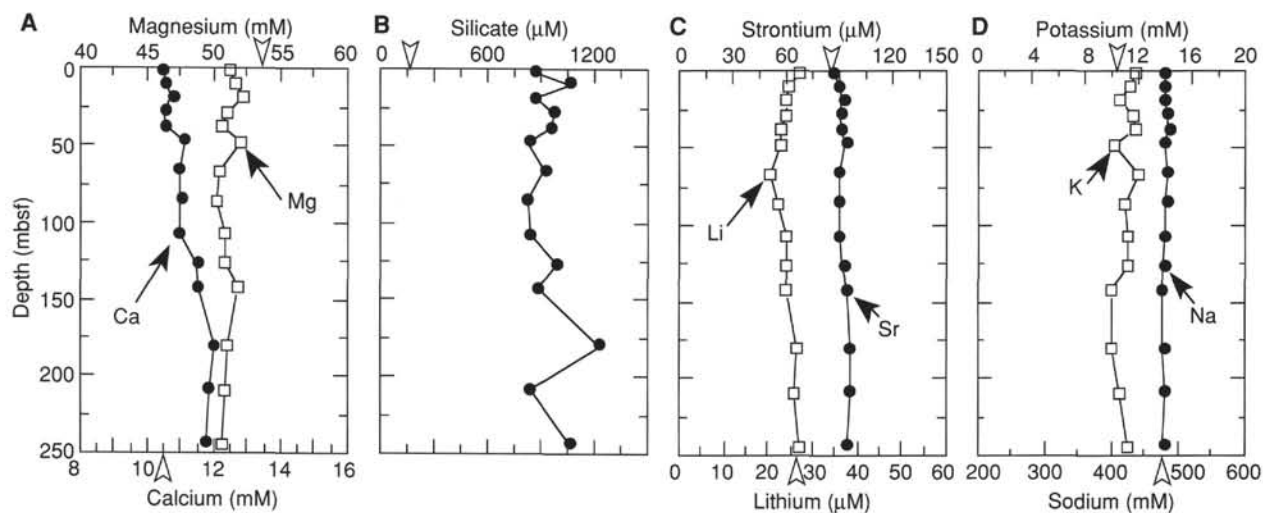


Figure 19. Interstitial-water profiles for Site 887. **A.** Magnesium and calcium. **B.** Silicate. **C.** Strontium and lithium. **D.** Potassium and sodium. Open arrowheads indicate respective concentrations in modern North Pacific Deep Water.

The boundary between Subunit IIB and Subunit IIC (235–270 mbsf) is gradational, based on the core smear slide observations (see “Lithostratigraphy” section, this chapter), and this transition is not easily recognized within the logging data.

The top of Unit III (270–289 mbsf), a clay with ash and iron oxides, is defined by a sharp contact with the overlying Subunit IIC. The resistivity and bulk density logs show variable, but significant, increases; a trend toward increased gamma-ray log values is seen within Unit III. The most dramatic changes occur within the alternating basalt-sediment lithologies of Unit IV (289–373 mbsf). Drilling within Unit IV indicated several zones having relatively rapid rates of penetration, which suggests possible sediment interbeds. Chalk was observed as a coherent sediment and as a coating on several of the basalt gravel pieces within Cores 145-887D-6R and -8R (see “Igneous Petrology” section, this chapter).

The interlayered basalt-sediment stratigraphy of lithologic Unit IV is illustrated by the bulk density and resistivity logs presented in Figure 33. The FMS caliper, SGR, resistivity, and bulk density data from this interval (265–345 mbsf) are shown at an expanded scale in Figure 35. These logs demonstrate that at least five separate basalt layers separated by sediment interbeds. In particular, the resistivity and density logs identify a thick, uniform basalt layer between 307 and 322 mbsf. This layer was probably recovered in Cores 145-887D-7R and -8R, which contained several long sections of highly plagioclase phryic basalt.

Comparison of Logs with Core-based Physical Property Measurements

The logging and core-based bulk density measurements are displayed in Figure 36. The logging bulk density measurements were taken from the HLDT and have been smoothed by a linear five-point (0.76-m) moving average filter. The core bulk density measurements were performed in discrete samples (see “Physical Properties” section, this chapter). Good overall correlation can be seen between the two types of measurements, although the discrete core samples are, on average, 0.1 g/cm³ less dense than those derived from the logs. The origin of this error is uncertain; core bulk density measurements were back-calculated from dry volumes to account for expansion of samples caused by the rebound effect, but the error may be related to water adsorption by the samples during recovery or while at the surface. A discrepancy in correlation between the core and logging values occurs with the basalt Unit IV, where the core density values exceed those of the logging estimates. Unlike the pycnometer analyses for the rest of

the hole, the core density estimates from this interval were calculated from 2-min GRAPE analysis integrations (see “Physical Properties” section, this chapter). The highly variable logging density data above 110 mbsf may be attributed to poor tool contact with the borehole wall over this interval; the FMS and density caliper data indicate wide borehole diameters within this interval (>18 in.). Although some measurement error is indicated by the density correction logging data, the core density data demonstrate that considerable real density variability exists within lithologic Subunits IA and IB. We have attributed this to the presence of discrete diatom-rich intervals that have high porosity and low bulk density values (see “Physical Properties” and “Lithostratigraphy” sections, this chapter).

Porosity can be determined from the resistivity logs by using Archie’s equation (Archie, 1942):

$$S_w a = a R_w / f m R_i,$$

Here, S_w is water saturation, equal to 1 for these virtually hydrocarbon-free sediments; R_w is resistivity of the formation water, f is the fractional porosity, R_i is the measured formation resistivity, and both a and m are constants, depending on lithology and pore geometry. In this case, we calculated porosity using the medium phasor induction resistivity log (IMPH) from the dual induction tool (DITE) with set values of $a = 1$ and $m = 2$. R_w was set at 0.4 ohm-m, based on seawater resistivity estimates at 2°C, the ambient borehole fluid temperature. Little borehole temperature variation was found during the Quad logging run; thus, R_w was set as a constant in this first-order porosity calculation. The calculated porosities have excellent overall correlation with those determined from discrete core samples (Fig. 37).

SEISMIC-LITHOLOGIC CORRELATION

All the Leg 145 drilling locations were surveyed in order to drop the beacon at the proper pre-selected location. In each case, the surveys were run in the figure of the number 4 with the long leg duplicating the site-survey trackline used to select the site, and the cross-leg being as nearly orthogonal as practical. The shipboard air-gun seismic reflection profiling system was used for all the surveys, except for Site 883 when it was inoperable; the 3.5-kHz profiling system was used to locate that drill site. Details of the surveying and seismic processing techniques are given in the Site 881 chapter (see “Seismic-Lithologic Correlation” section, “Site 881” chapter, this volume).

Site 887 is located on the platform level of the Patton-Murray Seamounts (Fig. 2), where just under 0.4 s of sediment overlies basaltic

Table 7. Results of headspace gas analyses from Holes 887A and 887C.

Core, section, interval (cm)	Depth (mbsf)	C ₁ (ppm)
145-887A-		
1H-2, 0-3	1.5	3
2H-3, 0-3	9.7	4
3H-3, 0-3	19.2	7
4H-3, 0-3	28.7	6
5H-3, 0-3	38.2	5
6H-3, 0-3	47.7	6
7H-3, 0-3	57.2	7
8H-3, 0-3	66.7	4
9H-3, 0-3	76.2	3
10H-3, 0-3	85.7	2
11H-5, 0-3	98.2	2
12H-5, 0-3	107.7	3
13H-5, 0-3	117.2	3
14H-5, 0-3	126.7	3
15X-3, 0-3	133.2	3
16X-3, 0-3	142.7	2
17X-3, 0-3	148.1	3
18X-3, 0-3	157.8	4
20X-5, 0-3	180.1	4
21X-2, 0-3	185.2	6
22H-3, 0-3	196.4	7
23H-5, 0-3	208.9	5
24H-4, 0-3	216.9	4
25H-4, 0-3	226.4	6
27H-3, 0-3	244.2	7
28H-5, 0-3	256.7	5
29H-2, 0-3	261.7	4
145-877C-		
6H-5, 0-3	48.3	4
7H-5, 0-3	57.8	4
8H-2, 0-3	62.8	4
9H-2, 0-3	66.3	3
10H-3, 0-3	77.3	3
11H-4, 0-3	88.3	3
12H-5, 0-3	99.3	3
13H-6, 0-3	110.3	3
14H-4, 0-3	116.8	3
15H-4, 0-3	126.3	3
16H-4, 0-3	135.8	2
17H-4, 0-3	145.3	3
18H-4, 0-3	154.8	4
19H-4, 0-3	164.3	3
20H-4, 0-3	173.8	4
22H-4, 0-3	192.8	6
23H-4, 0-3	202.3	6
24H-4, 0-3	211.8	3
25H-4, 0-3	221.3	3
26H-5, 0-3	232.3	7
27H-5, 0-3	241.8	2
28H-5, 0-3	251.3	7
29H-5, 0-3	260.8	5
30H-5, 0-3	270.3	4

Note: All samples are headspace samples. C₁ = methane.

basement (Fig. 38). The thin clays and gravels of Unit III are not readily distinguishable from basement. The siliceous oozes of lithologic Unit II form the more acoustically transparent middle part of the section. The upper more reflective portion of the profile corresponds to Unit I, siliceous clays and clays with ash and dropstones.

SUMMARY AND CONCLUSIONS

Geologic Record

Three sedimentary units having a total thickness of 289 m and basalt were recovered at Site 887 in the Gulf of Alaska (Figs. 1 and 2). The sedimentary section, early Miocene to Quaternary in age, can be divided into three lithologic units, two of which have subunits. Subunit IA (0–45 mbsf) is a greenish-gray, siliceous silty clay of Pleistocene age. Diatom layers averaging roughly 30 cm thick occur at a 1-m spacing in the silty clays. Ash layers are common, and dropstones are abundant in this unit. Subunit IB (45–90 mbsf) is a Pleistocene to

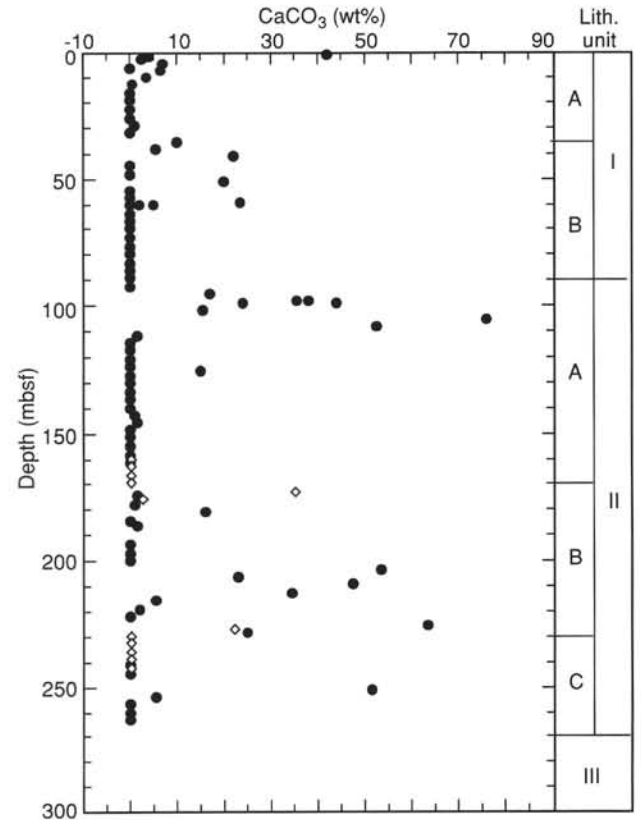


Figure 20. Plot of calcium carbonate contents vs. depth below the seafloor at Site 887. Lithologic units are shown at the right. Solid circles = Hole 887A; diamonds = Hole 887C.

upper Pliocene clay with a few diatomaceous layers. Dropstones and ash layers are common, and calcareous horizons occur intermittently in this subunit.

Lithologic Subunit IIA (90–174 mbsf) is an upper Pliocene to upper Miocene, gray-to-brown homogeneous diatom ooze. A few ash layers and one dropstone horizon, at approximately 130 mbsf, occur in this subunit. Subunit IIB (174–235 mbsf) is an upper Miocene to middle Miocene, gray calcareous diatom ooze. A few ash layers occur in the lower part of the subunit. Subunit IIC (235–270 mbsf) is a middle Miocene to lower Miocene, clayey siliceous ooze dominated by poorly preserved diatoms and radiolarians. Ash layers occur throughout the subunit. Lithologic Unit III (270–289 mbsf) is a lower Miocene brown clay that occurs just above the basalt in Hole 887D. In Hole 887A, several meters of basaltic pea gravel in a clay slurry was encountered at the bottom of the hole resting on basalt, evidence of the local variability of basement cover on this seamount platform.

Lithologic Unit IV is represented by the 16.3 m of basalt recovered from drilling 87.3 m into the basement. These basalts range from highly clinopyroxene-plagioclase phyric basalt in the upper portion to moderately plagioclase phyric basalt to sparsely plagioclase phyric basalt near the bottom of the hole. From logging runs into the basement, we were able to define a compound edifice that consists of at least three, and possibly four, flows or sills with intervening sediment layers. The upper intrabasalt sediment layer is an Oligocene nannofossil chalk. Hole 887D provides an intriguing glimpse into the geology of these kinds of volcanic constructions.

Calcareous fossils are present in the Miocene and lower Pliocene parts of the section, but in the Pleistocene section, sediments are present only in discrete, apparently cyclic, horizons; most of the Pleistocene section is barren. Diatoms are abundant and provide the

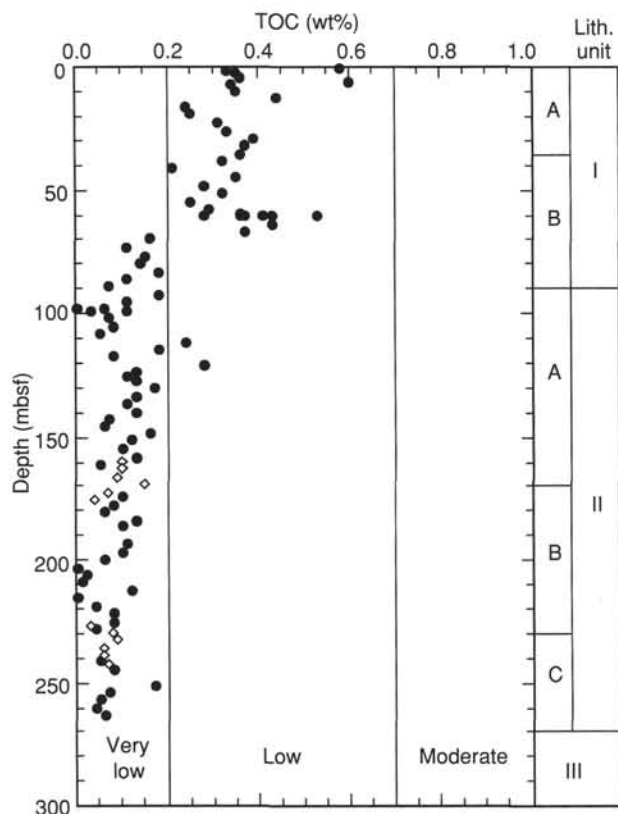


Figure 21. Plot of total organic carbon contents vs. depth below the seafloor at Site 887. Lithologic units are shown at the right. Solid circles = Hole 887A; diamonds = Hole 887C.

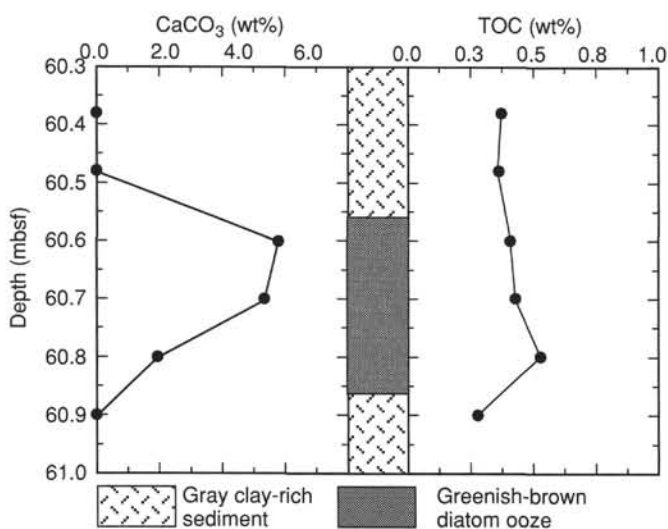


Figure 22. Plot of total organic carbon and calcium carbonate contents vs. depth below seafloor (Section 145-887A-7H-5). Sediment lithology and color are shown in the center.

basic biostratigraphic zonation, as they have for the other Leg 145 drill sites. Radiolarians are common throughout the section. Reworked middle Miocene forms of these fossils occur in the upper Miocene and lower Pliocene sediments.

In addition to the biostratigraphy provided by the siliceous microfossils, a magnetic reversal stratigraphy complete to 18 Ma has been

constructed for essentially the entire section of APC Hole 887C (0–270 mbsf). This stratigraphy provides a framework for calibration of microfossil zonation and allows one to determine well-constrained sedimentation rates. Subunit IA, the siliceous clays, has a linear sedimentation rate of about 61 m/m.y. that pertains from 0 to 0.74 Ma. Sedimentation rates decline more or less continuously down the core and are about 25 m/m.y. in the Pliocene and lower Pleistocene portions of the section, 0.74 to 5.8 m.y. in age, are 10 m/m.y. in the middle and upper Miocene parts. The lower Miocene clays may have a linear sedimentation rate of perhaps 2 m/m.y. Casting the sedimentation rates as mass accumulation rates (MAR) allows for differentiation of the flux of the major sedimentary components. Terrigenous materials, recorded aboard the ship as clay plus quartz, increased in flux by nearly an order of magnitude at the time of the onset of Northern Hemisphere glaciation from 0.10 to 0.15 $\text{g}(\text{cm}^2 \cdot \text{k.y.})^{-1}$ in the Miocene and lower and middle Pliocene sediments to about 1.0 $\text{g}(\text{cm}^2 \cdot \text{k.y.})^{-1}$ in sediments younger than 2.6 Ma. The greatest flux of terrigenous materials occurs in the youngest portion of the section, in materials younger than 0.74 Ma. Diatoms, the other major sedimentary component, reach their flux maxima in the lower and middle Pliocene portions of the section, where they accumulate at over more than 1.0 $\text{g}(\text{cm}^2 \cdot \text{k.y.})^{-1}$ in the time interval between 2.6 and 5.7 Ma. The lower Pliocene period of greatly enhanced diatom deposition, observed during Leg 145 throughout the North Pacific Ocean, also is present in the Gulf of Alaska.

Paleoceanography and Paleoclimatology

The Patton-Murray Seamount edifice was extruded during in the latest Oligocene onto seafloor that was already 10 to 12 m.y. old. Volcanic activity must have continued for at least one or two m.y., as demonstrated by the series of sills or flows with sedimentary interlayers. Seamount peaks stand as much as 3000 m above the platform level, which in turn is 1500 m above the seafloor. Those peaks must have stood above sea level, and the well-rounded pea gravel in the bottom core of Hole 887A implies shallow-water processes prior to downslope emplacement.

Sediment deposition was initially slow and with little carbonate. Calcite becomes a noticeable contributor to the sediments only within Subunit IIB, which is of late Miocene age. Clearly, the CCD did not become deeper through the past 10 to 15 m.y. at Patton-Murray Seamounts, as it did elsewhere in the Pacific Ocean (Berger, 1973; van Andel et al., 1975; Rea and Leinen, 1985). In that sense, its behavior is similar to that observed for the Northwest Pacific Ocean; However, it is not possible to discern the extent of any vertical excursions from a single site.

Diatom fluxes reflect the pattern observed during Leg 145 throughout the North Pacific Ocean and reached a maxima during the latest Miocene and early Pliocene. At Site 887 that maxima is on the order of 1 $\text{g}(\text{cm}^2 \cdot \text{k.y.})^{-1}$, approximately a three-fold increase in MAR compared to that in both underlying and overlying sediments.

The onset of Northern Hemisphere glaciation had a strong effect on sedimentation in the Gulf of Alaska. The flux of opal was greatly reduced, and the sediments have become dominated by terrigenous grains of clay and quartz. The timing of ice-rafting in the Gulf of Alaska was first studied by the scientists of DSDP Leg 18 (von Huene et al., 1973; 1976), based on recovery from rotary cores. The Site 887 information demonstrates that IRD became significant exactly at the 2.6-Ma magnetic reversal that marks the onset of glaciation. Lower Pliocene dropstone horizons that are about 4.5 m.y. old may represent the marine record of alpine glaciation in southeastern Alaska, indicated by the onshore geology (Lagoe et al., in press). Dropstones are far more abundant in the Gulf of Alaska than in the Northwest Pacific Ocean and are of different lithology, confirming the pronounced Alaskan source of IRD suggested by Rea and Schrader (1985). The pan-Pacific dropstone record should allow us to compare timing and pulses of glaciation in Siberia and North America.

The terrigenous materials, hemipelagic in the lower portion of the core with increasing contribution from ice-rafting up the section, become coarser and accumulate more rapidly in the upper 45 m of the section, in Subunit IA. The age of this change is approximated by the Brunhes/Matuyama reversal boundary at 0.74 Ma and may correspond to the increased amplitude of glacial cycles, as recorded in the marine oxygen-isotope signal.

REFERENCES*

- Archie, G.E., 1942. The electrical resistivity log as an aid in determining some reservoir characteristics. *Trans. Am. Inst. Min. Metall. Pet. Eng.*, 146:54–62.
- Baldauf, J.G., Thomas, E., Clement, B., Takayama, T., Weaver, P.P.E., Backman, J., Jenkins, G., Mudie, P.J., and Westberg-Smith, M.J., 1987. Magnetostratigraphic and biostratigraphic synthesis, Deep Sea Drilling Project Leg 94. In Ruddiman, W.F., Kidd, R.B., et al., *Init. Repts. DSDP*, 94 (Pt. 2): Washington (U.S. Govt. Printing Office), 1159–1205.
- Barron, J.A., 1985. Late Eocene to Holocene diatom biostratigraphy of the equatorial Pacific Ocean, Deep Sea Drilling Project Leg 85. In Mayer, L., Theyer, F., Thomas, E., et al., *Init. Repts. DSDP*, 85: Washington (U.S. Govt. Printing Office), 413–456.
- Barron, J.A., and Baldauf, J.G., 1990. Development of biosiliceous sedimentation in the North Pacific during the Miocene and Early Pliocene. In Tsuchi, R. (Ed.), *Pacific Neogene Events: Their Timing, Nature and Interrelationship*: Tokyo (Univ. of Tokyo Press), 43–63.
- Berger, W.H., 1973. Cenozoic sedimentation in the eastern tropical Pacific. *Geol. Soc. Am. Bull.*, 84:1941–1954.
- Cande, S.C., and Kent, D.V., 1992. A new geomagnetic polarity timescale for the Late Cretaceous and Cenozoic. *J. Geophys. Res.*, 97:13917–13951.
- Foreman, H.P., 1975. Radiolaria from the North Pacific, Deep Sea Drilling Project, Leg 32. In Larson, R.L., Moberly, R., et al., *Init. Repts. DSDP*, 32: Washington (U.S. Govt. Printing Office), 579–676.
- Hays, J.D., 1970. Stratigraphy and evolutionary trends of radiolaria in North Pacific deep sea sediments. In Hays, J.D. (Ed.), *Geological Investigations of the North Pacific*. Mem.—Geol. Soc. Am., 126:185–218.
- Hays, J.D., and Shackleton, N.J., 1976. Globally synchronous extinction of radiolarian *Stylatractus universus*. *Geology*, 4:649–652.
- Heath, G.R., Burckle, L.H., et al., 1985. *Init. Repts. DSDP*, 86: Washington (U.S. Govt. Printing Office).
- Keigwin, L.D., 1987. North Pacific deep water formation during the latest glaciation. *Nature*, 330:363–364.
- Lagoë, M.B., Eyles, C.H., Eyles, N., and Hale, C., in press. Timing of late Cenozoic tidewater glaciation in the far North Pacific Ocean. *Geol. Soc. Am. Bull.*
- Landing, W.M., and Bruland, K.W., 1980. Manganese in the North Pacific. *Earth Planet. Sci. Lett.*, 49:45–46.
- Ling, H.Y., 1973. Radiolaria: Leg 19 of the Deep Sea Drilling Project. In Creager, J.S., Scholl, D.W., et al., *Init. Repts. DSDP*, 19: Washington (U.S. Govt. Printing Office), 777–797.
- McDuff, R.E., 1985. The chemistry of interstitial waters, Deep Sea Drilling Project, Leg 86. In Heath, G.R., Burckle, L.H., et al., *Init. Repts. DSDP*, 86: Washington (U.S. Govt. Printing Office), 675–687.
- Morley, J.J., Hays, J.D., and Robertson, J.H., 1982. Stratigraphic framework for the late Pleistocene in the northwest Pacific ocean. *Deep-Sea Res. Part A*, 29:1485–1499.
- Morley, J.J., and Shackleton, N.J., 1978. Extension of the radiolarian *Stylatractus universus* as a biostratigraphic datum to the Atlantic Ocean. *Geology*, 6:309–311.
- Perch-Nielsen, K., 1985. Silicoflagellates. In Bolli, H.M., Saunders, J.B., and Perch-Nielsen, K. (Eds.), *Plankton Stratigraphy*: Cambridge (Cambridge Univ. Press), 811–846.
- Rea, D.K., and Leinen, M., 1985. Neogene history of the calcite compensation depth and lysocline in the South Pacific Ocean. *Nature*, 316:805–807.
- Rea, D.K., and Schrader, H., 1985. Late Pliocene onset of glaciation: ice rafting and diatom stratigraphy of North Pacific DSDP cores. *Palaeogeogr. Palaeoclimatol., Palaeoecol.*, 49:313–325.
- Riedel, W.R., and Sanfilippo, A., 1970. Radiolaria, Leg 4, Deep Sea Drilling Project. In Bader, R.G., Gerard, R.D., et al., *Init. Repts. DSDP*, 4: Washington (U.S. Govt. Printing Office), 503–575.
- , 1978. Stratigraphy and evolution of tropical Cenozoic radiolarians. *Micropaleontology*, 24:61–96.
- Sakai, T., 1980. Radiolarians from Sites 434, 435, and 436, Northwest Pacific, Leg 56, Deep Sea Drilling Project. In von Huene, R., Nasu, N., et al., *Init. Repts. DSDP*, 56, 57 (Pt. 2): Washington (U.S. Govt. Printing Office), 695–733.
- Scheidegger, K.F., and Kulm, L.D., 1975. Late Cenozoic volcanism in the Aleutian Arc: information from ash layers in the northeastern Gulf of Alaska. *Geol. Soc. Am. Bull.*, 86:1407–1412.
- Scholl, D.W., Marlow, M.S., MacLeod, N.S., and Buffington, E.C., 1976. Episodic Aleutian Ridge igneous activity: implications of Miocene and younger submarine volcanism west of Buldir Island. *Geol. Soc. Am. Bull.*, 87:547–554.
- Thiede, J., and Rea, D.K., 1981. Mass accumulation rates of Barremian to Recent biogenic sediments from the Mid-Pacific Mountains (Deep Sea Drilling Project Site 463) and Hess Rise (Sites 464, 465, 466) central North Pacific Ocean. In Thiede, J., Vallier, T.L., et al., *Init. Repts. DSDP*, 62: Washington (U.S. Govt. Printing Office), 637–651.
- van Andel, T.H., Heath, G.R., and Moore, T.C., 1975. Cenozoic history and paleoceanography of the central equatorial Pacific Ocean. *Mem.—Geol. Soc. Am.*, 143.
- van Morkhoven, F.P.C.M., Berggren, W.A., and Edwards, A.S., 1986. Cenozoic cosmopolitan deep-water benthic foraminifera. *Bull. Cent. Rech. Explor.-Prod. Elf-Aquitaine*, Mem. 11.
- von Huene, R., Crouch, J., and Larson, E., 1976. Glacial advance in the Gulf of Alaska area implied by ice rafted material. In Cline, R.M., and Hays, J.D. (Eds.), *Investigation of Late Quaternary Paleocceanography and Paleoclimatology*. Mem.—Geol. Soc. Am., 145:411–422.
- von Huene, R., Larson, E., and Crouch, J., 1973. Preliminary study of ice-rafted erratics as indicators of glacial advances in the Gulf of Alaska. In Kulm, L.D., von Huene, R., et al., *Init. Repts. DSDP*, 18: Washington (U.S. Govt. Printing Office), 835–842.
- Woodruff, F., and Savin, S.M., 1989. Miocene deepwater oceanography. *Paleoceanography*, 4:87–140.
- Zahn, R., Pedersen, T.F., Bornhold, B.D., and Mix, A.C., 1991. Water mass conversion in the glacial subarctic Pacific (54°N, 148°W): physical constraints and the benthic-planktonic stable isotope record. *Paleoceanography*, 6:543–560.

* Abbreviations for names of organizations and publication titles in ODP reference lists follow the style given in *Chemical Abstracts Service Source Index* (published by American Chemical Society).

Ms 145IR-110

NOTE: For all sites drilled, core-description forms (“barrel sheets”) and core photographs can be found in Section 3, beginning on page 395. Forms containing smear-slide data can be found in Section 4, beginning on page 985. Thin-section data are given in Section 5, beginning on page 1013. Conventional log and FMS data can be found in CD-ROM form (back pocket).

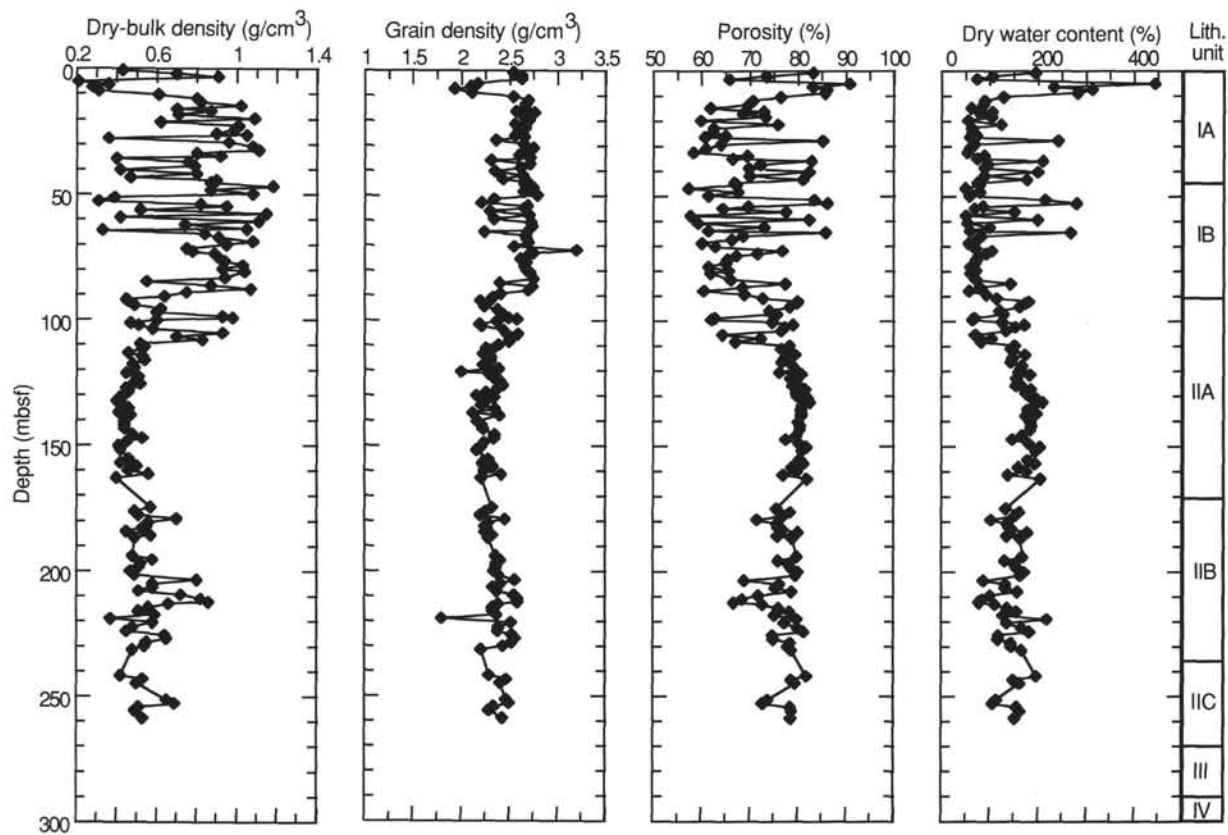


Figure 23. Plots of index property data vs. depth for Hole 887A. Lithologic units are shown at right.

Table 8. Results of geochemical analyses from Holes 887A and 887C.

Core, section, interval (cm)	Depth (mbsf)	TC (wt%)	IC (wt%)	TOC (wt%)	CaCO ₃ (wt%)	TN (wt%)
145-887A-						
1H-1, 72-73	0.72	5.56	4.98	0.58	41.50	0.08
1H-2, 76-77	2.26	0.77	0.44	0.33	3.70	0.04
1H-3, 41-42	3.41	0.63	0.28	0.35	2.30	0.05
1H-4, 73-74	5.23	1.16	0.80	0.36	6.70	0.06
1H-5, 32-33	6.32	0.60	0.00	0.60	0.00	0.08
2H-1, 72-73	7.42	1.13	0.79	0.34	6.60	0.06
2H-3, 72-73	10.42	0.74	0.39	0.35	3.20	0.06
2H-5, 76-77	13.46	0.51	0.07	0.44	0.60	0.06
3H-1, 71-72	16.91	0.24	0.00	0.24	0.00	0.04
3H-3, 71-72	19.91	0.34	0.00	0.25	0.00	0.04
3H-5, 71-72	22.91	0.31	0.00	0.31	0.00	0.05
4H-1, 70-71	26.40	0.33	0.00	0.33	0.00	0.04
4H-3, 74-75	29.44	0.48	0.09	0.39	0.70	0.05
4H-5, 91-92	32.61	0.37	0.00	0.37	0.00	0.05
5H-1, 71-72	35.91	1.54	1.18	0.36	9.80	0.05
5H-3, 71-72	38.91	0.99	0.67	0.32	5.60	0.05
5H-5, 76-77	41.96	2.82	2.61	0.21	21.70	0.00
6H-1, 73-74	45.43	0.35	0.00	0.35	0.00	0.05
6H-3, 73-74	48.43	0.28	0.00	0.28	0.00	0.04
6H-5, 71-72	51.41	2.70	2.38	0.32	19.80	0.04
7H-1, 70-71	54.90	0.25	0.00	0.25	0.00	0.05
7H-3, 70-71	57.90	0.29	0.00	0.29	0.00	0.04
7H-4, 123-124	59.93	3.13	2.77	0.36	23.10	0.04
7H-5, 18-19	60.38	0.37	0.00	0.37	0.00	0.04
7H-5, 28-29	60.48	0.36	0.00	0.36	0.00	0.04
7H-5, 40-41	60.60	1.02	0.61	0.41	5.10	0.06
7H-5, 50-51	60.70	0.99	0.56	0.43	4.70	0.05
7H-5, 60-61	60.80	0.73	0.20	0.53	1.70	0.06
7H-5, 70-71	60.90	0.28	0.00	0.28	0.00	0.02
8H-1, 83-84	64.53	0.43	0.00	0.43	0.00	0.03
8H-3, 65-66	67.35	0.37	0.00	0.37	0.00	0.03
8H-5, 71-72	70.41	0.16	0.00	0.16	0.00	0.03
9H-1, 70-71	73.90	0.11	0.00	0.11	0.00	0.03
9H-3, 70-71	76.90	0.15	0.00	0.15	0.00	0.01
9H-5, 70-71	79.90	0.14	0.00	0.14	0.00	0.01
10H-1, 71-72	83.41	0.18	0.00	0.18	0.00	0.04
10H-3, 86-87	86.56	0.11	0.00	0.11	0.00	0.01
10H-5, 74-75	89.44	0.07	0.00	0.07	0.00	0.01
11H-1, 68-69	92.88	0.18	0.00	0.18	0.00	0.01
11H-3, 67-68	95.87	2.13	2.02	0.11	16.80	0.01
11H-4, 147-148	98.17	4.50	4.53	0.00	37.70	0.03
11H-5, 62-63	98.82	4.30	4.24	0.06	35.30	0.03
11H-5, 71-72	98.91	2.90	2.87	0.03	23.90	0.01
11H-6, 5-6	99.75	5.33	5.22	0.11	43.50	0.02
12H-1, 71-72	102.41	1.92	1.85	0.07	15.40	0.03
12H-3, 85-86	105.55	9.15	9.07	0.08	75.60	0.01
12H-5, 66-67	108.36	6.30	6.25	0.05	52.10	0.02
13H-1, 71-72	111.91	0.41	0.17	0.24	1.40	0.02
13H-3, 68-69	114.88	0.18	0.00	0.18	0.00	0.01
13H-5, 68-69	117.88	0.08	0.00	0.08	0.00	0.02
14H-1, 77-78	121.47	0.28	0.00	0.28	0.00	0.02
14H-3, 77-78	124.47	0.13	0.00	0.13	0.00	0.02
14H-4, 26-27	125.46	1.90	1.79	0.11	14.90	0.02
14H-5, 67-68	127.37	0.13	0.00	0.13	0.00	0.02
15X-1, 71-72	130.91	0.17	0.00	0.17	0.00	0.02
15X-3, 71-72	133.91	0.13	0.00	0.13	0.00	0.03
15X-5, 71-72	136.91	0.11	0.00	0.11	0.00	0.02
16X-1, 69-70	140.39	0.13	0.00	0.13	0.00	0.02
16X-3, 71-72	143.41	0.20	0.13	0.07	1.10	0.02
17X-1, 72-73	145.82	0.20	0.14	0.06	1.20	0.02
17X-3, 73-74	148.83	0.16	0.00	0.16	0.00	0.01
17X-5, 73-74	151.83	0.12	0.00	0.12	0.00	0.02
18X-1, 72-73	155.52	0.10	0.00	0.10	0.00	0.02
18X-3, 70-71	158.50	0.13	0.00	0.13	0.00	0.02
18X-5, 71-72	161.51	0.05	0.00	0.05	0.00	0.01
20X-1, 72-73	174.82	0.26	0.16	0.10	1.30	0.02
20X-3, 71-72	177.81	0.18	0.10	0.08	0.80	0.01
20X-5, 71-72	180.81	1.98	1.92	0.06	16.00	0.01
21X-1, 72-73	184.42	0.13	0.00	0.13	0.00	0.02
21X-3, 71-72	186.91	0.26	0.16	0.10	1.30	0.02
22H-1, 70-71	194.10	0.11	0.00	0.11	0.00	0.01
22H-3, 70-71	197.10	0.10	0.00	0.10	0.00	0.02
22H-5, 70-71	200.10	0.06	0.00	0.06	0.00	0.02
23H-1, 68-69	203.58	6.33	6.39	0.00		

Table 8 (continued).

Core, section, interval (cm)	Depth (mbsf)	TC (wt%)	IC (wt%)	TOC (wt%)	CaCO ₃ (wt%)	TN (wt%)
23H-3, 72-73	206.62	2.74	2.71	0.02	22.60	0.00
23H-5, 80-81	209.70	5.70	5.69	0.01	47.40	0.01
24H-1, 80-81	213.20	4.22	4.10	0.12	34.20	0.01
24H-3, 71-72	216.11	0.61	0.63	0.00	5.20	0.01
24H-5, 71-72	219.11	0.29	0.25	0.04	2.10	0.01
25H-1, 71-72	222.61	0.08	0.00	0.08	0.00	0.02
25H-3, 71-72	225.61	7.65	7.57	0.08	63.10	0.01
25H-5, 71-72	228.61	3.00	2.96	0.04	24.70	0.00
27H-1, 71-72	241.91	0.05	0.00	0.05	0.00	0.00
27H-3, 71-72	244.91	0.08	0.00	0.08	0.00	0.00
28H-1, 71-72	251.41	6.30	6.13	0.17	51.10	0.01
28H-3, 71-72	254.41	0.70	0.63	0.07	5.20	0.02
28H-5, 71-72	257.41	0.05	0.00	0.05	0.00	0.01
29H-1, 71-72	260.91	0.04	0.00	0.04	0.00	0.01
29H-3, 41-42	263.61	0.06	0.00	0.06	0.00	0.02
145-887C-						
19H-1, 72-73	160.52	0.10	0.00	0.10	0.00	0.01
19H-3, 72-73	163.52	0.10	0.00	0.10	0.00	0.02
19H-5, 72-73	166.52	0.09	0.00	0.09	0.00	0.00
20H-1, 72-73	170.02	0.15	0.00	0.15	0.00	0.01
20H-3, 72-73	173.02	4.27	4.20	0.07	35.00	0.02
20H-5, 72-73	176.02	0.37	0.33	0.04	2.70	0.00
26H-1, 71-72	227.01	2.66	2.63	0.03	21.90	0.02
26H-3, 71-72	230.01	0.08	0.00	0.08	0.00	0.02
26H-5, 71-72	233.01	0.09	0.00	0.09	0.00	0.03
27H-1, 71-72	236.51	0.06	0.00	0.06	0.00	0.01
27H-3, 71-72	239.51	0.06	0.00	0.06	0.00	0.00
27H-5, 71-72	242.51	0.07	0.00	0.07	0.00	0.01

Notes: All samples are CARB (carbonate) samples. TC = total carbon, IC = inorganic carbon, TOC = total organic carbon, and TN = total nitrogen. All results are given in weight percent of bulk dry sediment.

Table 9. Summary of physical properties measurements, Site 887.

	Hole 887A	Hole 887B	Hole 887C	Hole 887D
Magnetic susceptibility	X	X	X	
GRAPE density	X	X	X	
P-wave logger velocity	X	X	X	
Thermal conductivity	X	X	X	
DSV velocity	X		X	
Hamilton Frame velocity				X
Vane shear strength	X		X	
Index properties	X	X	X	X

Table 10. Index properties data from Hole 887A.

Core, section, interval (cm)	Depth (mbsf)	Wet-bulk density (g/cm ³)	Dry-bulk density (g/cm ³)	Grain density (g/cm ³)	Wet porosity (%)	Dry porosity (%)	Wet water content (%)	Dry water content (%)	Void ratio 1	Void ratio 2
145-887A-										
1H-1, 70	0.70	1.28	0.43	2.54	82.60	83.20	66.10	195.20	4.74	4.85
1H-2, 74	2.24	1.45	0.70	2.63	73.00	73.50	51.60	106.70	2.70	2.74
1H-3, 40	3.40	1.57	0.91	2.63	65.30	65.80	42.50	73.80	1.88	1.90
1H-4, 71	5.21	1.13	0.21	2.17	90.00	90.80	81.60	443.80	9.02	9.41
1H-5, 33	6.33	1.21	0.36	2.10	82.40	83.10	70.00	233.00	4.68	4.78
2H-1, 70	7.40	1.15	0.28	1.93	85.20	86.00	75.80	312.90	5.75	5.91
2H-2, 70	8.90	1.18	0.31	2.11	85.00	85.70	73.80	282.20	5.66	5.81
2H-3, 70	10.40	1.38	0.61	2.54	75.80	76.40	56.20	128.30	3.13	3.18
2H-4, 79	11.99	1.52	0.80	2.70	70.00	70.60	47.30	89.80	2.34	2.36
2H-5, 79	13.49	1.52	0.82	2.67	69.20	69.70	46.50	86.90	2.24	2.27
2H-6, 70	14.90	1.65	1.02	2.66	61.40	61.80	38.20	61.70	1.59	1.60
2H-7, 49	16.19	1.44	0.70	2.57	72.40	72.90	51.30	105.50	2.62	2.65
3H-1, 69	16.89	1.57	0.87	2.76	68.10	68.60	44.50	80.10	2.13	2.16
3H-2, 69	18.39	1.46	0.71	2.65	72.70	73.30	51.10	104.40	2.67	2.70
3H-3, 69	19.89	1.70	1.09	2.71	59.40	59.90	35.80	55.80	1.46	1.47
3H-4, 69	21.39	1.39	0.62	2.56	75.30	75.90	55.40	124.20	3.06	3.10
3H-5, 69	22.89	1.64	1.01	2.67	62.00	62.50	38.70	63.10	1.63	1.65
3H-6, 69	24.39	1.62	0.99	2.62	61.90	62.40	39.10	64.10	1.62	1.64
3H-7, 69	25.89	1.56	0.90	2.56	64.50	65.00	42.30	73.40	1.82	1.83
4H-1, 74	26.44	1.67	1.05	2.66	60.20	60.70	37.00	58.80	1.51	1.52
4H-2, 69	27.89	1.22	0.36	2.36	84.50	85.20	70.80	242.00	5.44	5.58
4H-3, 69	29.39	1.61	0.96	2.65	63.50	64.00	40.50	68.00	1.74	1.76
4H-4, 79	30.99	1.70	1.08	2.75	60.50	60.90	36.50	57.50	1.53	1.54
4H-5, 89	32.59	1.70	1.11	2.64	57.80	58.30	34.90	53.50	1.37	1.38
4H-6, 69	33.89	1.50	0.80	2.60	69.00	69.50	47.00	88.70	2.23	2.25
4H-7, 29	34.99	1.59	0.92	2.72	66.00	66.50	42.50	73.90	1.95	1.96
5H-1, 69	35.89	1.24	0.40	2.31	82.30	82.90	67.80	210.40	4.64	4.74
5H-2, 69	37.39	1.49	0.76	2.72	71.80	72.30	49.20	96.80	2.54	2.57
5H-3, 69	38.89	1.51	0.79	2.62	69.40	69.90	47.20	89.50	2.27	2.29
5H-4, 69	40.39	1.26	0.42	2.35	81.80	82.40	66.70	200.30	4.49	4.58
5H-5, 74	41.94	1.51	0.80	2.64	69.50	70.00	47.20	89.30	2.28	2.30
5H-6, 69	43.39	1.29	0.47	2.43	80.50	81.10	63.90	177.00	4.12	4.20
5H-7, 39	44.59	1.58	0.90	2.69	66.30	66.80	43.00	75.60	1.97	1.99
6H-1, 69	45.39	1.56	0.87	2.66	66.80	67.30	43.90	78.30	2.01	2.03
6H-2, 69	46.89	1.76	1.18	2.75	56.90	57.30	33.20	49.60	1.32	1.33
6H-3, 69	48.39	1.55	0.87	2.65	67.10	67.60	44.30	79.40	2.04	2.06
6H-4, 69	49.89	1.71	1.08	2.79	61.00	61.40	36.60	57.80	1.56	1.58
6H-5, 69	51.39	1.24	0.39	2.34	82.70	83.40	68.20	214.70	4.79	4.90
6H-6, 69	52.89	1.19	0.31	2.21	85.50	86.20	73.70	280.70	5.89	6.05
6H-7, 39	54.09	1.53	0.82	2.69	69.30	69.80	46.50	86.80	2.25	2.28
7H-1, 69	54.89	1.60	0.95	2.66	64.00	64.50	40.90	69.10	1.78	1.80
7H-2, 69	56.39	1.31	0.52	2.30	77.00	77.60	60.20	151.50	3.35	3.40
7H-3, 69	57.89	1.74	1.15	2.71	57.20	57.70	33.70	50.90	1.34	1.35
7H-4, 69	59.39	1.26	0.42	2.34	81.70	82.40	66.60	199.70	4.47	4.56
7H-5, 69	60.89	1.72	1.11	2.73	58.90	59.30	35.10	54.10	1.43	1.44
7H-6, 69	62.39	1.49	0.74	2.74	72.50	73.00	49.90	99.80	2.64	2.67
7H-7, 69	63.89	1.67	1.05	2.70	60.90	61.40	37.30	59.50	1.56	1.57
8H-1, 81	64.51	1.20	0.33	2.24	85.10	85.80	72.80	268.00	5.70	5.85
8H-2, 69	65.89	1.54	0.84	2.67	68.10	68.60	45.30	82.70	2.14	2.16
8H-3, 63	67.33	1.58	0.91	2.68	65.80	66.30	42.70	74.40	1.93	1.95
8H-4, 69	68.89	1.69	1.08	2.70	59.70	60.10	36.10	56.50	1.48	1.49
8H-5, 69	70.39	1.59	0.95	2.55	62.40	62.90	40.30	67.40	1.66	1.68
8H-6, 69	71.89	1.53	0.75	3.20	76.30	76.80	51.20	104.80	3.23	3.27
8H-7, 34	73.04	1.51	0.78	2.75	71.20	71.70	48.30	93.30	2.47	2.50
9H-1, 69	73.89	1.57	0.89	2.70	66.80	67.30	43.50	77.10	2.01	2.03
9H-2, 69	75.39	1.58	0.91	2.62	64.90	65.40	42.20	73.00	1.85	1.87
9H-3, 69	76.89	1.60	0.94	2.68	64.60	65.10	41.30	70.50	1.83	1.84
9H-4, 69	78.39	1.65	1.03	2.66	61.00	61.50	37.80	60.90	1.57	1.58
9H-5, 69	79.89	1.59	0.93	2.68	65.10	65.60	41.90	72.00	1.87	1.88
9H-6, 19	80.89	1.67	1.04	2.72	61.40	61.90	37.70	60.60	1.59	1.61
10H-10, 69	83.39	1.61	0.94	2.75	65.60	66.10	41.80	71.80	1.91	1.93
10H-20, 79	84.99	1.34	0.55	2.40	76.80	77.40	58.90	143.20	3.30	3.35
10H-30, 87	86.57	1.56	0.87	2.74	68.00	68.50	44.60	80.40	2.13	2.15
10H-40, 75	87.95	1.68	1.07	2.70	60.10	60.50	36.60	57.60	1.51	1.52
10H-50, 75	89.45	1.45	0.75	2.41	68.50	69.00	48.30	93.40	2.18	2.20
10H-60, 75	90.95	1.38	0.64	2.33	72.20	72.80	53.50	115.30	2.59	2.62
10H-70, 42	92.12	1.26	0.45	2.20	79.30	80.00	64.50	181.60	3.83	3.90
11H-11, 69	92.89	1.28	0.46	2.28	79.30	79.90	63.60	174.90	3.83	3.89
11H-21, 69	94.39	1.29	0.49	2.24	77.80	78.40	62.00	162.90	3.50	3.56
11H-31, 69	95.89	1.38	0.62	2.38	73.50	74.10	54.70	120.90	2.77	2.81
11H-41, 69	97.39	1.37	0.60	2.43	75.00	75.60	56.30	128.60	3.01	3.05
11H-51, 69	98.89	1.57	0.93	2.49	62.30	62.80	40.70	68.50	1.65	1.66
11H-51, 13	99.51	1.61	0.98	2.58	61.70	62.10	39.10	64.30	1.61	1.62
11H-61, 69	100.39	1.36	0.60	2.37	74.10	74.70	55.70	125.70	2.87	2.91
11H-71, 39	101.59	1.27	0.47	2.19	78.40	79.00	63.30	172.60	3.62	3.68
12H-12, 69	102.39	1.29	0.51	2.21	76.60	77.30	60.60	153.90	3.28	3.32
12H-22, 69	103.89	1.36	0.58	2.44	76.00	76.60	57.40	134.90	3.17	3.21
12H-32, 83	105.53	1.58	0.93	2.59	63.90	64.40	41.30	70.50	1.77	1.78
12H-42, 73	106.93	1.43	0.70	2.51	71.90	72.40	51.30	105.50	2.55	2.58
12H-52, 64	108.34	1.51	0.83	2.50	66.60	67.10	45.10	82.20	1.99	2.01
12H-62, 69	109.89	1.32	0.52	2.39	77.80	78.40	60.40	152.40	3.50	3.55
12H-72, 39	111.09	1.31	0.54	2.26	75.90	76.60	59.20	145.00	3.16	3.20
13H-13, 72	111.92	1.32	0.53	2.32	76.90	77.50	59.90	149.20	3.32	3.37

Table 10 (continued).

Core, section, interval (cm)	Depth (mbsf)	Wet-bulk density (g/cm ³)	Dry-bulk density (g/cm ³)	Grain density (g/cm ³)	Wet porosity (%)	Dry porosity (%)	Wet water content (%)	Dry water content (%)	Void ratio 1	Void ratio 2
13H-23, 79	113.49	1.27	0.46	2.23	78.80	79.50	63.50	174.00	3.72	3.79
13H-33, 69	114.89	1.32	0.53	2.31	76.70	77.30	59.60	147.50	3.28	3.33
13H-43, 69	116.39	1.32	0.54	2.30	76.10	76.70	59.00	144.10	3.19	3.23
13H-53, 69	117.89	1.28	0.48	2.23	78.20	78.90	62.60	167.50	3.59	3.65
13H-63, 69	119.39	1.30	0.49	2.39	79.00	79.60	62.20	164.30	3.76	3.83
13H-73, 39	120.59	1.26	0.48	2.00	75.50	76.20	61.60	160.20	3.08	3.13
14H-14, 79	121.49	1.27	0.45	2.29	80.20	80.80	64.90	184.50	4.05	4.12
14H-24, 79	122.99	1.31	0.51	2.34	77.80	78.50	61.00	156.50	3.51	3.57
14H-34, 79	124.49	1.31	0.50	2.41	78.70	79.30	61.50	160.00	3.70	3.76
14H-44, 28	125.48	1.30	0.49	2.42	79.30	80.00	62.30	165.30	3.84	3.91
14H-44, 69	125.89	1.32	0.52	2.44	78.40	79.00	60.80	155.30	3.63	3.69
14H-54, 69	127.39	1.27	0.45	2.38	80.90	81.60	65.10	186.20	4.24	4.32
14H-64, 69	128.89	1.27	0.46	2.26	79.20	79.80	63.70	175.40	3.80	3.87
14H-74, 39	130.09	1.25	0.44	2.16	79.20	79.90	64.80	184.40	3.82	3.89
15X-15, 79	130.99	1.26	0.42	2.34	81.60	82.20	66.40	197.40	4.42	4.51
15X-25, 79	132.49	1.24	0.40	2.25	81.90	82.60	67.80	210.10	4.53	4.62
15X-35, 79	133.99	1.25	0.43	2.21	80.30	80.90	65.70	191.70	4.07	4.14
15X-45, 79	135.49	1.28	0.46	2.35	80.10	80.70	64.10	178.60	4.02	4.10
15X-55, 79	136.99	1.24	0.41	2.12	80.10	80.80	66.40	197.80	4.02	4.10
15X-65, 39	138.09	1.29	0.47	2.40	80.10	80.70	63.50	174.30	4.02	4.09
16X-16, 69	140.39	1.25	0.44	2.17	79.50	80.20	65.00	185.80	3.87	3.94
16X-26, 69	141.89	1.26	0.44	2.22	79.90	80.60	65.20	187.10	3.98	4.05
16X-36, 69	143.39	1.26	0.44	2.23	79.80	80.50	64.90	185.20	3.95	4.03
17X-17, 69	145.79	1.29	0.48	2.35	79.10	79.80	62.70	168.00	3.79	3.86
17X-27, 69	147.29	1.32	0.53	2.34	76.80	77.50	59.60	147.40	3.32	3.37
17X-37, 69	148.79	1.26	0.45	2.24	79.60	80.30	64.50	181.70	3.91	3.98
17X-47, 69	150.29	1.24	0.41	2.21	81.30	81.90	67.20	205.10	4.33	4.42
17X-57, 69	151.79	1.24	0.42	2.16	80.20	80.90	66.20	196.00	4.05	4.13
18X-18, 74	155.54	1.27	0.46	2.28	79.60	80.30	64.20	179.20	3.91	3.98
18X-28, 69	156.99	1.25	0.42	2.22	80.60	81.30	66.10	195.20	4.15	4.23
18X-38, 69	158.49	1.30	0.50	2.33	78.10	78.80	61.50	159.90	3.57	3.63
18X-48, 69	159.99	1.27	0.46	2.24	79.20	79.90	63.90	177.10	3.81	3.88
18X-58, 69	161.49	1.35	0.56	2.42	76.40	77.00	58.10	138.60	3.23	3.28
18X-68, 69	162.99	1.24	0.40	2.21	81.30	82.00	67.40	206.30	4.35	4.44
20X-10, 69	174.79	1.34	0.57	2.32	75.00	75.60	57.40	134.50	3.00	3.05
20X-20, 69	176.29	1.29	0.49	2.25	77.90	78.50	61.90	162.60	3.52	3.58
20X-30, 69	177.79	1.29	0.51	2.20	76.50	77.10	60.60	153.60	3.26	3.30
20X-40, 69	179.29	1.43	0.70	2.46	71.10	71.60	50.90	103.50	2.46	2.48
20X-50, 69	180.79	1.33	0.56	2.28	75.20	75.80	58.00	138.00	3.03	3.07
20X-60, 69	182.29	1.32	0.55	2.25	75.30	75.90	58.50	140.70	3.05	3.09
20X-70, 49	183.09	1.31	0.53	2.27	76.20	76.80	59.40	146.60	3.20	3.24
21X-11, 69	184.39	1.27	0.45	2.25	79.40	80.10	64.20	179.00	3.85	3.92
21X-21, 69	185.89	1.34	0.57	2.32	75.20	75.80	57.60	136.10	3.04	3.08
21X-31, 69	186.89	1.29	0.49	2.28	78.30	78.90	62.20	164.60	3.61	3.67
22H-12, 69	194.09	1.29	0.48	2.36	79.20	79.90	62.80	168.80	3.81	3.88
22H-22, 69	195.59	1.36	0.58	2.41	75.40	76.00	56.90	132.30	3.07	3.11
22H-32, 69	197.09	1.32	0.52	2.37	77.60	78.20	60.40	152.40	3.47	3.53
22H-42, 69	198.59	1.31	0.51	2.36	78.00	78.70	61.10	157.00	3.56	3.61
22H-52, 69	200.09	1.29	0.47	2.34	79.50	80.10	63.30	172.60	3.87	3.94
22H-62, 69	201.59	1.30	0.49	2.39	79.00	79.60	62.10	164.10	3.76	3.83
23H-13, 69	203.59	1.50	0.80	2.56	68.40	68.90	46.60	87.40	2.16	2.18
23H-23, 69	205.09	1.35	0.58	2.41	75.60	76.20	57.10	133.30	3.09	3.14
23H-33, 69	206.59	1.34	0.58	2.33	74.80	75.40	57.10	132.80	2.97	3.01
23H-43, 69	208.09	1.31	0.51	2.37	78.20	78.80	61.20	158.00	3.59	3.65
23H-53, 69	209.59	1.45	0.72	2.55	71.40	71.90	50.30	101.20	2.49	2.52
23H-63, 69	211.09	1.52	0.82	2.59	68.00	68.50	45.90	84.90	2.13	2.15
23H-73, 59	212.49	1.54	0.86	2.59	66.30	66.80	44.10	78.80	1.97	1.99
24H-14, 79	213.19	1.40	0.66	2.39	72.20	72.70	52.90	112.30	2.59	2.62
24H-24, 69	214.59	1.34	0.56	2.33	75.50	76.10	57.80	137.20	3.08	3.12
24H-34, 69	216.09	1.31	0.51	2.33	77.80	78.40	60.90	156.00	3.50	3.55
24H-44, 69	217.59	1.36	0.59	2.37	74.60	75.20	56.30	128.80	2.94	2.98
24H-54, 69	219.09	1.18	0.37	1.80	79.10	79.90	68.70	219.40	3.78	3.85
24H-64, 69	220.59	1.36	0.58	2.52	76.70	77.30	57.70	136.30	3.30	3.35
25H-15, 69	222.59	1.30	0.48	2.39	79.40	80.00	62.60	167.70	3.85	3.92
25H-25, 69	224.09	1.28	0.45	2.38	80.70	81.30	64.70	183.10	4.18	4.26
25H-35, 69	225.59	1.40	0.64	2.53	74.30	74.80	54.20	118.30	2.89	2.93
25H-45, 69	227.09	1.41	0.65	2.56	74.40	75.00	54.10	118.00	2.91	2.95
25H-55, 69	228.59	1.35	0.55	2.53	77.90	78.50	59.10	144.50	3.52	3.57
25H-65, 69	230.09	1.34	0.54	2.44	77.40	78.00	59.40	146.30	3.43	3.49
25H-75, 69	231.59	1.28	0.48	2.21	78.20	78.80	62.70	168.20	3.58	3.64
27H-17, 69	241.89	1.25	0.42	2.29	81.20	81.90	66.40	197.50	4.33	4.41
27H-27, 69	243.39	1.33	0.53	2.47	78.10	78.70	60.00	149.90	3.56	3.62
27H-37, 69	244.89	1.31	0.50	2.41	79.00	79.60	62.00	162.80	3.76	3.83
28H-18, 69	251.39	1.40	0.65	2.47	73.20	73.80	53.50	114.90	2.74	2.77
28H-28, 69	252.89	1.43	0.69	2.50	72.10	72.70	51.70	107.10	2.59	2.62
28H-38, 69	254.39	1.31	0.51	2.34	77.90	78.50	61.10	157.00	3.52	3.58
28H-48, 69	255.89	1.29	0.49	2.29	78.20	78.80	62.00	163.00	3.58	3.64
28H-68, 69	258.89	1.32	0.53	2.43	78.00	78.60	60.30	152.20	3.55	3.61

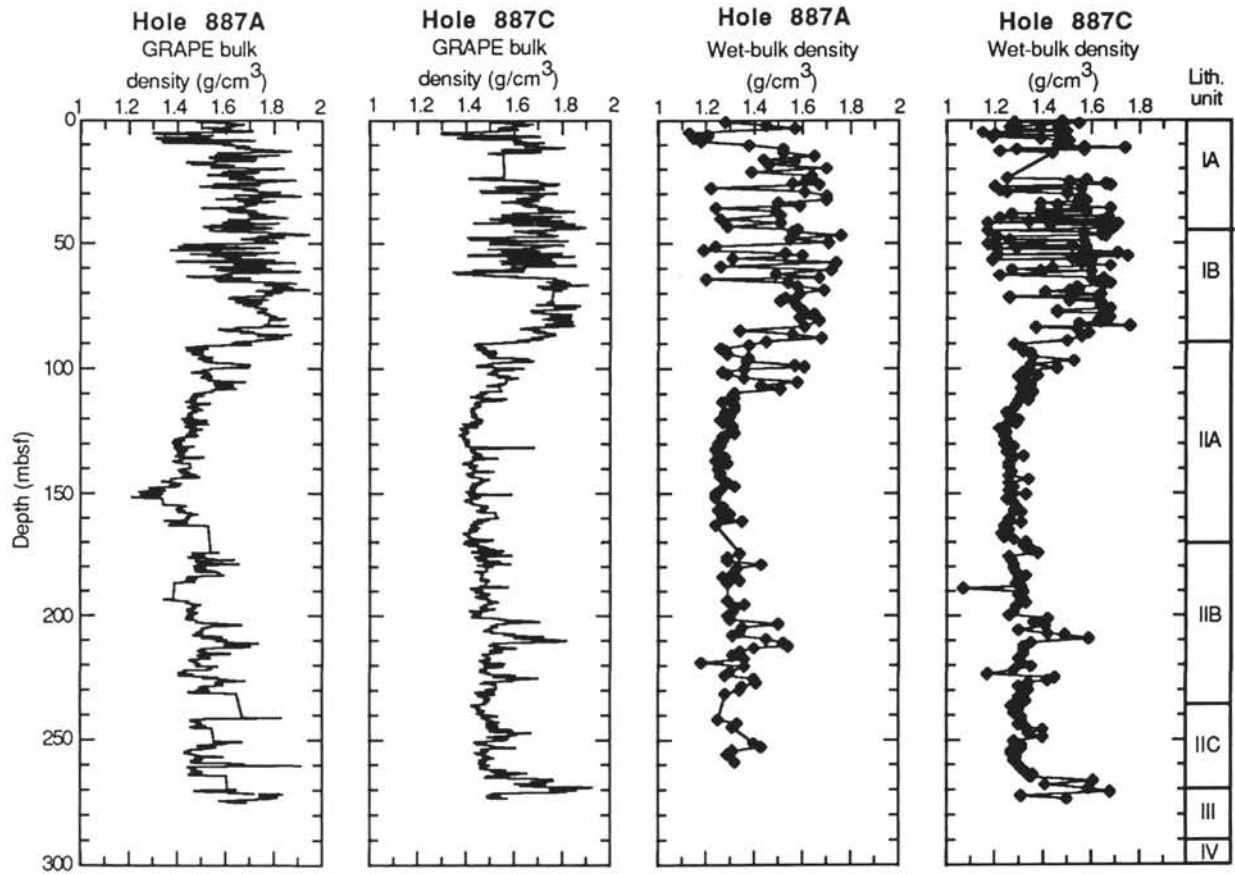


Figure 24. Plots of GRAPE bulk density and wet-bulk density vs. sub-bottom depth for Holes 887A and 887C. Lithologic units also are shown on the right.

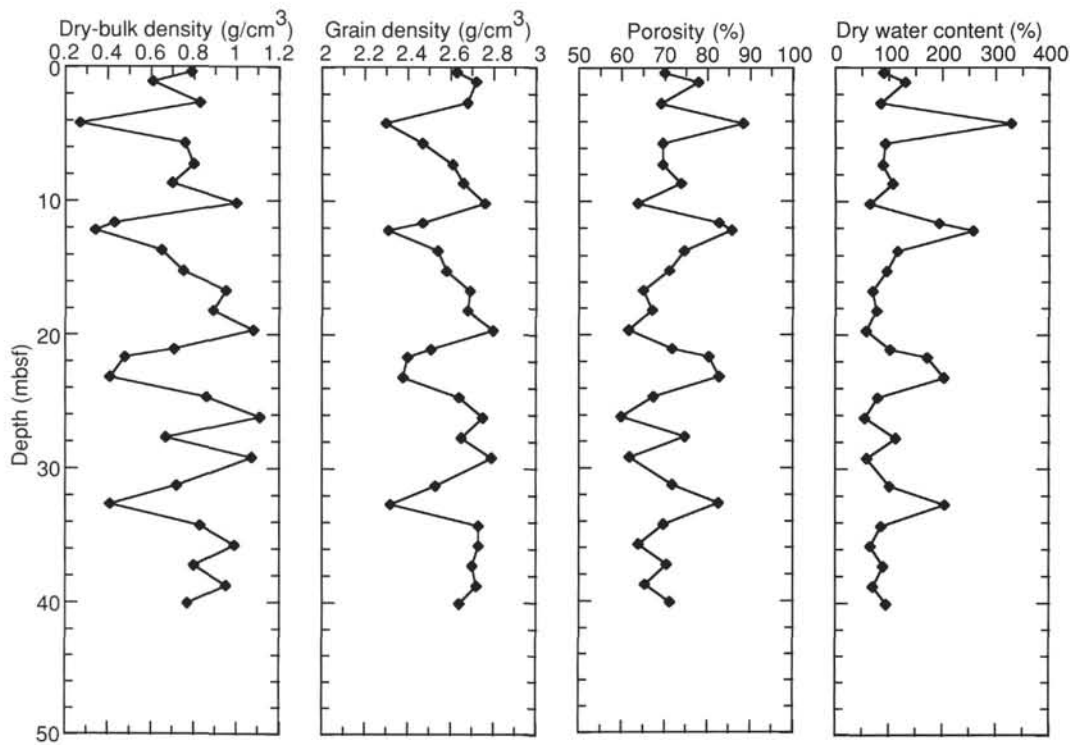


Figure 25. Plots of index property data vs. depth for Hole 887B.

Table 11. Index properties data from Holes 887B and 887D.

Core, section, interval (cm)	Depth (mbsf)	Wet-bulk density (g/cm ³)	Dry-bulk density (g/cm ³)	Grain density (g/cm ³)	Wet porosity (%)	Dry porosity (%)	Wet water content (%)	Dry water content (%)	Void ratio 1	Void ratio 2
145-887B-										
1H-1, 39	0.39	1.50	0.79	2.63	69.60	70.10	47.40	90.20	2.29	2.31
1H-1, 109	1.09	1.40	0.61	2.72	77.30	77.90	56.70	130.70	3.41	3.46
2H-1, 39	2.69	1.53	0.83	2.68	68.70	69.20	45.90	84.80	2.20	2.22
2H-2, 109	4.19	1.17	0.27	2.30	87.70	88.40	76.70	329.50	7.15	7.39
2H-3, 69	5.69	1.46	0.76	2.47	69.00	69.60	48.30	93.50	2.23	2.25
2H-4, 69	7.29	1.51	0.80	2.61	69.10	69.60	47.00	88.60	2.23	2.26
2H-5, 69	8.69	1.45	0.70	2.66	73.40	73.90	51.80	107.40	2.76	2.79
2H-6, 79	10.19	1.65	1.00	2.76	63.30	63.80	39.30	64.70	1.73	1.74
2H-7, 69	11.64	1.27	0.43	2.47	82.10	82.70	66.00	194.00	4.59	4.68
3H-1, 69	12.19	1.21	0.34	2.31	85.00	85.70	72.10	257.90	5.67	5.82
3H-2, 64	13.69	1.41	0.65	2.54	74.00	74.60	53.80	116.30	2.85	2.89
3H-3, 69	15.19	1.47	0.75	2.58	70.50	71.10	49.00	96.10	2.39	2.42
3H-4, 69	16.69	1.61	0.95	2.69	64.50	65.00	41.10	69.80	1.82	1.83
3H-5, 69	18.19	1.57	0.89	2.68	66.60	67.10	43.50	77.00	2.00	2.01
3H-6, 69	19.69	1.70	1.08	2.80	61.30	61.70	36.80	58.30	1.58	1.60
3H-7, 69	21.09	1.44	0.71	2.51	71.30	71.80	50.60	102.60	2.48	2.51
4H-1, 69	21.69	1.29	0.48	2.40	79.80	80.40	63.20	171.90	3.95	4.02
4H-2, 59	23.19	1.26	0.41	2.38	82.20	82.80	67.00	203.20	4.61	4.71
4H-3, 69	24.69	1.55	0.86	2.64	66.90	67.40	44.20	79.20	2.02	2.04
4H-4, 69	26.19	1.72	1.11	2.75	59.50	59.90	35.50	55.00	1.47	1.48
4H-5, 69	27.69	1.43	0.67	2.65	74.20	74.80	53.00	112.80	2.88	2.92
4H-6, 69	29.19	1.70	1.07	2.79	61.40	61.80	37.00	58.80	1.59	1.60
5H-1, 69	31.29	1.45	0.72	2.53	71.30	71.80	50.40	101.40	2.48	2.51
5H-2, 69	32.69	1.25	0.41	2.32	81.90	82.60	67.10	204.30	4.52	4.62
5H-3, 79	34.29	1.54	0.83	2.73	69.30	69.80	46.10	85.50	2.25	2.28
5H-4, 69	35.79	1.64	0.99	2.73	63.50	63.90	39.60	65.60	1.74	1.75
5H-5, 79	37.29	1.52	0.80	2.70	70.00	70.50	47.20	89.20	2.33	2.35
5H-6, 79	38.79	1.61	0.95	2.72	64.90	65.40	41.20	70.10	1.85	1.86
5H-7, 59	40.09	1.49	0.77	2.64	70.70	71.20	48.60	94.60	2.41	2.44
145-877C-										
3R-1, 49	277.59	1.57	0.89	2.67	66.40	66.90	43.30	76.40	1.98	1.99
4R-1, 69	287.39	1.36	0.57	2.53	77.30	77.90	58.30	140.00	3.40	3.45
4R-2, 119	366.39	1.63	1.03	2.50	58.50	58.90	36.80	58.10	1.41	1.42

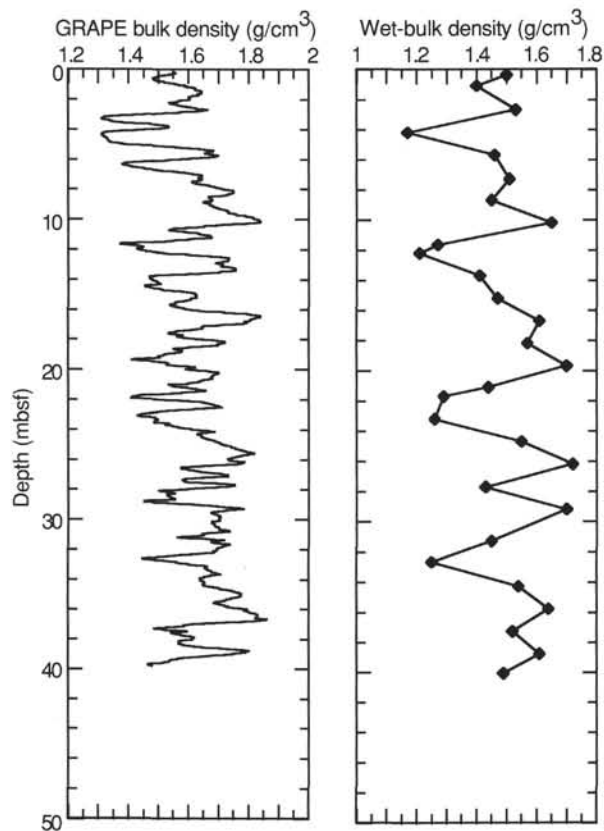


Figure 26. Plots of GRAPE density and wet-bulk density vs. depth for Hole 887B.

Table 12. Index properties data from Hole 887C.

Core, section, interval (cm)	Depth (mbsf)	Wet-bulk density (g/cm ³)	Dry-bulk density (g/cm ³)	Grain density (g/cm ³)	Wet porosity (%)	Dry porosity (%)	Wet water content (%)	Dry water content (%)	Void ratio 1	Void ratio 2
145-887C-										
1H-1, 39	0.39	1.48	0.76	2.58	70.30	70.80	48.80	95.20	2.37	2.39
1H-1, 69	0.69	1.28	0.44	2.42	81.30	81.90	65.20	187.60	4.35	4.43
1H-1, 131	1.31	1.55	0.86	2.67	67.40	67.90	44.50	80.10	2.07	2.09
1H-2, 39	1.89	1.46	0.70	2.73	73.90	74.40	51.90	107.70	2.83	2.87
1H-2, 74	2.24	1.39	0.62	2.54	75.10	75.70	55.30	123.50	3.02	3.06
1H-2, 139	2.89	1.26	0.42	2.39	82.10	82.80	66.80	201.20	4.59	4.69
1H-3, 54	3.54	1.30	0.49	2.36	79.10	79.70	62.50	166.50	3.78	3.84
1H-3, 109	4.09	1.46	0.73	2.63	72.10	72.70	50.50	101.90	2.59	2.62
2H-1, 39	4.69	1.50	0.79	2.62	69.70	70.20	47.60	90.80	2.30	2.32
2H-1, 69	4.99	1.15	0.24	2.15	88.50	89.30	79.20	379.70	7.69	7.97
2H-1, 134	5.64	1.20	0.34	2.24	84.60	85.30	72.00	257.40	5.49	5.63
2H-2, 67	6.47	1.47	0.73	2.62	71.70	72.20	50.00	99.90	2.53	2.56
2H-2, 129	7.09	1.19	0.31	2.23	85.60	86.30	73.80	281.50	5.95	6.11
2H-3, 49	7.79	1.39	0.61	2.53	75.40	76.00	55.70	125.70	3.06	3.11
2H-3, 129	8.59	1.51	0.80	2.67	69.80	70.30	47.30	89.70	2.31	2.34
2H-4, 139	10.19	1.46	0.72	2.65	72.40	72.90	50.70	102.70	2.62	2.65
2H-5, 19	10.49	1.49	0.76	2.74	72.10	72.60	49.40	97.80	2.59	2.62
2H-5, 69	10.99	1.57	0.93	2.50	62.30	62.80	40.60	68.30	1.65	1.67
2H-5, 122	11.52	1.74	1.27	2.37	46.40	46.80	27.30	37.50	0.87	0.87
2H-6, 11	11.91	1.29	0.46	2.52	81.50	82.10	64.60	182.40	4.39	4.48
2H-6, 64	12.44	1.57	0.89	2.68	66.30	66.80	43.20	76.00	1.97	1.98
2H-6, 99	12.79	1.22	0.35	2.37	84.90	85.60	71.40	250.20	5.63	5.78
2H-7, 39	13.69	1.44	0.69	2.62	73.10	73.70	51.90	108.00	2.72	2.76
4H-1, 49	23.79	1.25	0.42	2.25	81.10	81.80	66.60	199.10	4.29	4.38
4H-1, 129	24.59	1.58	0.90	2.69	66.10	66.50	42.80	74.80	1.95	1.96
4H-2, 49	25.29	1.51	0.80	2.62	69.30	69.80	47.10	89.10	2.25	2.28
4H-2, 129	26.09	1.66	1.03	2.74	62.30	62.70	38.30	62.10	1.65	1.66
4H-3, 24	26.54	1.68	1.06	2.72	60.60	61.00	36.90	58.40	1.54	1.55
4H-3, 86	27.16	1.20	0.35	2.14	83.30	84.00	70.90	243.30	4.98	5.09
4H-4, 49	28.29	1.56	0.87	2.71	67.60	68.10	44.30	79.50	2.09	2.11
4H-4, 99	28.79	1.22	0.35	2.36	84.60	85.30	71.00	245.40	5.51	5.65
4H-5, 29	29.59	1.25	0.38	2.54	84.50	85.20	69.30	226.30	5.46	5.60
4H-5, 92	30.22	1.50	0.79	2.63	69.90	70.40	47.70	91.10	2.32	2.34
4H-6, 49	31.29	1.56	0.88	2.66	66.50	66.90	43.50	77.00	1.98	2.00
4H-7, 39	32.19	1.55	0.86	2.64	67.20	67.70	44.60	80.30	2.05	2.07
5H-1, 24	33.04	1.58	0.91	2.64	65.30	65.80	42.40	73.60	1.88	1.90
5H-1, 112	33.92	1.39	0.62	2.50	75.00	75.60	55.50	124.60	3.00	3.04
5H-2, 24	34.54	1.46	0.74	2.55	70.70	71.20	49.40	97.80	2.41	2.44
5H-2, 85	35.15	1.54	0.83	2.67	68.50	69.00	45.70	84.00	2.17	2.19
5H-3, 31	36.11	1.68	1.06	2.71	60.60	61.10	36.90	58.60	1.54	1.55
5H-3, 109	36.89	1.39	0.62	2.51	75.00	75.60	55.50	124.50	3.00	3.05
5H-4, 24	37.54	1.58	0.91	2.66	65.50	66.00	42.50	74.00	1.90	1.92
5H-4, 109	38.39	1.27	0.46	2.21	79.00	79.60	63.90	177.00	3.75	3.82
5H-5, 59	39.39	1.67	1.07	2.62	58.90	59.40	36.10	56.40	1.43	1.44
5H-5, 115	39.95	1.22	0.37	2.22	82.80	83.50	69.40	227.10	4.82	4.92
5H-6, 59	40.89	1.64	1.01	2.67	61.80	62.20	38.50	62.60	1.62	1.63
5H-6, 114	41.44	1.34	0.54	2.47	77.70	78.30	59.50	146.80	3.48	3.54
5H-7, 19	41.99	1.17	0.27	2.33	88.20	88.90	77.20	338.40	7.45	7.71
5H-7, 41	42.21	1.71	1.10	2.71	59.10	59.50	35.40	54.90	1.45	1.45
6H-1, 39	42.69	1.43	0.68	2.51	72.40	73.00	52.00	108.30	2.63	2.66
6H-1, 109	43.39	1.70	1.09	2.69	59.20	59.60	35.70	55.50	1.45	1.46
6H-2, 39	44.19	1.69	1.07	2.76	61.10	61.50	37.00	58.60	1.57	1.58
6H-2, 129	45.09	1.17	0.31	1.99	83.90	84.70	73.40	275.30	5.22	5.34
6H-3, 39	45.69	1.57	0.90	2.61	65.00	65.50	42.40	73.70	1.86	1.88
6H-3, 129	46.59	1.64	1.01	2.64	61.60	62.10	38.50	62.70	1.61	1.62
6H-4, 24	47.04	1.66	1.03	2.68	61.20	61.60	37.80	60.70	1.57	1.59
6H-4, 77	47.57	1.21	0.36	2.19	83.00	83.70	70.00	233.40	4.88	4.99
6H-5, 34	48.64	1.26	0.43	2.31	81.00	81.70	65.90	193.30	4.27	4.35
6H-5, 84	49.14	1.57	0.90	2.64	65.70	66.10	42.80	74.70	1.91	1.93
6H-6, 63	50.43	1.17	0.30	2.04	85.10	85.90	74.70	295.00	5.71	5.86
6H-6, 127	51.07	1.52	0.83	2.61	68.00	68.50	45.80	84.40	2.13	2.15
6H-7, 24	51.54	1.58	0.91	2.64	65.30	65.80	42.50	73.90	1.89	1.90
6H-7, 61	51.91	1.29	0.46	2.40	80.40	81.00	64.00	178.10	4.10	4.18
7H-1, 53	52.33	1.21	0.34	2.30	85.00	85.70	72.10	258.30	5.66	5.81
7H-1, 103	52.83	1.57	0.89	2.68	66.30	66.80	43.10	75.90	1.97	1.98
7H-2, 69	53.99	1.71	1.11	2.70	58.60	59.00	35.10	54.10	1.42	1.43
7H-2, 129	54.59	1.21	0.35	2.27	84.30	85.00	71.30	248.30	5.36	5.49
7H-3, 39	55.19	1.75	1.17	2.70	56.50	56.90	33.10	49.60	1.30	1.30
7H-3, 135	56.15	1.52	0.82	2.65	68.70	69.20	46.20	85.90	2.20	2.22
7H-4, 52	56.82	1.19	0.32	2.16	85.00	85.70	73.40	276.00	5.67	5.82
7H-4, 61	56.91	1.60	0.93	2.67	64.80	65.30	41.60	71.30	1.84	1.86
7H-4, 103	57.33	1.57	0.90	2.66	65.90	66.40	42.90	75.20	1.93	1.95
7H-5, 46	58.26	1.56	0.88	2.63	66.10	66.60	43.40	76.60	1.95	1.97
7H-5, 124	59.04	1.68	1.08	2.62	58.60	59.10	35.80	55.80	1.42	1.43
7H-6, 49	59.79	1.44	0.69	2.62	73.20	73.80	51.90	108.10	2.73	2.77
7H-6, 124	60.54	1.27	0.45	2.31	80.30	81.00	64.90	184.60	4.09	4.16
7H-7, 22	61.02	1.39	0.61	2.55	75.60	76.20	55.70	125.90	3.10	3.14
7H-7, 44	61.24	1.60	0.95	2.67	64.30	64.80	41.10	69.70	1.80	1.82
8H-2, 15	62.95	1.22	0.35	2.29	84.20	84.90	71.00	244.30	5.33	5.46
8H-2, 133	64.13	1.65	1.01	2.67	61.80	62.20	38.40	62.40	1.62	1.63
8H-3, 19	64.49	1.60	0.94	2.63	63.90	64.40	41.00	69.40	1.77	1.78
9H-1, 66	65.46	1.62	0.96	2.69	63.90	64.40	40.40	67.90	1.77	1.78
9H-1, 125	66.05	1.68	1.07	2.70	60.00	60.50	36.50	57.50	1.50	1.51

Table 12 (continued).

Core, section, interval (cm)	Depth (mbsf)	Wet-bulk density (g/cm ³)	Dry-bulk density (g/cm ³)	Grain density (g/cm ³)	Wet porosity (%)	Dry porosity (%)	Wet water content (%)	Dry water content (%)	Void ratio 1	Void ratio 2
9H-2, 66	66.96	1.65	1.04	2.61	60.10	60.50	37.20	59.30	1.50	1.51
9H-2, 125	67.55	1.54	0.84	2.72	69.00	69.50	45.80	84.60	2.22	2.25
9H-3, 39	68.19	1.55	0.86	2.66	67.40	67.90	44.60	80.40	2.07	2.09
9H-3, 113	68.93	1.51	0.81	2.58	68.40	68.90	46.50	86.80	2.17	2.19
9H-4, 34	69.64	1.41	0.65	2.53	73.80	74.40	53.60	115.60	2.82	2.86
9H-4, 124	70.54	1.64	1.00	2.67	62.30	62.80	39.00	63.90	1.65	1.66
9H-5, 39	71.19	1.63	0.97	2.73	64.10	64.50	40.30	67.50	1.78	1.80
9H-5, 85	71.65	1.26	0.42	2.43	82.40	83.10	66.90	202.50	4.69	4.79
9H-6, 29	72.59	1.63	0.98	2.74	64.00	64.50	40.10	67.00	1.78	1.79
9H-6, 84	73.14	1.51	0.80	2.66	69.50	70.00	47.10	88.90	2.28	2.31
9H-7, 39	73.69	1.64	1.00	2.72	63.10	63.50	39.40	64.90	1.71	1.72
10H-1, 49	74.79	1.64	0.98	2.72	63.50	64.00	39.80	66.10	1.74	1.76
10H-1, 124	75.54	1.64	0.99	2.72	63.30	63.70	39.50	65.20	1.72	1.73
10H-2, 39	76.19	1.68	1.07	2.64	59.10	59.50	36.10	56.40	1.44	1.45
10H-2, 124	77.04	1.46	0.72	2.59	71.80	72.30	50.50	102.00	2.55	2.58
10H-3, 39	77.69	1.46	0.72	2.61	72.30	72.80	50.90	103.50	2.61	2.64
10H-3, 109	78.39	1.65	1.01	2.70	62.40	62.90	38.80	63.50	1.66	1.68
10H-4, 39	79.19	1.65	1.00	2.76	63.70	64.10	39.60	65.50	1.75	1.77
10H-4, 87	79.67	1.68	1.05	2.75	61.50	61.90	37.50	59.90	1.60	1.61
10H-5, 52	80.82	1.63	0.98	2.69	63.10	63.60	39.70	65.80	1.71	1.73
10H-5, 127	81.57	1.64	1.01	2.67	61.80	62.20	38.50	62.50	1.62	1.63
10H-6, 39	82.19	1.55	0.85	2.67	67.80	68.30	44.90	81.40	2.10	2.12
10H-6, 125	83.05	1.76	1.17	2.79	57.70	58.10	33.50	50.40	1.36	1.37
10H-7, 39	83.69	1.37	0.68	2.11	67.40	67.90	50.30	101.10	2.06	2.08
11H-1, 69	84.49	1.54	0.85	2.66	68.00	68.50	45.20	82.40	2.12	2.14
11H-2, 69	85.99	1.59	0.93	2.65	64.70	65.20	41.60	71.30	1.83	1.85
11H-3, 59	87.39	1.56	0.87	2.73	68.00	68.50	44.60	80.50	2.13	2.15
11H-4, 79	89.09	1.50	0.79	2.61	69.30	69.80	47.20	89.30	2.26	2.28
11H-5, 69	90.49	1.28	0.49	2.15	76.80	77.40	61.50	159.80	3.30	3.36
11H-6, 69	91.99	1.31	0.52	2.32	77.40	78.00	60.50	153.50	3.42	3.47
11H-7, 59	93.39	1.32	0.53	2.29	76.30	76.90	59.40	146.30	3.22	3.27
12H-1, 69	93.99	1.35	0.57	2.45	76.20	76.80	57.70	136.20	3.21	3.25
12H-2, 69	95.49	1.36	0.58	2.46	76.00	76.60	57.30	134.10	3.17	3.22
12H-3, 69	96.99	1.53	0.86	2.53	65.70	66.20	43.90	78.40	1.92	1.94
12H-4, 69	98.49	1.35	0.57	2.43	76.10	76.70	57.70	136.30	3.19	3.24
12H-5, 69	99.99	1.46	0.73	2.51	70.40	71.00	49.60	98.40	2.38	2.41
12H-6, 69	101.49	1.32	0.57	2.19	73.80	74.40	57.10	133.20	2.81	2.85
12H-7, 59	102.89	1.38	0.62	2.44	74.10	74.60	54.90	121.60	2.85	2.89
13H-1, 71	103.51	1.30	0.48	2.41	79.80	80.40	63.10	171.30	3.96	4.03
13H-2, 71	105.01	1.33	0.53	2.48	78.30	78.90	60.20	151.30	3.60	3.66
13H-3, 79	106.59	1.35	0.57	2.43	76.20	76.80	57.90	137.60	3.21	3.26
13H-4, 69	107.99	1.31	0.53	2.24	76.10	76.80	59.70	148.20	3.19	3.24
13H-5, 69	109.49	1.36	0.62	2.25	72.20	72.80	54.50	119.70	2.60	2.63
13H-6, 69	110.99	1.31	0.53	2.22	75.80	76.40	59.40	146.30	3.13	3.17
13H-7, 69	112.49	1.34	0.57	2.32	75.30	75.90	57.70	136.50	3.05	3.09
14H-1, 69	112.99	1.30	0.51	2.22	76.50	77.10	60.40	152.60	3.26	3.30
14H-2, 69	114.49	1.29	0.49	2.24	77.80	78.40	61.90	162.30	3.50	3.56
14H-3, 69	115.99	1.28	0.48	2.21	78.10	78.80	62.70	168.40	3.57	3.63
14H-4, 69	117.49	1.25	0.45	2.09	78.20	78.90	64.10	178.90	3.59	3.65
14H-5, 69	118.99	1.26	0.47	2.12	77.60	78.20	62.90	169.60	3.46	3.51
14H-6, 69	120.49	1.30	0.50	2.34	78.30	79.00	61.60	160.60	3.61	3.67
14H-7, 49	121.79	1.29	0.50	2.28	77.80	78.50	61.60	160.30	3.51	3.57
15H-1, 69	122.49	1.25	0.42	2.23	81.00	81.70	66.60	199.30	4.26	4.34
15H-2, 69	123.99	1.22	0.39	2.18	81.90	82.60	68.50	217.70	4.53	4.63
15H-3, 69	125.49	1.25	0.43	2.22	80.20	80.90	65.60	190.90	4.05	4.13
15H-4, 69	126.99	1.24	0.41	2.22	81.00	81.70	66.70	200.00	4.26	4.34
15H-5, 69	128.49	1.25	0.42	2.31	81.60	82.20	66.70	200.50	4.43	4.52
15H-6, 69	129.99	1.24	0.41	2.20	80.90	81.60	66.80	200.80	4.23	4.32
15H-7, 49	131.29	1.28	0.49	2.16	77.00	77.60	61.60	160.60	3.34	3.39
16H-1, 69	131.99	1.27	0.47	2.21	78.40	79.10	63.20	171.50	3.64	3.70
16H-2, 69	133.49	1.25	0.45	2.12	78.40	79.10	64.10	178.90	3.64	3.70
16H-3, 69	134.99	1.32	0.53	2.36	77.40	78.00	60.10	150.80	3.42	3.47
16H-4, 69	136.49	1.27	0.46	2.23	79.00	79.60	63.70	175.70	3.76	3.82
16H-5, 69	137.99	1.26	0.44	2.23	79.80	80.50	64.90	185.10	3.95	4.03
16H-6, 69	139.49	1.26	0.44	2.23	79.70	80.40	64.70	183.70	3.93	4.00
17H-1, 69	141.49	1.27	0.46	2.25	79.30	79.90	63.90	177.10	3.82	3.89
17H-2, 69	142.99	1.26	0.44	2.23	80.10	80.80	65.40	188.60	4.04	4.11
17H-3, 69	144.49	1.34	0.58	2.28	74.20	74.90	56.80	131.40	2.88	2.92
17H-4, 69	145.99	1.26	0.46	2.16	78.10	78.80	63.30	172.70	3.57	3.63
17H-5, 69	147.49	1.28	0.48	2.24	78.30	78.90	62.60	167.30	3.60	3.66
17H-6, 69	148.99	1.26	0.47	2.13	77.60	78.30	63.00	169.90	3.47	3.53
17H-7, 69	150.49	1.33	0.55	2.35	76.30	76.90	58.80	142.60	3.22	3.27
18H-1, 69	150.99	1.27	0.46	2.23	79.20	79.90	64.00	178.10	3.81	3.87
18H-2, 69	152.49	1.25	0.43	2.17	79.90	80.60	65.70	191.30	3.98	4.06
18H-3, 69	153.99	1.28	0.47	2.24	78.50	79.10	62.90	169.70	3.64	3.71
18H-4, 69	155.49	1.29	0.49	2.24	77.60	78.30	61.70	161.30	3.47	3.52
18H-5, 69	156.99	1.28	0.48	2.24	78.10	78.70	62.40	165.90	3.56	3.62
18H-6, 49	157.79	1.31	0.53	2.25	76.30	76.90	59.70	148.30	3.22	3.26
19H-1, 69	160.49	1.26	0.44	2.28	80.40	81.10	65.30	187.90	4.10	4.18
19H-2, 69	161.99	1.31	0.52	2.29	76.80	77.40	60.10	150.30	3.31	3.36
19H-3, 69	163.49	1.24	0.43	2.04	78.40	79.10	64.90	185.10	3.63	3.69
19H-4, 69	164.99	1.26	0.45	2.20	79.00	79.70	64.10	178.40	3.76	3.83
19H-5, 69	166.49	1.23	0.39	2.23	82.10	82.80	68.30	215.40	4.59	4.68
19H-6, 69	167.99	1.24	0.41	2.18	80.70	81.40	66.70	200.20	4.19	4.27

Table 12 (continued).

Core, section, interval (cm)	Depth (mbsf)	Wet-bulk density (g/cm ³)	Dry-bulk density (g/cm ³)	Grain density (g/cm ³)	Wet porosity (%)	Dry porosity (%)	Wet water content (%)	Dry water content (%)	Void ratio 1	Void ratio 2
19H-7, 49	168.79	1.28	0.49	2.22	77.70	78.30	62.00	162.80	3.48	3.54
20H-1, 69	169.99	1.33	0.55	2.35	76.10	76.70	58.50	140.90	3.19	3.23
20H-2, 69	171.49	1.32	0.52	2.40	78.00	78.60	60.50	153.10	3.54	3.59
20H-3, 69	172.99	1.35	0.58	2.38	75.10	75.70	56.90	132.20	3.02	3.07
20H-4, 69	174.49	1.38	0.63	2.39	73.40	74.00	54.60	120.10	2.76	2.80
20H-5, 69	175.99	1.26	0.46	2.20	78.90	79.60	64.00	177.60	3.75	3.81
20H-6, 69	177.49	1.27	0.47	2.20	78.10	78.80	62.90	169.30	3.57	3.63
21H-1, 69	179.49	1.28	0.46	2.26	79.10	79.80	63.60	174.50	3.79	3.86
21H-2, 69	180.99	1.28	0.47	2.28	79.00	79.60	63.20	171.60	3.76	3.82
21H-3, 69	182.49	1.29	0.48	2.32	78.90	79.50	62.70	168.00	3.74	3.80
21H-4, 69	183.99	1.33	0.55	2.37	76.50	77.10	58.80	142.60	3.25	3.29
21H-5, 69	185.49	1.30	0.51	2.24	76.70	77.30	60.50	153.10	3.29	3.34
21H-6, 69	186.99	1.29	0.49	2.28	78.20	78.80	62.10	163.80	3.58	3.64
21H-7, 39	188.19	1.31	0.52	2.30	76.90	77.50	60.10	150.70	3.33	3.38
22H-1, 69	188.99	1.07	0.21	1.34	83.60	85.20	79.90	398.20	5.08	5.20
22H-2, 69	190.49	1.32	0.51	2.47	78.80	79.40	61.10	157.20	3.72	3.78
22H-3, 69	191.99	1.30	0.49	2.36	78.90	79.60	62.30	165.30	3.74	3.81
22H-4, 69	193.49	1.32	0.53	2.35	77.20	77.80	60.00	150.10	3.38	3.44
22H-5, 69	194.99	1.33	0.55	2.35	76.10	76.70	58.50	141.10	3.19	3.24
22H-6, 69	196.49	1.29	0.50	2.24	77.20	77.90	61.10	157.30	3.39	3.44
23H-1, 69	198.49	1.28	0.47	2.30	79.20	79.90	63.30	172.50	3.81	3.88
23H-2, 69	199.99	1.26	0.46	2.20	78.90	79.60	63.90	177.10	3.74	3.80
23H-3, 69	201.49	1.42	0.68	2.49	72.50	73.00	52.20	109.40	2.63	2.66
23H-4, 69	202.99	1.36	0.62	2.29	72.60	73.20	54.50	119.90	2.65	2.68
23H-5, 69	204.49	1.41	0.59	3.10	80.70	81.30	58.50	141.20	4.19	4.27
23H-6, 69	205.99	1.30	0.51	2.27	77.30	77.90	60.90	155.90	3.40	3.45
23H-7, 69	207.49	1.42	0.67	2.50	72.60	73.20	52.50	110.30	2.66	2.69
24H-1, 69	207.99	1.49	0.75	2.72	72.10	72.70	49.60	98.50	2.59	2.62
24H-2, 69	209.49	1.59	0.92	2.71	65.80	66.30	42.40	73.50	1.92	1.94
24H-3, 69	210.99	1.35	0.59	2.30	73.90	74.50	56.10	127.70	2.83	2.86
24H-4, 69	212.49	1.32	0.56	2.24	74.80	75.40	57.90	137.70	2.97	3.01
24H-5, 69	213.99	1.32	0.53	2.33	77.00	77.60	59.90	149.40	3.34	3.39
24H-6, 69	215.49	1.32	0.52	2.44	78.20	78.80	60.50	153.50	3.59	3.65
25H-1, 79	217.59	1.30	0.49	2.40	79.30	79.90	62.40	166.20	3.83	3.90
25H-2, 79	219.09	1.31	0.53	2.30	76.80	77.40	59.90	149.50	3.30	3.35
25H-3, 79	220.59	1.35	0.56	2.56	77.90	78.50	59.00	143.80	3.53	3.59
25H-4, 79	222.09	1.28	0.45	2.39	80.90	81.50	64.90	185.30	4.23	4.31
25H-5, 79	223.59	1.17	0.38	1.72	77.70	78.60	67.90	211.20	3.49	3.55
25H-6, 79	225.09	1.45	0.74	2.48	70.00	70.60	49.40	97.60	2.34	2.36
25H-7, 49	226.29	1.42	0.65	2.61	74.70	75.30	54.00	117.50	2.95	2.99
26H-1, 69	226.99	1.34	0.52	2.69	80.50	81.00	61.50	159.70	4.12	4.19
26H-2, 69	228.49	1.30	0.51	2.22	76.60	77.30	60.60	153.50	3.28	3.33
26H-3, 69	229.99	1.34	0.54	2.49	77.90	78.50	59.60	147.70	3.53	3.59
26H-4, 69	231.49	1.32	0.53	2.31	76.60	77.20	59.60	147.20	3.27	3.32
26H-5, 69	232.99	1.30	0.49	2.31	78.20	78.80	61.80	162.00	3.59	3.65
26H-6, 69	234.49	1.33	0.54	2.38	77.00	77.60	59.40	146.20	3.34	3.39
26H-7, 29	235.59	1.29	0.49	2.29	78.40	79.10	62.30	165.20	3.63	3.69
27H-1, 59	236.39	1.27	0.46	2.29	79.60	80.30	64.10	178.40	3.91	3.98
27H-2, 59	237.89	1.30	0.50	2.32	78.20	78.80	61.70	161.00	3.59	3.64
27H-3, 59	239.39	1.28	0.46	2.34	80.10	80.80	64.30	179.90	4.03	4.10
27H-4, 59	240.89	1.31	0.50	2.41	78.70	79.30	61.50	159.70	3.69	3.76
27H-5, 59	242.39	1.31	0.49	2.47	79.80	80.40	62.50	166.90	3.96	4.03
27H-6, 59	243.89	1.30	0.50	2.29	77.70	78.30	61.20	157.90	3.48	3.53
27H-7, 29	245.09	1.33	0.51	2.55	79.70	80.30	61.50	159.90	3.91	3.99
28H-1, 69	245.99	1.40	0.64	2.51	74.30	74.90	54.40	119.50	2.89	2.93
28H-2, 69	247.49	1.34	0.56	2.44	76.90	77.50	58.60	141.80	3.32	3.37
28H-3, 69	248.99	1.40	0.66	2.44	72.60	73.20	53.00	112.60	2.65	2.69
28H-4, 69	250.49	1.28	0.48	2.24	78.10	78.80	62.30	165.60	3.57	3.63
28H-5, 69	251.99	1.31	0.51	2.35	77.80	78.50	60.90	155.80	3.51	3.57
28H-6, 69	253.49	1.31	0.51	2.34	77.70	78.40	60.80	155.30	3.49	3.55
28H-7, 19	254.49	1.27	0.47	2.18	77.90	78.60	62.80	168.80	3.53	3.58
29H-1, 69	255.49	1.27	0.46	2.22	78.80	79.50	63.60	174.40	3.72	3.78
29H-2, 69	256.99	1.29	0.47	2.42	80.10	80.70	63.40	173.00	4.02	4.09
29H-3, 64	258.44	1.28	0.44	2.43	81.40	82.00	65.30	187.80	4.37	4.46
29H-4, 69	259.99	1.30	0.48	2.39	79.50	80.20	62.90	169.30	3.88	3.95
29H-5, 64	261.44	1.31	0.51	2.34	77.70	78.30	60.80	154.90	3.48	3.54
29H-6, 69	262.99	1.33	0.54	2.41	77.40	78.00	59.50	147.20	3.42	3.47
29H-7, 19	263.99	1.36	0.59	2.41	75.20	75.80	56.70	131.10	3.04	3.08
30H-1, 69	264.99	1.35	0.57	2.41	76.00	76.60	57.70	136.60	3.17	3.21
30H-2, 69	266.49	1.61	0.96	2.64	63.20	63.70	40.20	67.30	1.72	1.73
30H-3, 69	267.99	1.41	0.68	2.38	71.10	71.70	51.70	107.00	2.46	2.49
30H-4, 69	269.49	1.59	0.92	2.68	65.40	65.80	42.10	72.80	1.89	1.90
30H-5, 69	270.99	1.68	1.07	2.68	59.80	60.20	36.40	57.30	1.49	1.50
30H-6, 69	272.49	1.31	0.52	2.27	76.50	77.20	59.90	149.60	3.26	3.31
30H-7, 39	273.69	1.50	0.79	2.59	69.30	69.90	47.50	90.30	2.26	2.29

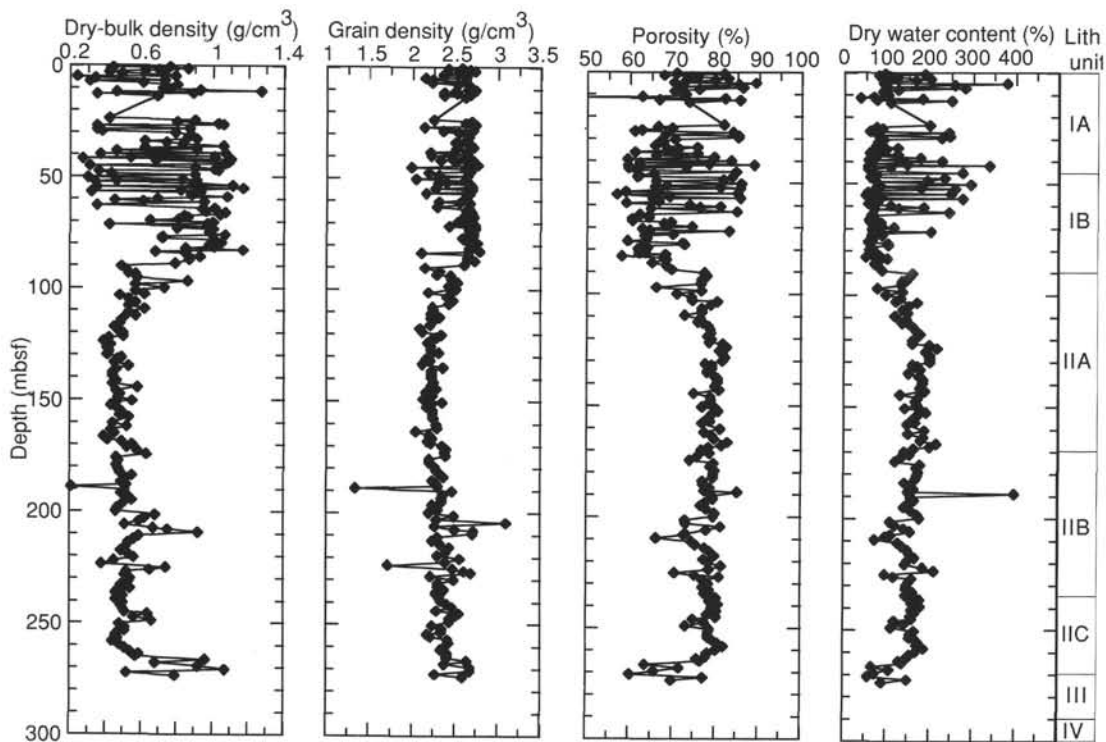


Figure 27. Plots of index property data vs. depth for Hole 887C. Lithologic units also are shown.

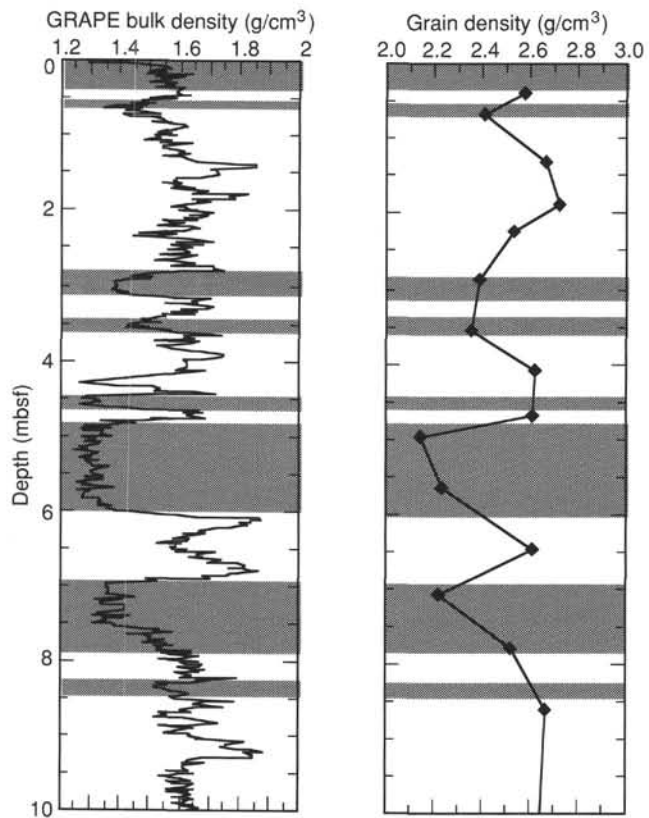


Figure 28. Plots of GRAPE density and grain density data vs. depth in the upper 10 mbsf of the Hole 887C.

Table 13. Vane shear strength data from Hole 887A.

Core, section, interval (cm)	Depth (mbsf)	Vane shear strength (kPa)
145-887A-		
1H-1, 110	1.10	14.01
1H-2, 105	2.55	18.62
1H-3, 110	4.10	24.05
1H-4, 110	5.60	45.91
2H-1, 110	7.80	38.49
2H-2, 110	9.30	45.45
2H-3, 110	10.80	42.20
2H-4, 110	12.30	44.06
2H-5, 125	13.95	42.67
2H-6, 110	15.30	50.09
3H-1, 85	17.05	48.70
3H-2, 110	18.80	39.42
3H-3, 110	20.30	54.26
3H-4, 110	21.80	69.79
3H-5, 110	23.30	70.55
3H-6, 115	24.85	78.80
4H-1, 110	26.80	57.79
4H-2, 110	28.30	50.28
4H-3, 110	29.80	60.04
4H-4, 110	31.30	66.04
4H-5, 110	32.80	78.80
4H-6, 110	34.30	76.55
5H-1, 110	36.30	53.28
5H-2, 110	37.80	60.79
5H-3, 110	39.30	58.54
5H-4, 110	40.80	100.56
5H-5, 110	42.30	54.03
5H-6, 110	43.80	69.79
6H-1, 110	45.80	74.30
6H-2, 110	47.30	75.80
6H-3, 110	48.80	76.55
6H-4, 100	50.20	77.30
6H-5, 120	51.90	72.80
6H-6, 110	53.30	177.11
7H-1, 110	55.30	76.55
7H-2, 110	56.80	78.05
7H-3, 110	58.30	74.30
7H-4, 110	59.80	70.55
7H-5, 110	61.30	89.31
7H-6, 110	62.80	105.82
8H-1, 100	64.70	59.29
8H-1, 120	64.90	57.79
8H-2, 110	66.30	70.55
8H-3, 110	67.80	55.54
8H-4, 110	69.30	78.05
8H-5, 110	70.80	60.04
8H-6, 110	72.30	74.30
9H-1, 120	74.40	35.27
9H-2, 110	75.80	24.02
9H-3, 110	77.30	24.02
9H-4, 110	78.80	24.02
9H-5, 110	80.30	40.53
10H-1, 110	83.80	93.06
10H-2, 105	85.25	78.80
10H-3, 100	86.70	148.59
10H-4, 110	88.30	104.32
10H-5, 115	89.85	159.85
10H-6, 110	91.30	92.31
11H-1, 110	93.30	51.78
11H-2, 110	94.80	63.04
11H-3, 115	96.35	64.54
11H-4, 110	97.80	87.81
11H-5, 110	99.30	84.80
11H-6, 110	100.80	75.80
12H-1, 110	102.80	77.30
12H-2, 110	104.30	85.55
12H-3, 110	105.80	101.31
12H-4, 110	107.30	114.07
12H-5, 110	108.80	120.83
12H-6, 100	110.20	78.80
13H-1, 110	112.30	52.53
13H-2, 110	113.80	42.78
13H-3, 110	115.30	76.55
13H-4, 110	116.80	111.07
13H-5, 110	118.30	116.32
13H-6, 110	119.80	126.08
14H-1, 110	121.80	36.77
14H-2, 110	123.30	88.56
14H-3, 110	124.80	102.82
14H-4, 110	126.30	112.57
14H-5, 110	127.80	91.56
14H-6, 115	129.35	87.06
15X-1, 110	131.30	24.77

Table 13 (continued).

Core, section, interval (cm)	Depth (mbsf)	Vane shear strength (kPa)
15X-2, 130	133.00	16.70
15X-3, 110	134.30	17.16
15X-4, 115	135.85	18.55
15X-5, 110	137.30	17.16
16X-1, 110	140.80	34.78
16X-2, 110	142.30	31.54
16X-3, 110	143.80	34.78
17X-1, 110	146.20	41.28
17X-2, 110	147.70	31.07
17X-3, 110	149.20	25.51
17X-4, 120	150.80	20.41
17X-5, 110	152.20	19.02
18X-1, 110	155.90	20.87
18X-2, 110	157.40	26.44
18X-3, 110	158.90	35.25
18X-4, 110	160.40	38.49
18X-5, 110	161.90	47.31
20X-1, 110	175.20	22.26
20X-2, 110	176.70	26.90
20X-3, 110	178.20	22.26
20X-4, 110	179.70	25.51
20X-5, 110	181.20	27.36
21X-1, 115	184.85	12.97
21X-3, 60	186.80	17.15
22H-1, 110	194.50	21.54
22H-2, 110	196.00	44.52
22H-3, 110	197.50	36.64
22H-4, 110	199.00	40.35
22H-5, 110	200.50	38.96
23H-1, 110	204.00	70.55
23H-2, 110	205.50	95.31
23H-3, 110	207.00	111.82
23H-4, 110	208.50	118.58
23H-5, 110	210.00	111.82
23H-6, 110	211.50	101.31
24H-1, 110	213.50	81.80
24H-2, 110	215.00	87.06
24H-3, 110	216.50	78.05
24H-4, 110	218.00	80.30
25H-3, 110	226.00	93.81
25H-4, 110	227.50	109.57
25H-5, 110	229.00	133.58
25H-6, 105	230.45	111.07
27H-1, 120	242.40	41.28
27H-2, 110	243.80	38.49
27H-3, 110	245.30	43.60
28H-1, 115	251.85	55.65
28H-2, 110	253.30	81.63
28H-3, 110	254.80	168.11
28H-4, 110	256.30	195.87

Table 14. Vane shear strength data from Hole 887C.

Core, section, interval (cm)	Depth (mbsf)	Vane shear strength (kPa)
145-887-H-		
1H-1, 110	1.10	9.20
1H-2, 110	2.60	14.85
1H-3, 110	4.10	16.52
2H-1, 110	5.40	17.15
2H-3, 115	8.45	24.89
2H-5, 108	11.38	34.32
4H-1, 133	24.63	40.35
4H-3, 115	27.45	39.89
4H-5, 110	30.40	63.54
5H-1, 110	33.90	51.03
5H-3, 85	36.65	58.54
5H-5, 110	39.90	132.83
6H-1, 90	43.20	66.79
6H-3, 110	46.40	57.79
6H-5, 100	49.30	47.28
7H-1, 105	52.85	69.04
7H-3, 110	55.90	61.54
7H-5, 110	58.90	59.29
8H-1, 110	62.40	26.27
9H-1, 115	65.95	65.29
9H-3, 110	68.90	71.30
9H-5, 110	71.90	72.80
10H-1, 110	75.40	73.55
10H-3, 100	78.30	67.54
10H-5, 102	81.32	102.06
11H-1, 110	84.90	71.30
11H-3, 110	87.90	90.81
11H-5, 110	90.90	63.04
12H-1, 110	94.40	66.04
12H-3, 110	97.40	81.80
12H-5, 110	100.40	73.55
13H-1, 110	103.90	120.08
13H-3, 110	106.90	126.83
13H-5, 110	109.90	111.07
14H-2, 110	114.90	55.54
14H-3, 110	116.40	59.29
14H-5, 110	119.40	89.31
15H-2, 110	124.40	56.29
15H-4, 110	127.40	57.04
15H-6, 110	130.40	58.54
16H-2, 110	133.90	44.06
16H-4, 110	136.90	65.86
16H-6, 110	139.90	144.84
17H-2, 110	143.40	58.54
17H-4, 110	146.40	78.05
17H-6, 110	149.40	87.06
18H-1, 110	151.40	69.04
18H-3, 110	154.40	65.29
19H-1, 110	160.90	74.30
19H-3, 110	163.90	76.55
19H-5, 110	166.90	42.78
20H-2, 110	171.90	62.29
20H-4, 110	174.90	81.80
20H-6, 110	177.90	93.06
21H-2, 110	181.40	98.31
21H-4, 110	184.40	147.84
22H-2, 110	190.90	104.32
22H-4, 110	193.90	121.58
22H-6, 110	196.90	120.83
23H-2, 110	200.40	98.31
23H-4, 110	203.40	97.56
23H-6, 110	206.40	121.58
24H-1, 110	208.40	63.79
24H-3, 30	210.60	72.05
24H-5, 110	214.40	135.09
25H-1, 110	217.90	67.54
25H-3, 110	220.90	60.04
25H-5, 110	223.90	148.59
26H-1, 110	227.40	48.78
26H-3, 110	230.40	180.11
26H-5, 110	233.40	155.35
27H-1, 110	236.90	85.55
27H-3, 110	239.90	112.57
27H-5, 110	242.90	182.37
28H-1, 110	246.40	105.82
28H-3, 110	249.40	114.07
28H-5, 110	252.40	179.36
29H-1, 105	255.85	41.28
29H-3, 110	258.90	81.80
29H-6, 100	263.30	99.81
30H-1, 110	265.40	129.08
30H-3, 110	268.40	139.59
30H-5, 110	271.40	187.62

Table 15. Thermal conductivity data from Site 887.

Core, section, interval (cm)	Depth (mbsf)	Thermal conductivity (W/(m ² ·°C))
145-887A-		
1H-2, 75	2.25	1.2145
1H-4, 75	5.25	0.8099
2H-2, 75	8.95	0.8864
2H-4, 75	11.95	1.1712
2H-6, 75	14.95	1.3546
3H-2, 75	18.45	1.1768
3H-4, 75	21.45	1.1726
3H-6, 75	24.45	1.2552
4H-2, 75	27.95	0.9743
4H-4, 75	30.95	1.2103
4H-6, 75	33.95	1.1322
5H-2, 75	37.45	1.2340
5H-4, 75	40.45	1.2524
5H-6, 75	43.45	0.8557
6H-2, 75	46.95	1.8807
6H-4, 75	49.95	1.5990
6H-6, 75	52.95	1.4403
7H-2, 75	56.45	0.8312
7H-4, 75	59.45	0.9794
7H-6, 75	62.45	0.8259
8H-2, 75	65.95	1.0705
8H-4, 75	68.95	1.7990
8H-6, 75	71.95	1.4880
9H-2, 75	75.45	1.4006
9H-4, 75	78.45	1.1619
9H-6, 40	81.10	1.2719
10H-2, 75	84.95	1.2653
10H-4, 75	87.95	1.0038
10H-6, 75	90.95	1.7301
11H-2, 75	94.45	1.0027
11H-4, 75	97.45	0.9678
11H-6, 75	100.45	1.1107
12H-2, 75	103.95	0.9872
12H-4, 75	106.95	1.0549
12H-6, 75	109.95	1.0859
13H-2, 70	113.40	0.8747
13H-4, 70	116.40	0.9667
13H-6, 70	119.40	0.8932
14H-2, 70	122.90	0.8721
14H-4, 70	125.90	0.9436
14H-6, 70	128.90	0.8444
15X-2, 7	132.40	0.8816
15X-4, 7	135.04	0.9335
15X-6, 3	138.00	0.8474
16X-2, 7	141.90	0.8667
16X-3, 7	143.40	0.9295
17X-2, 7	147.30	0.8695
18X-2, 7	157.00	1.0513
18X-4, 7	160.00	0.9121
18X-6, 6	162.97	0.8780
20X-2, 7	176.30	0.8916
20X-4, 7	179.30	0.9459
20X-6, 7	182.30	1.0174
21X-2, 7	185.90	0.8633
21X-1, 7	184.40	1.0618
22H-2, 70	195.60	0.8862
22H-4, 70	198.60	0.9795
22H-6, 70	201.60	0.8959
23H-2, 70	205.10	0.8836
23H-4, 70	211.10	1.0529
23H-6, 70	214.60	1.2293
24H-2, 70	217.59	0.8916
24H-4, 69	220.59	1.0198
24H-6, 69	224.10	1.0256
25H-2, 70	227.10	0.8499
25H-4, 70	230.10	0.9491
25H-6, 70	233.10	1.1070
27H-2, 75	243.45	0.9179
27H-3, 75	244.95	0.9914
28H-2, 75	252.95	0.9134
28H-4, 75	255.95	1.1635
28H-6, 75	258.95	0.9429
29H-2, 40	262.10	0.9178
29H-4, 40	264.25	0.9937
30X-4, 80	275.00	0.8816
145-887C-		
2H-4, 75	9.55	0.8790
2H-6, 75	12.55	1.3509
4H-2, 70	25.50	1.3754
4H-4, 70	28.50	1.0842
4H-6, 70	31.50	1.2579

Table 15 (continued).

Core, section, interval (cm)	Depth (mbsf)	Thermal conductivity (W/(m ² ·°C))
5H-2, 70	35.00	1.2325
5H-4, 70	38.00	0.8293
5H-6, 70	41.00	1.4637
6H-2, 70	44.50	1.4733
6H-4, 70	47.50	0.8726
6H-6, 70	50.50	0.8572
7H-2, 67	53.97	1.5694
7H-5, 70	58.50	1.1316
7H-6, 70	60.00	1.0003
8H-1, 70	62.00	1.1161
8H-2, 70	63.50	1.0781
9H-1, 70	65.50	1.0091
9H-2, 70	67.00	1.4566
10H-2, 70	76.50	1.2466
10H-4, 70	79.50	1.3810
10H-6, 70	82.50	1.2910
11H-2, 70	86.00	1.4740
11H-4, 70	89.00	1.0493
11H-6, 70	92.00	0.9196
14H-2, 70	114.50	0.9731
14H-4, 70	117.50	0.8569
14H-6, 70	120.50	0.8586
12H-2, 70	95.50	1.0510
12H-4, 70	98.50	0.9588
12H-6, 70	101.50	0.9236
13H-1, 40	103.20	1.0833
13H-6, 100	111.30	0.8910
15H-2, 70	124.00	0.9092
15H-4, 70	127.00	0.8298
15H-6, 70	130.00	0.8698
16H-2, 70	133.50	0.7809
16H-4, 70	136.50	0.8266
16H-6, 70	139.50	0.8575
17H-2, 75	143.05	0.9080
17H-4, 75	146.05	0.9752
17H-6, 75	149.05	0.8321
18H-2, 75	152.55	0.9537
18H-4, 75	155.55	0.8918
18H-6, 40	157.70	0.8802
19H-2, 75	162.05	0.9918
19H-4, 75	165.05	0.8880
19H-6, 75	168.05	0.8926
20H-2, 75	171.55	0.9844
20H-4, 75	174.55	1.0361
20H-6, 75	177.55	0.8814
22H-2, 75	190.55	0.9566
22H-4, 75	193.55	0.9610
22H-6, 75	196.55	0.9344
23H-2, 75	200.05	1.0221
23H-4, 75	203.05	1.1783
23H-6, 75	206.05	0.8967
24H-2, 75	209.55	1.3521
24H-4, 75	212.55	1.0304
24H-6, 75	215.55	0.9823
25H-2, 75	219.05	0.9627
25H-4, 75	222.05	0.9725
25H-6, 75	225.05	1.2079
26H-2, 75	228.55	0.9766
26H-4, 75	231.55	0.9092
26H-6, 75	234.55	0.9029
26H-2, 75	228.55	0.9525
26H-4, 75	231.55	0.9027
26H-6, 75	234.55	0.9639
28H-2, 70	247.50	1.3780
28H-4, 70	250.50	0.9256
29H-2, 70	257.00	0.9280
29H-4, 70	260.00	0.8811
29H-6, 70	263.00	0.8726
30H-2, 70	266.50	1.5121
30H-4, 70	269.50	1.2702
30H-6, 70	272.50	0.8545

Table 16. Compressional wave velocity data (DSV and Hamilton Frame) from Site 887.

Core, section, interval (cm)	Depth (mbsf)	Compress. wave velocity (DSV)(m/s)
145-887A-		
1H-1, 40	0.40	1504.0
1H-2, 50	2.00	1507.2
1H-3, 40	3.40	1508.9
1H-4, 65	5.15	1523.5
2H-1, 40	7.10	1512.1
2H-2, 30	8.50	1526.8
2H-3, 40	10.10	1513.7
2H-4, 40	11.60	1499.3
2H-5, 50	13.20	1533.4
2H-6, 45	14.65	1533.4
3H-2, 40	18.10	1530.1
3H-3, 40	19.60	1517.0
3H-4, 40	21.10	1530.1
3H-5, 40	22.60	1543.4
3H-6, 40	24.10	1520.2
4H-1, 75	26.45	1530.1
4H-2, 40	27.60	1536.7
4H-3, 40	29.10	1530.1
4H-4, 40	30.60	1553.6
4H-5, 40	32.10	1531.7
4H-6, 40	33.60	1521.9
5H-1, 40	35.60	1520.2
5H-2, 40	37.10	1515.3
5H-3, 40	38.60	1528.4
5H-4, 40	40.10	1604.8
5H-5, 40	41.60	1512.1
5H-6, 40	43.10	1540.1
6H-1, 50	45.20	1526.8
6H-2, 40	46.60	1555.3
6H-3, 40	48.10	1541.8
6H-5, 40	51.10	1553.6
6H-6, 50	52.70	1558.8
7H-1, 50	54.70	1588.5
7H-2, 40	56.10	1520.2
7H-3, 40	57.60	1553.6
7H-4, 40	59.10	1433.9
7H-5, 40	60.60	1543.4
7H-6, 40	62.10	1536.7
8H-1, 45	64.15	1538.4
8H-2, 53	65.73	1528.4
8H-3, 48	67.18	1595.7
8H-4, 53	68.73	1730.5
8H-5, 53	70.23	1517.0
8H-6, 53	71.73	1518.6
9H-1, 53	73.73	1507.2
9H-2, 53	75.23	1526.8
9H-3, 53	76.73	1533.4
9H-4, 53	78.23	1525.1
9H-5, 53	79.73	1553.6
10H-1, 53	83.23	1574.4
10H-2, 35	84.55	1535.1
10H-3, 44	86.14	1545.1
10H-4, 53	87.73	1577.9
10H-5, 58	89.28	1551.9
10H-6, 85	91.05	1546.8
11H-1, 53	92.73	1553.6
11H-2, 53	94.23	1541.8
11H-3, 53	95.73	1530.1
11H-4, 53	97.23	1545.1
11H-5, 53	98.73	1551.9
11H-6, 42	100.12	1540.1
12H-1, 53	102.23	1543.4
12H-2, 53	103.73	1540.1
12H-3, 53	105.23	1546.8
12H-4, 53	106.73	1548.5
12H-5, 53	108.23	1546.8
12H-6, 43	109.63	1538.4
13H-1, 58	111.78	1543.4
13H-2, 53	113.23	1538.4
13H-3, 53	114.73	1540.1
13H-4, 53	116.23	1548.5
13H-6, 53	119.23	1563.9
14H-1, 53	121.23	1553.6
14H-2, 53	122.73	1548.5
14H-3, 53	124.23	1560.5
14H-4, 53	125.73	1553.6
14H-5, 53	127.23	1551.9
14H-6, 80	129.00	1543.4
14H-6, 80	129.00	1555.3
15X-1, 53	130.73	1550.2

Table 16 (continued).

Core, section, interval (cm)	Depth (mbsf)	Compress. wave velocity (DSV)(m/s)
15X-2, 53	132.23	1550.2
15X-3, 53	133.73	1551.9
15X-4, 53	135.23	1553.6
15X-5, 53	136.73	1545.1
16X-1, 40	140.10	1546.8
16X-2, 40	141.60	1551.9
16X-3, 40	143.10	1553.6
17X-1, 40	145.50	1540.1
17X-2, 40	147.00	1546.8
17X-3, 40	148.50	1536.7
17X-4, 40	150.00	1545.1
17X-5, 40	151.50	1545.1
18X-1, 40	155.20	1540.1
18X-2, 40	156.70	1551.9
18X-3, 40	158.20	1548.5
18X-4, 40	159.70	1562.2
18X-5, 60	161.40	1557.0
18X-6, 40	162.70	1540.1
20X-1, 40	174.50	1536.7
20X-2, 40	176.00	1536.7
20X-3, 40	177.50	1540.1
20X-4, 40	179.00	1538.4
20X-5, 40	180.50	1567.4
20X-6, 40	182.00	1557.0
21X-1, 40	184.10	1546.8
21X-2, 40	185.60	1550.2
21X-3, 40	186.60	1545.1
22H-1, 40	193.80	1538.4
22H-2, 40	195.30	1535.1
22H-3, 40	196.80	1533.4
22H-4, 40	198.30	1545.1
22H-5, 40	199.80	1535.1
22H-6, 40	201.30	1551.9
23H-1, 40	203.30	1536.7
23H-2, 40	204.80	1548.5
23H-3, 40	206.30	1550.2
23H-4, 40	207.80	1563.9
23H-5, 40	209.30	1562.2
23H-6, 40	210.80	1562.2
24H-1, 40	212.80	1515.3
24H-3, 40	215.80	1531.7
24H-4, 40	217.30	1555.3
25H-1, 40	222.30	1538.4
25H-2, 50	223.90	1518.6
25H-3, 40	225.30	1523.5
25H-4, 40	226.80	1533.4
25H-5, 40	228.30	1543.4
25H-6, 40	229.80	1555.3
27H-1, 80	242.00	1525.1
27H-2, 40	243.10	1528.4
27H-3, 40	244.60	1531.7
28H-4, 40	255.60	1574.4
29H-1, 70	260.90	1562.2
145-887C-		
1H-1, 53	0.53	1508.9
1H-2, 53	2.03	1518.6
1H-3, 35	3.35	1515.3
2H-1, 53	4.83	1526.8
2H-3, 40	7.70	1530.1
2H-5, 58	10.88	1521.9
4H-1, 40	23.70	1536.7
4H-3, 53	26.83	1546.8
4H-5, 53	29.83	1570.9
5H-1, 53	33.33	1545.1
5H-3, 22	36.02	1545.1
5H-5, 39	39.19	1551.9
6H-1, 33	42.63	1579.7
6H-3, 46	45.76	1528.4
6H-5, 22	48.52	1530.1
7H-1, 53	52.33	1533.4
7H-3, 40	55.20	1588.5
7H-5, 55	58.35	1543.4
8H-2, 35	63.15	1513.7
9H-1, 53	65.33	1574.4
9H-3, 53	68.33	1550.2
9H-5, 53	71.33	1545.1
10H-1, 60	74.90	1555.3
10H-3, 53	77.83	1517.0
10H-5, 22	80.52	1553.6
11H-3, 40	87.20	1518.6
11H-5, 40	90.20	1583.2
12H-3, 40	96.70	1548.5
12H-5, 40	99.70	1551.9
13H-1, 40	103.20	1550.2

Table 16 (continued).

Core, section, interval (cm)	Depth (mbsf)	Compress. wave velocity (DSV)(m/s)
13H-3, 40	106.20	1551.9
13H-5, 40	109.20	1567.4
14H-2, 30	114.10	1555.3
14H-3, 40	115.70	1560.5
14H-5, 40	118.70	1570.9
15H-2, 40	123.70	1543.4
15H-4, 40	126.70	1551.9
15H-6, 40	129.70	1553.6
16H-2, 40	133.20	1546.8
16H-4, 40	136.20	1570.9
16H-6, 40	139.20	1604.8
17H-2, 40	142.70	1555.3
17H-4, 40	145.70	1567.4
17H-6, 40	148.70	1599.3
18H-1, 40	150.70	1557.0
18H-3, 40	153.70	1563.9
18H-5, 40	156.70	1574.4
19H-1, 40	160.20	1558.8
19H-3, 40	163.20	1562.2
19H-5, 40	166.20	1576.1
20H-2, 40	171.20	1576.1
20H-4, 40	174.20	1563.9
20H-6, 40	177.20	1563.9
21H-2, 40	180.70	1585.0
21H-4, 40	183.70	1572.6
22H-2, 40	190.20	1570.9
22H-4, 40	193.20	1565.7
22H-6, 40	196.20	1562.2
23H-2, 53	199.83	1563.9
23H-4, 53	202.83	1545.1
23H-4, 53	202.83	1543.4
23H-6, 53	205.83	1574.4
24H-1, 53	207.83	1530.1
24H-3, 15	210.45	1530.1
24H-5, 53	213.83	1548.5
25H-1, 53	217.33	1533.4
25H-3, 53	220.33	1541.8
25H-5, 53	223.33	1541.8
26H-1, 53	226.83	1538.4
26H-3, 53	229.83	1553.6
26H-5, 53	232.83	1572.6
27H-1, 53	236.33	1550.2
27H-3, 53	239.33	1546.8
27H-5, 53	242.33	1550.2
28H-1, 53	245.83	1536.7
28H-3, 53	248.83	1546.8
28H-5, 30	251.60	1572.6
29H-1, 53	255.33	1536.7
29H-3, 53	258.33	1555.3
29H-6, 53	262.83	1555.3
30H-1, 53	264.83	1546.8
30H-3, 53	267.83	1551.9
30H-5, 53	270.83	1565.7
145-877D-		
4R-3, 52	289.92	
4R-4, 50	291.04	
5R-2, 2	293.42	
7R-4, 72	310.85	
10R-2, 60	336.60	

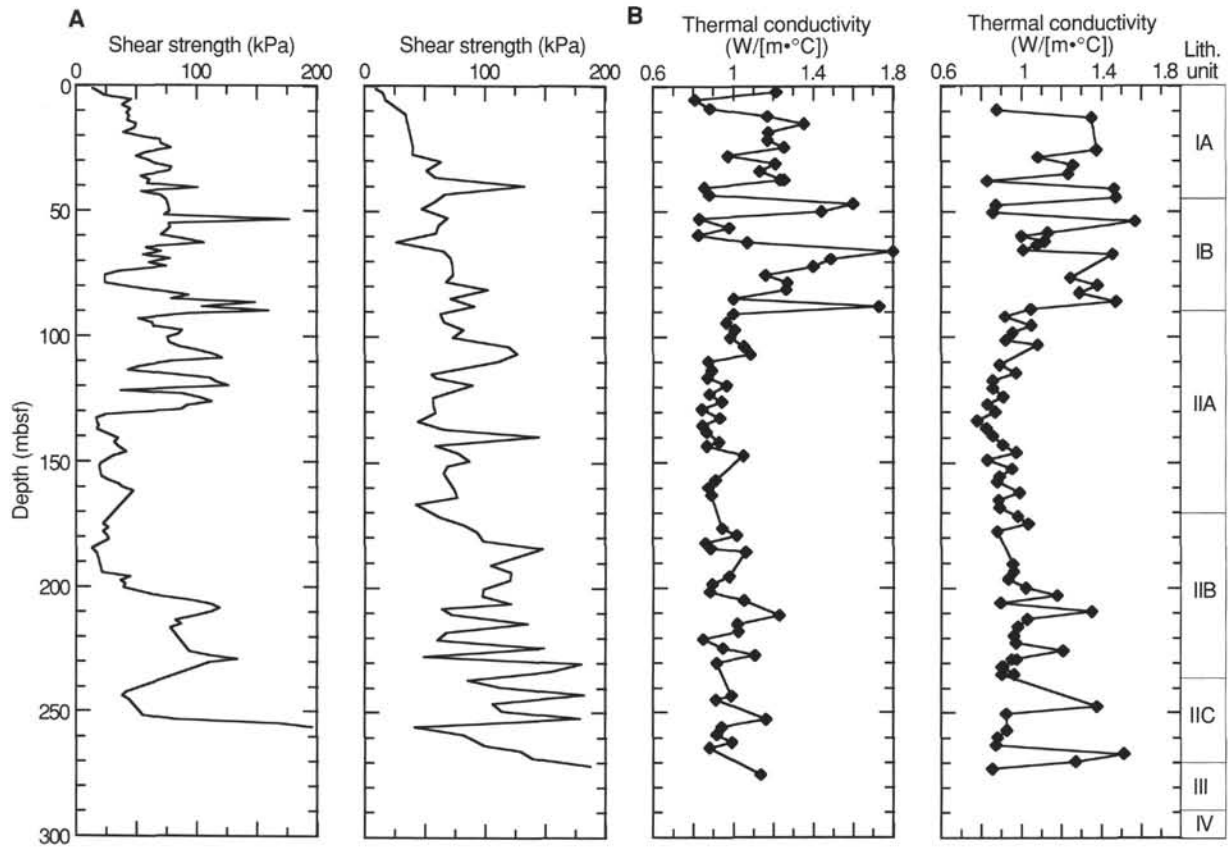


Figure 29. Plots of vane shear strength (A) and thermal conductivity (B) data vs. depth for Holes 887A and 887C. Lithologic units are shown at right.

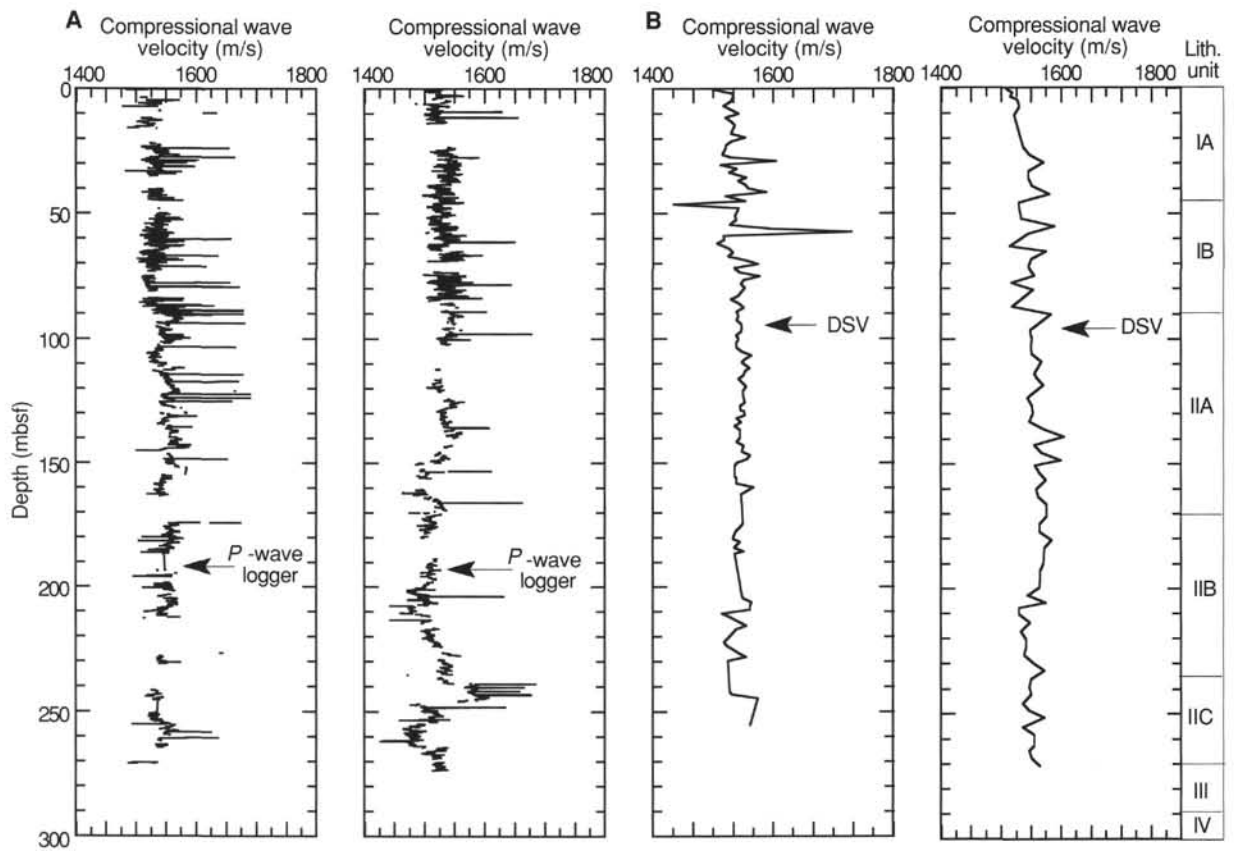


Figure 30. Plots of compressional wave velocity (P-wave logger [A] and DSV [B]) data vs. depth for Holes 887A and 887C. Lithologic units are shown at right.

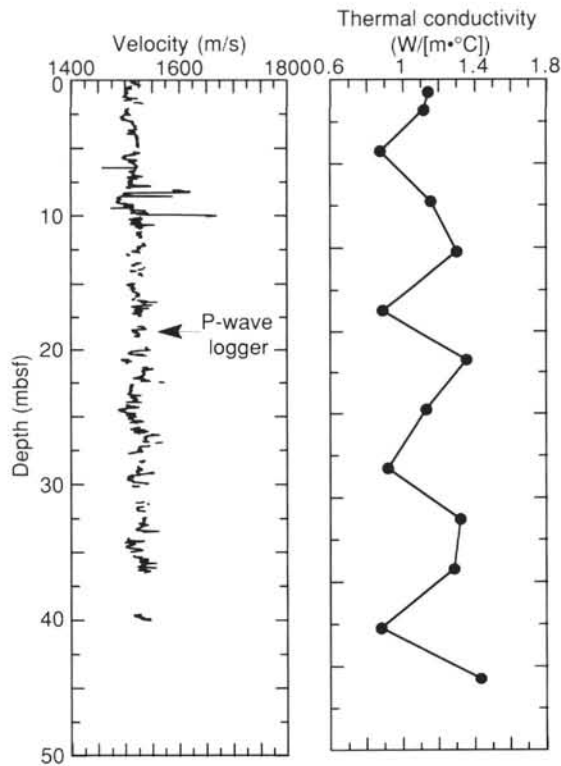


Figure 31. Plots of compressional wave velocity and thermal conductivity data vs. depth for Hole 887B.

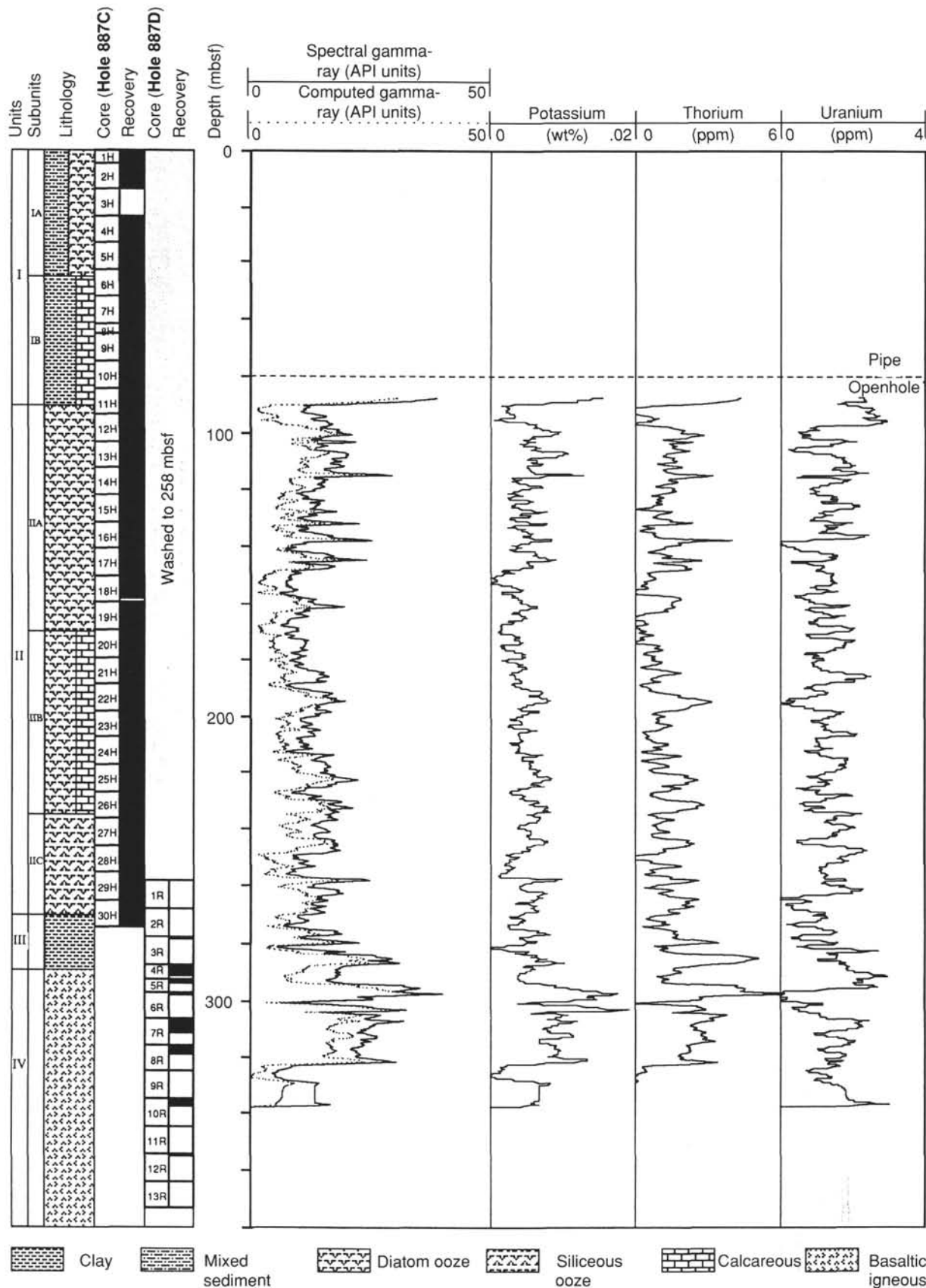


Figure 32. Data from the NGT recorded on the FMS tool string. Displayed data have been smoothed by a linear nine-point (1.37-m) moving average filter.

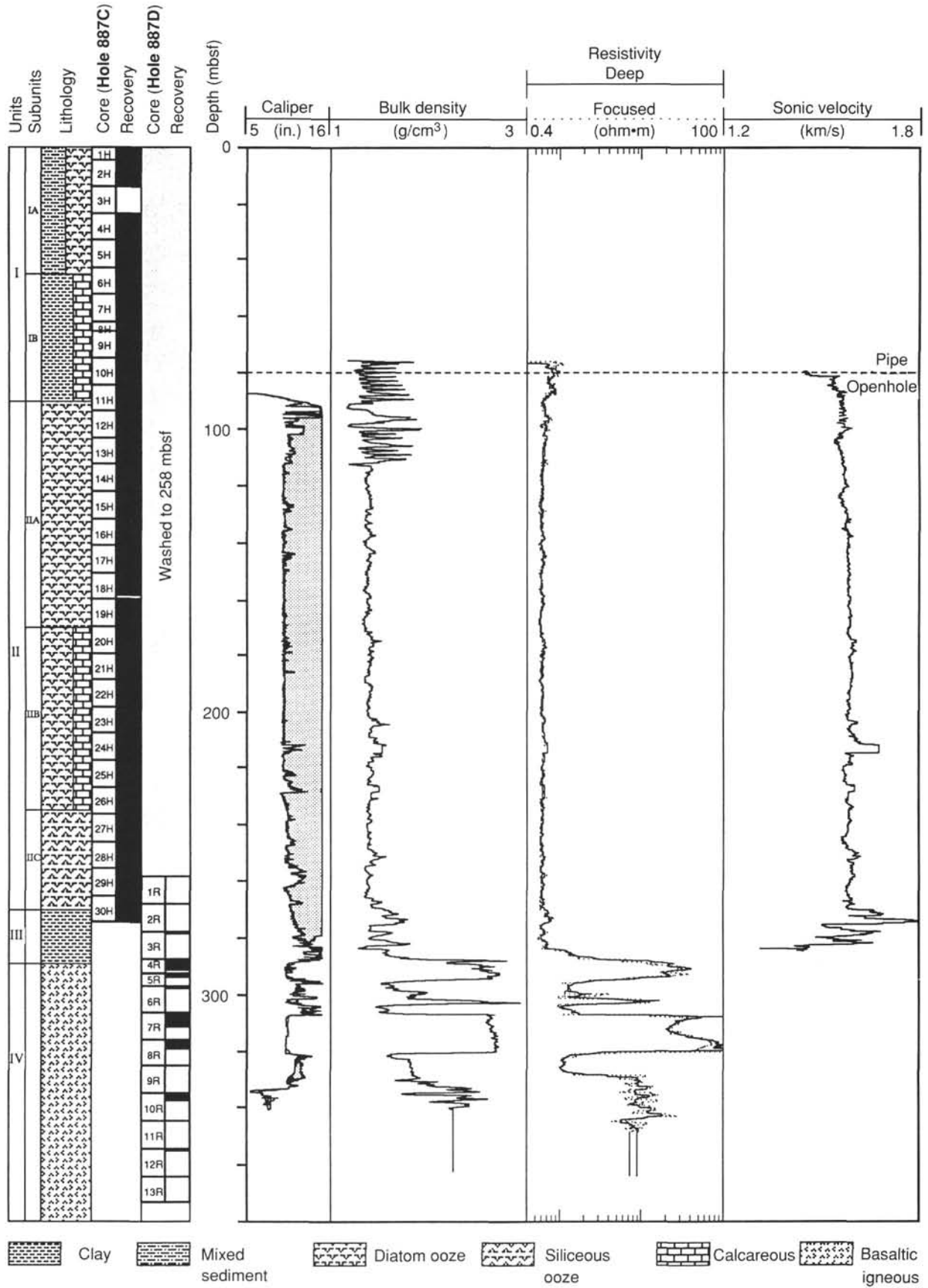


Figure 33. Orthogonal caliper pair data from the FMS, shown with other logs from the Quad combination tool string; bulk density data from the HLDT; deep phasor induction and spherically focused resistivity from the DIT. Long- and short-spacing sonic velocity from the digital sonic tool (SDT). The displayed data have been smoothed by a linear nine-point (1.37-m) moving average filter.

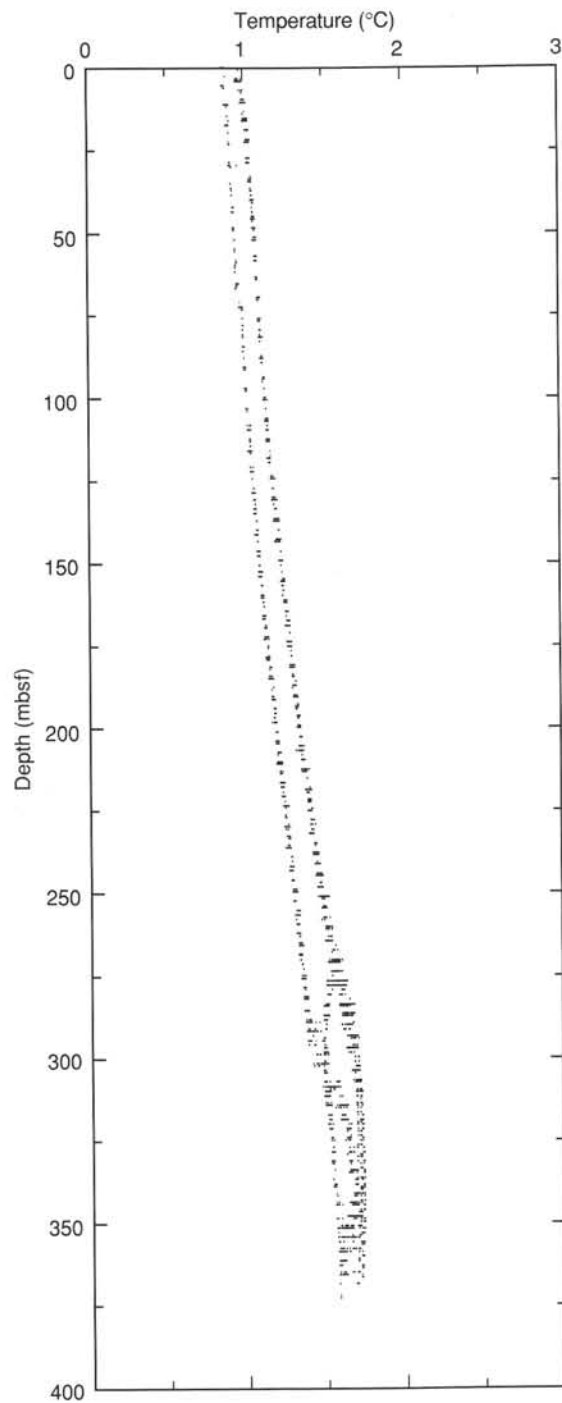


Figure 34. Temperature data recorded by the Lamont temperature tool on the Quad combination tool string, the first tool string to be run into Hole 887D.

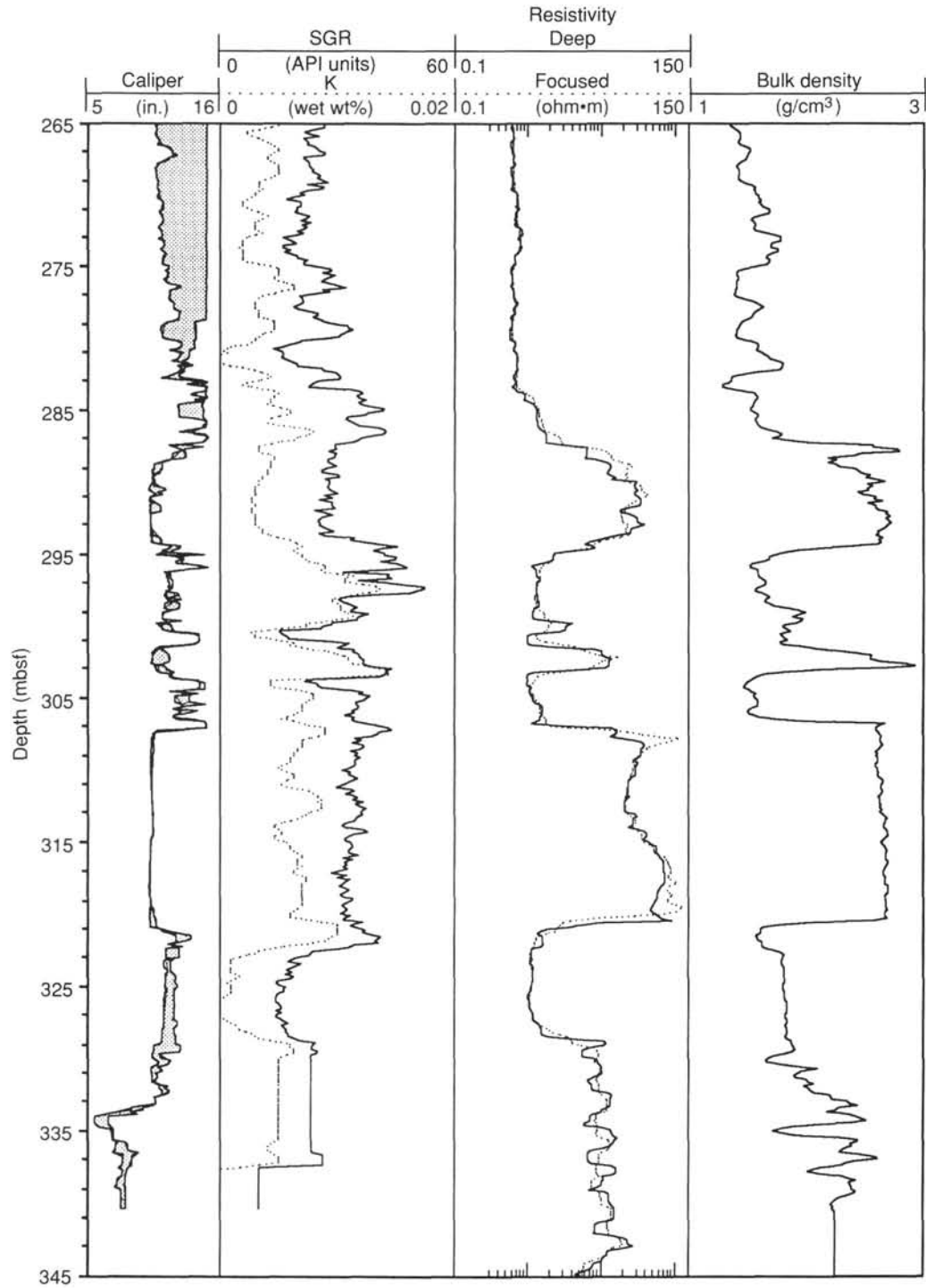


Figure 35. Detail of the logs representing the basalt-sediment interbeds within lithologic Unit IV. The sharp increases in resistivity and bulk density correspond to several basalt sills and/or flows; the decreases correspond to sediment interbeds. The layer between 307 and 322 mbsf may have been recovered in Cores 145-887D-7R and -8R, which contained several long sections of highly plagioclase phyric basalt.

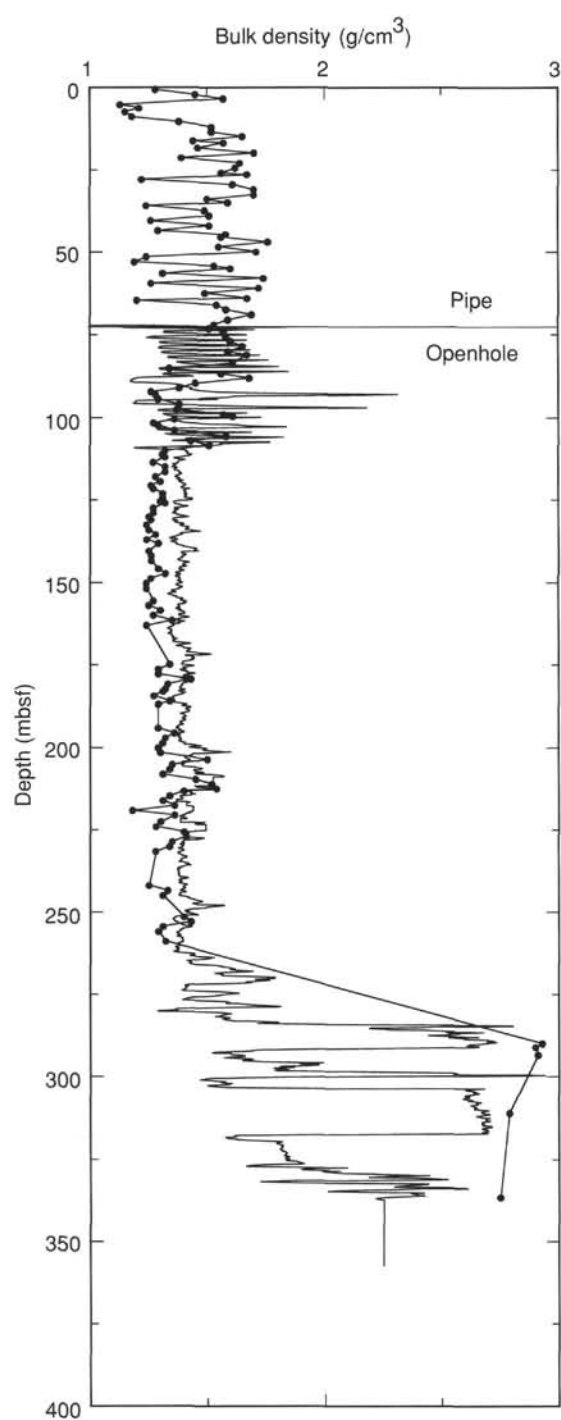


Figure 36. Comparison of logging and core (points)-derived bulk density measurements. Logging data are from the HLDT and have been smoothed by a linear seven-point moving average filter. Core density data have been based on pycnometer measurements above 280 mbsf; data below 280 mbsf were based on 2-min GRAPE analyses (see "Physical Properties" section, this chapter).

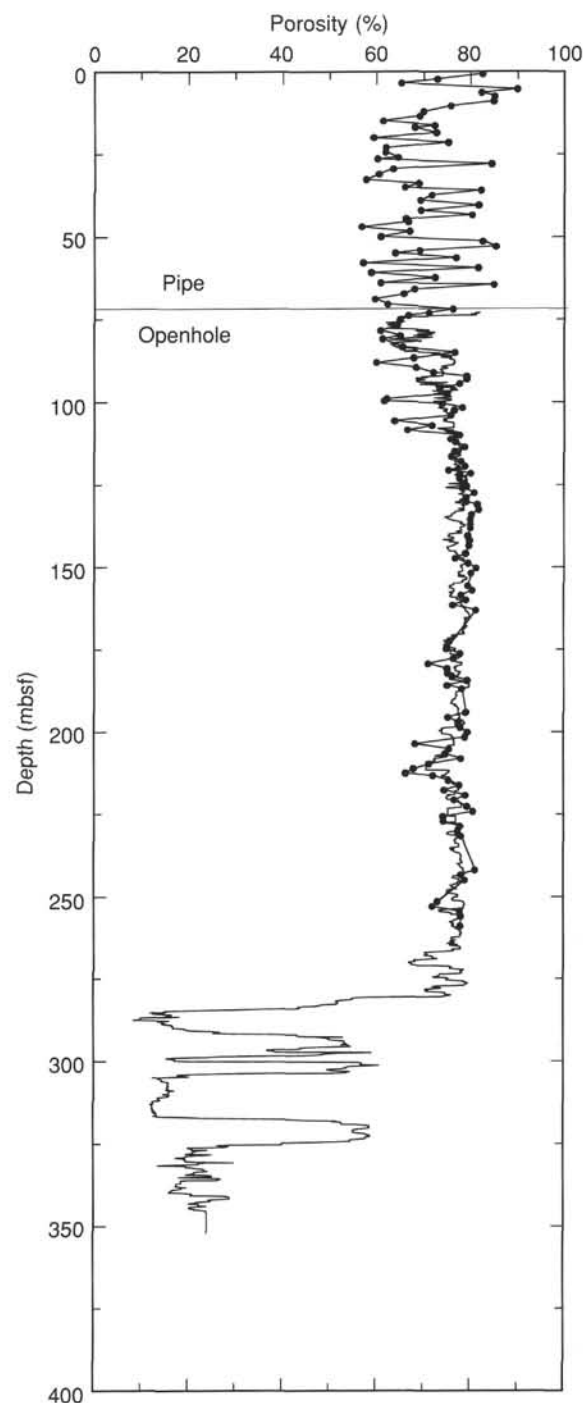


Figure 37. Porosity derived from the medium phasor induction logging of the DIT compared with core porosity measurements in discrete samples (points). The flux resistivity data and the final porosity logging data are unsmoothed.

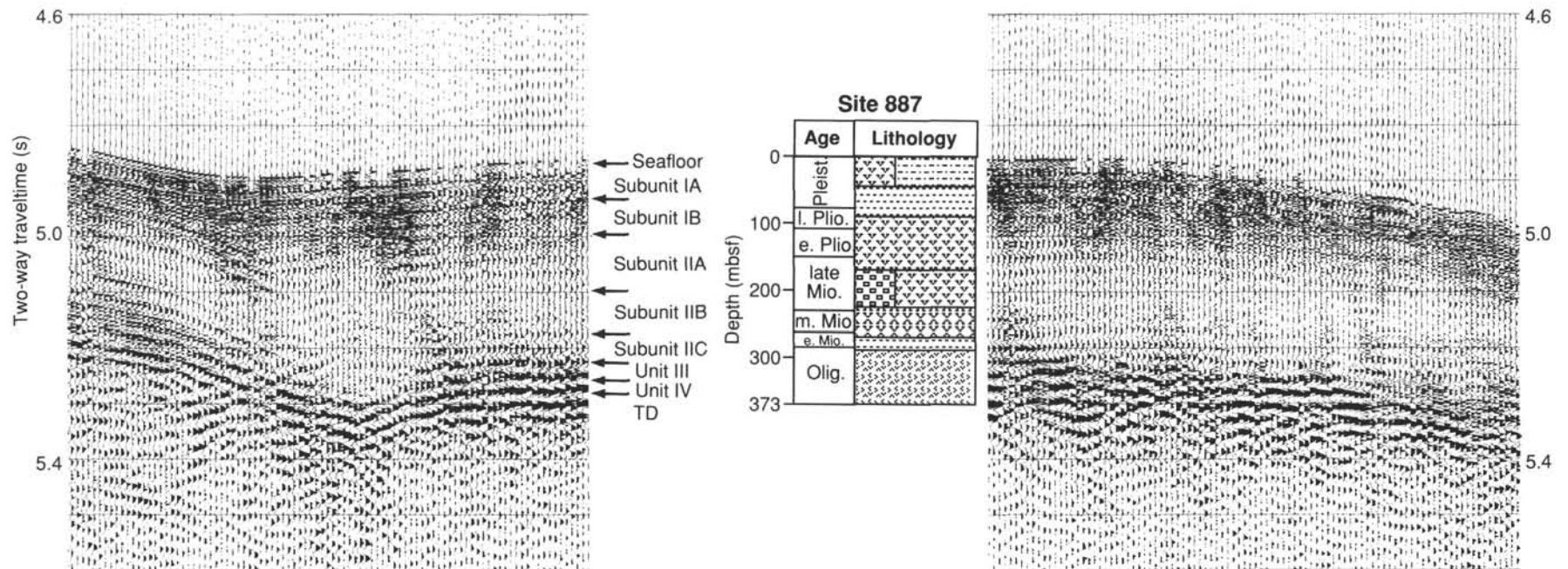
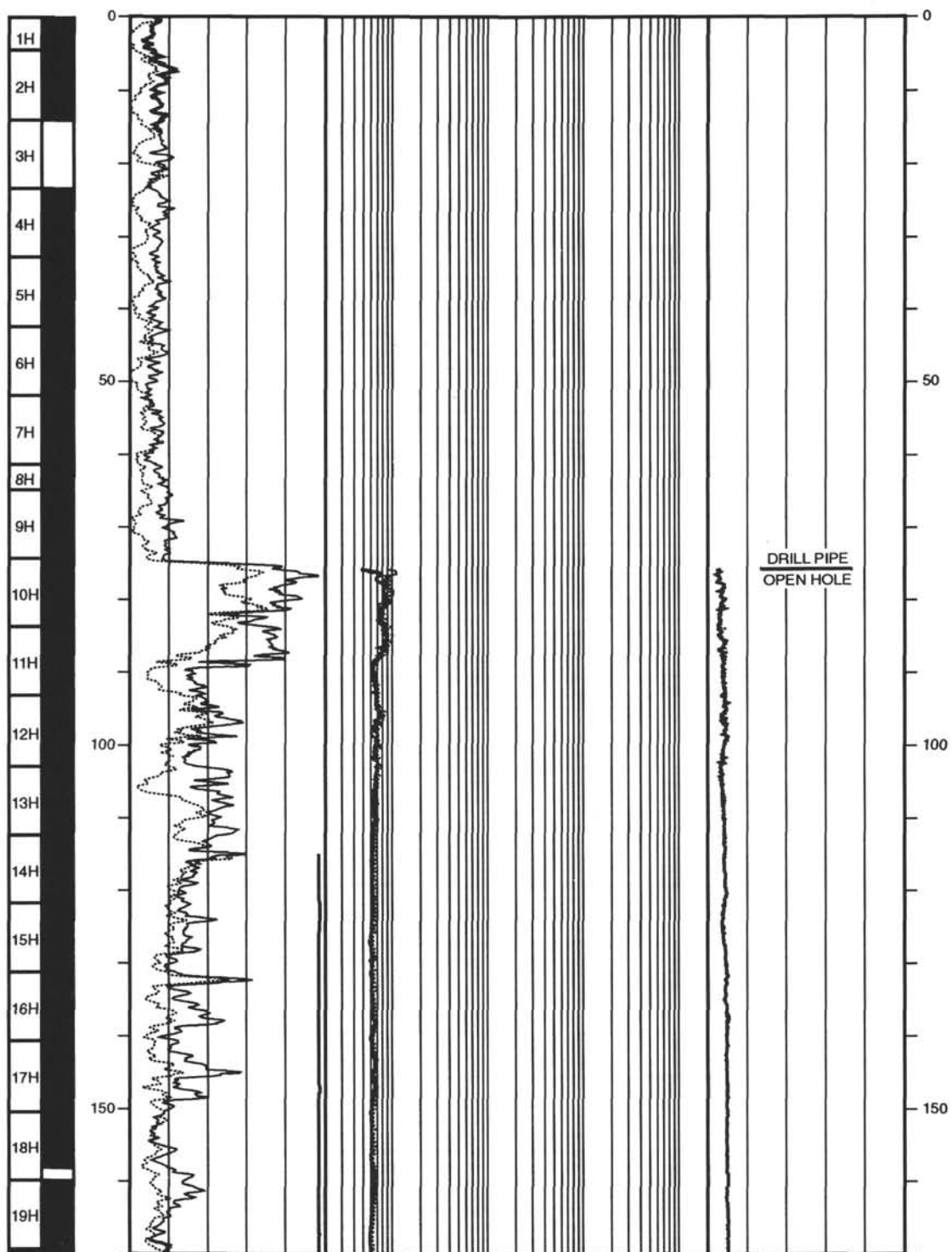


Figure 38: Processed seismic reflection profile from the *JOIDES Resolution* site-survey crossing Site 887. Line trends east-west (east is to the right). The depth ranges of lithologic Units I through III are indicated in the profile inset. Unit IV is basalt. An unidentified electronic glitch prevented the seafloor arrival from every shot from being picked up by the data recorder.

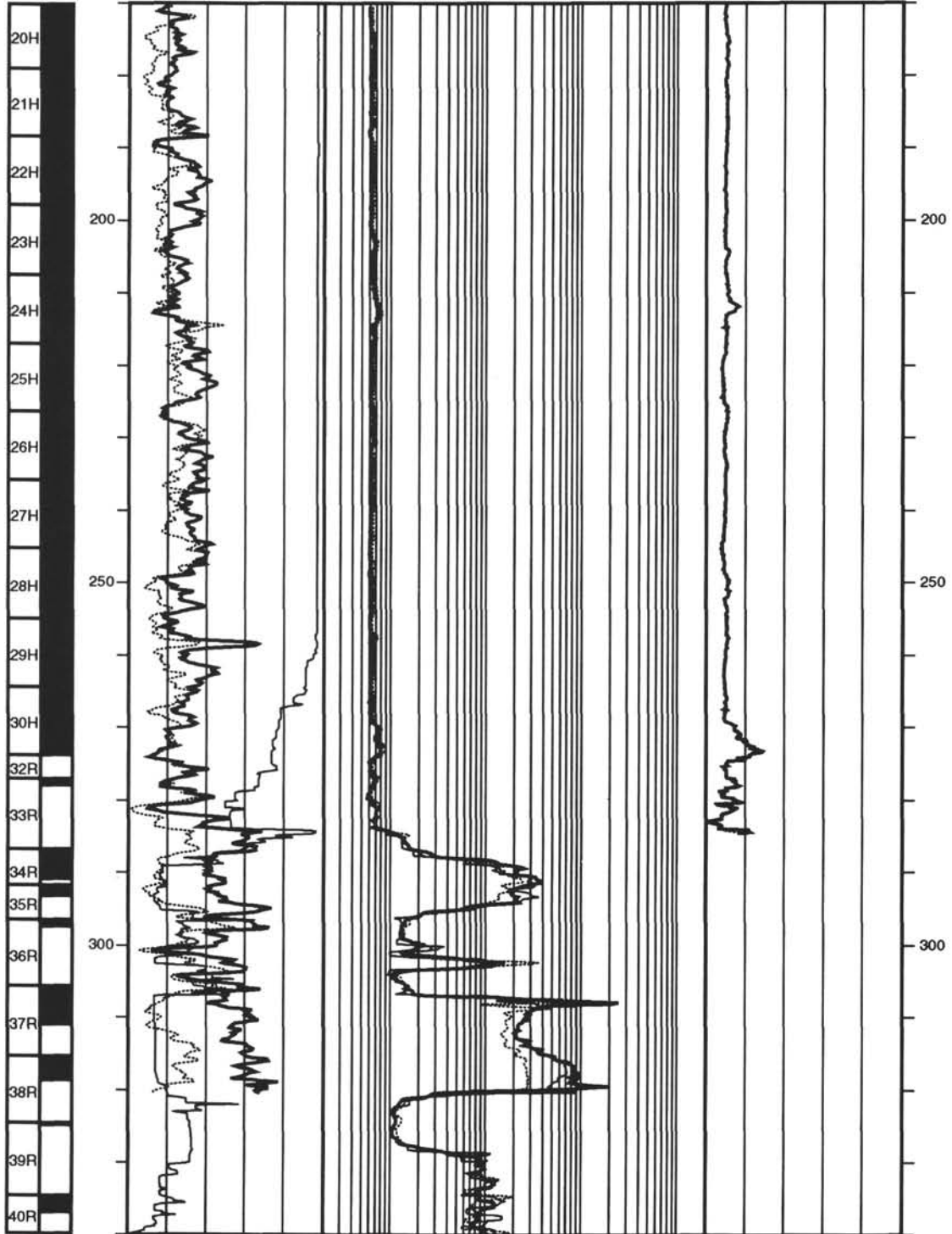
Hole 887D: Resistivity-Velocity-Natural Gamma Ray Log Summary

CORE RECOVERY	SPECTRAL GAMMA RAY			RESISTIVITY			VELOCITY		
	TOTAL			FOCUSED			LONG-SPACING		
	DEPTH BELOW SEA FLOOR (m)	API units		ohm-m		2000	1.4	km/s	2.8
	0	60	.2						
	COMPUTED			MEDIUM			LONG-SPACING		
	0	60	.2	ohm-m		2000	1.4	km/s	2.8
	CALIPER			DEEP			SHORT-SPACING		
	9	in	19.2	ohm-m		2000	1.4	km/s	2.8



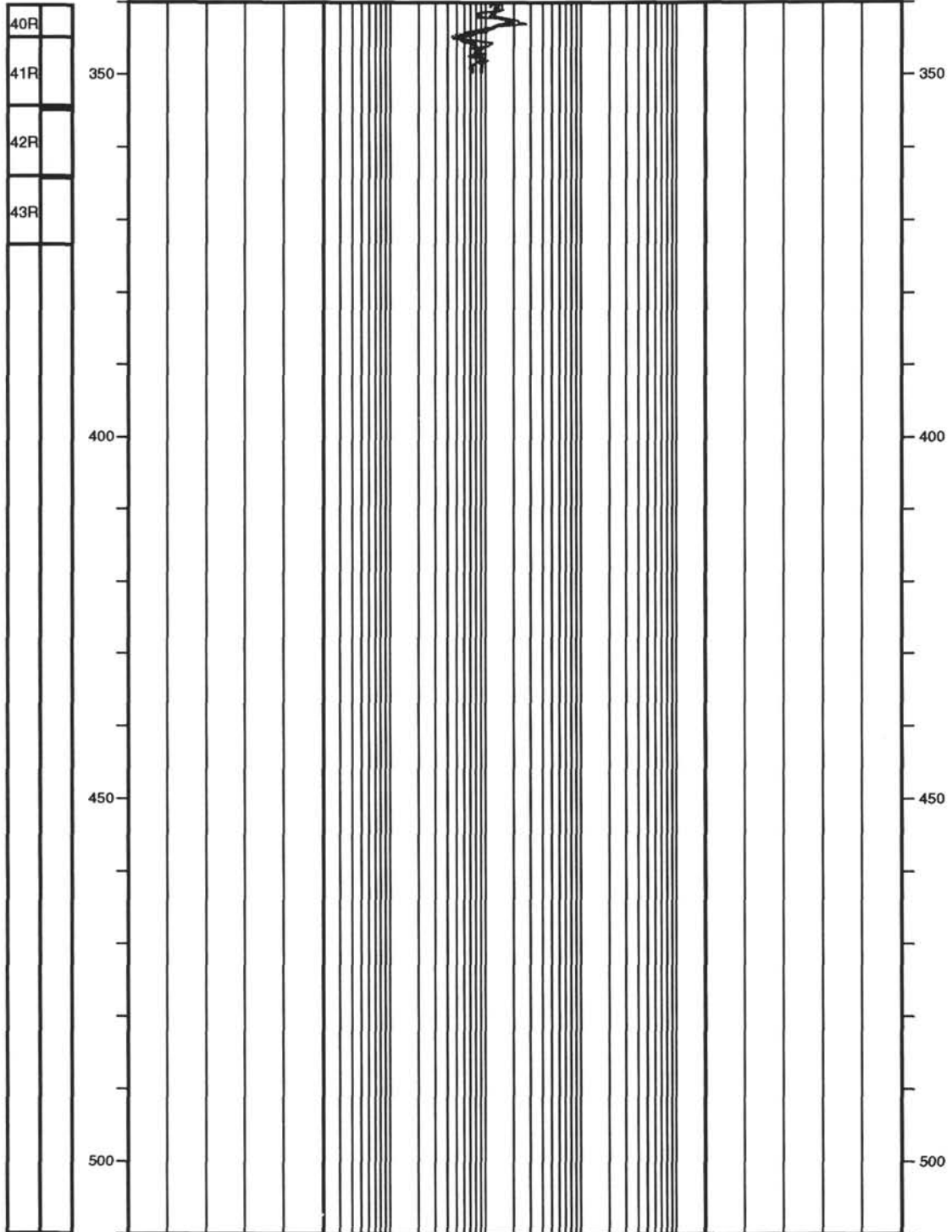
Hole 887D: Resistivity-Velocity-Natural Gamma Ray Log Summary (continued)

CORE RECOVERY	SPECTRAL GAMMA RAY			RESISTIVITY		VELOCITY			DEPTH BELOW SEA FLOOR (m)
	TOTAL			FOCUSED		LONG-SPACING			
	0	API units	60 .2	ohm-m	2000	1.4	km/s	2.8	
	COMPUTED			MEDIUM		SHORT-SPACING			
	0	API units	60 .2	ohm-m	2000	1.4	km/s	2.8	
	CALIPER			DEEP					
	9	in	19 .2	ohm-m	2000	1.4	km/s	2.8	

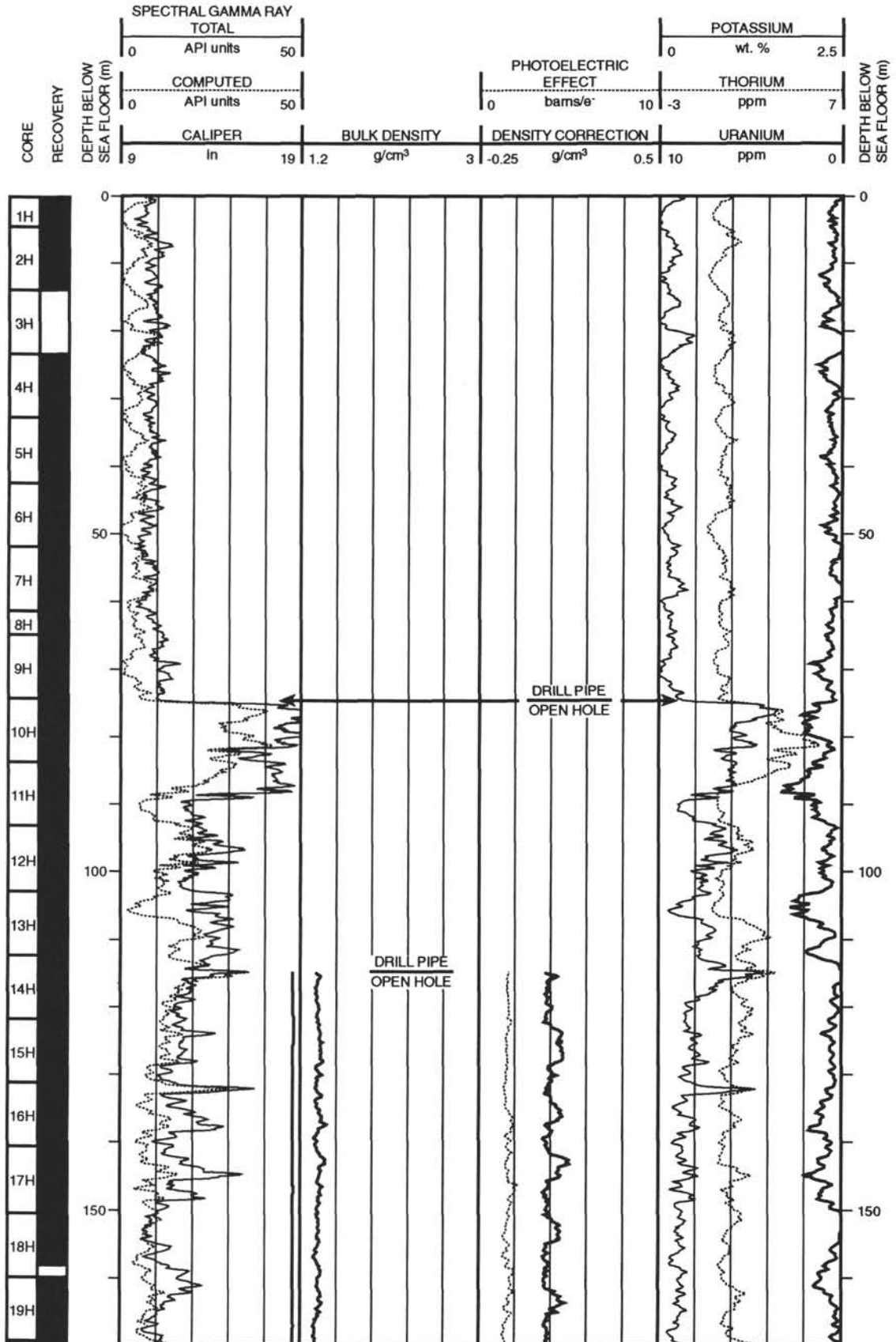


Hole 887D: Resistivity-Velocity-Natural Gamma Ray Log Summary (continued)

CORE RECOVERY	SPECTRAL GAMMA RAY				RESISTIVITY			VELOCITY			DEPTH BELOW SEA FLOOR (m)
	TOTAL				FOCUSED			LONG-SPACING			
	0	API units	60	.2	ohm-m	2000	1.4	km/s	2.8		
	COMPUTED				MEDIUM			SHORT-SPACING			
	0	API units	60	.2	ohm-m	2000	1.4	km/s	2.8		
	CALIPER				DEEP						
	9	in	19	.2	ohm-m	2000	1.4	km/s	2.8		



Hole 887D: Density-Natural Gamma Ray Log Summary



Hole 887D: Density-Natural Gamma Ray Log Summary (continued)

